DOT/FAA/CT-84/30

The Role of Aircraft Panel Materials in Cabin Fires and their Properties

J.G. Quintiere
V. Babrauskas
L. Cooper
M. Harkleroad
K. Steckler

National Bureau of Standards
Gaithersburg, MD 20899

A. Tewarson

Factory Mutual Research Corp.
Norwood, MA 02062

June 1985

Final Report

U.S Department of Transportation
Federal Aviation Administration
Technical Center
Atlantic City Airport, N.J. 08405

NOTICE

This document is disseminated under the sponsorship of the Department of Transportation in the interest of information exchange. The United States Government assumes no liability for the contents or use thereof.

The United States Government does not endorse products or manufacturers. Trade or manufacturer's names appear herein solely because they are considered essential to the object of this report.

Technical Report Documentation Page

1. Report No.	2. Government Accession No.	3. Recipient's Catalog No.
DOT/FAA/CT-84/30		

4. Title and Subtitle	5. Report Date
The Role of Aircraft Panel Materials in Cabin Fires and Their Properties	June 1985
	6. Performing Organization Code
	8. Performing Organization Report No.
7. Author(s) J. C. Quintiere, Coordinating Editor, V.Babrauskas, L. Cooper, M. Harkleroad, K. Steckler, A. Tewarson	
9. Performing Organization Name and Address Department of Commerce National Bureau of Standards Bldg 224, Room A-345 Gaithersburg, Maryland 20899	10. Work Unit No. (TRAIS)
	11. Contract or Grant No.
	13. Type of Report and Period Covered
12. Sponsoring Agency Name and Address U.S. Department of Transportation Federal Aviation Administration Technical Center Atlantic City Airport, New Jersey 08405	14. Sponsoring Agency Code
15. Supplementary Notes	

16. Abstract

Analyses were performed on full-scale aircraft post-crash fire data. In particular the rate and involvement of aircraft wall and ceiling panels are examined. For two full-scale experiments the energy release rate of the interior cabin furnishings were estimated and an estimate of ceiling ignition computed. Also an extensive set of measurements, by several advanced state-of-the-art laboratory flammability devices, was conducted for fire aircraft panel materials. The measurements included piloted ignition by thermal radiation, energy release rate, combustion produce generation rates, lateral flame spread rates in a vertical orientation, flame heights and their heat transfer to a contiguous vertical surface, and for one devices results were obtained at conditions of oxygen concentrations lower than normal air. Comparison among the results for each device show good consistency of the ignition data, but only fair agreement for energy release rate data.

17. Key Words	18. Distribution Statement
Aircraft interior panels, experimental analysis, material fire data, post-crash fires, theoretical modeling.	This document is available to the U.S. public through the National Technical Information Service, Springfield, Virginia 22161

19. Security Classif. (of this report)	20. Security Classif. (of this page)	21. No. of Pages	22. Price
Unclassified	Unclassified	109	

Form DOT F 1700.7 (8-72) Reproduction of completed page authorized

TABLE OF CONTENTS

LIST OF ILLUSTRATIONS

LIST OF ILLUSTRATIONS (Continued)

LIST OF ILLUSTRATIONS (Continued)

LIST OF ILLUSTRATIONS (Continued)

LIST OF TABLES

EXECUTIVE SUMMARY

This report attempts to analyze the role and response of aircraft cabin wall and ceiling panel materials in cabin fires. In particular several post crash fire experiments, previously conducted by the FAA Technical Center, were analyzed. These included tests of a fully furnished cabin section with regular and blocking layer seats. Flashover, the onset of full cabin involvement, occurred for both tests. This was manifested by the ignition of the ceiling panels and subsequent fire spread over the furnishings as flaming ceiling panel debris fell. Analysis was made for these two experiments to estimate the rate of energy release of the cabin furnishings during the growth rate of the fire to flashover. It appears from these estimates that an energy release rate of approximately 1000 kW coincided with the perceived events of flashover in both tests. Flashover was noted to have occurred at 140 s for the regular seat test and 210 s for the blocking layer seat test. Consistent predicted times for ceiling panel ignition based on modeling of the fuel and cabin fire heat fluxes and temperature rise at a typical ceiling panel were demonstrated. These times were estimated as 148 s and 204 s for the regular and blocking-layer seat tests, respectively.

An extensive set of measurements, by several advanced state-of-the-art laboratory flammability devices, was conducted for five aircraft panel materials. These panels only differed in their facing layer materials and binders (epoxy or phenolic). The results are presented in tables and graphs for a wide range of phenomena: ignition, combustion in air and vitiated air ($< 21\%$ O_2 by volume), and flame spread. Fair consistency for the ignition data was found among the devices, but incomplete consistency was observed for peak energy release rate. For the epoxy panels the minimum radiative heat flux for piloted ignition is approximately 2 W/cm^2 and approximately 3.5 W/cm^2 for the phenolic panels. The ignition times roughly range from 10 to 60 s over fluxes greater than the critical value and up to 6 W/cm^2. The peak energy release rate per unit area over these same irradiance levels appears roughly monotonic with heat flux and ranges from 100 to 300 kW/m^2. More precise results for each panel should be derived from the text, but these values have been offered as an indication of performance in summary. Moreover, these data can serve as a reference source in establishing correlation and analysis of full-scale and model experiments.

INTRODUCTION

PURPOSE.

The purpose of this investigation was to provide the Federal Aviation Administration (FAA) with information in order to develop a correlation study for the flammability of aircraft cabin interior panel materials.

BACKGROUND.

The approach taken involved the following. Video records of FAA post-crash fire experiments were to be examined to identify the factors which contributed to fire growth and flashover, with particular attention focused on the role of the cabin interior panels. Also experimental data on a selected series of aircraft panels were to be derived from heat (energy) release rate and flame spread apparatuses at the National Bureau of Standards (NBS) and from the flammability apparatus of the Factory Mutual Research Corporation (FMRC). These results would then be supplemented with additional experimental data from the FAA on the select series of aircraft panels involving their performance in laboratory, model-scale and full-scale experiments.

Flashover, the event in which fire growth beyond a localized region of combustion is rapid and extensive, marks a critical state in the development of a fire. In particular, it has been concluded from post-crash aircraft fire experiments that flashover is the most significant factor in affecting survivability and escape time. Consequently, it is important to understand the flame spread and combustion characteristics of the cabin materials and their role in promoting flashover. Currently it is not possible to predict the general fire growth for a compartment with interior finish materials and furnishings. However, measurement techniques are being developed which attempt to display fire parameters or properties of materials which may be used to describe some particular aspect of fire growth. Hopefully, someday mathematical models will use these "property" data to predict fire growth. In this way, we might unravel the events leading to flashover and clearly quantify the roles of each component in the compartment. Moreover, the phenomenological mechanisms possible for flashover are not completely included in predictive models, but some mechanisms can be quantified. Thus, any attempt to understand the development of flashover in aircraft cabin fires, and to correlate results with laboratory data must be based on partial analyses.

In terms of our current knowledge it may be possible in an experiment to identify the mechanism or mechanisms responsible for flashover and relate it to the contribution of a particular furnishing material. This would require observations and data from that particular experiment, and appropriate data for the materials involved in combustion. For example, if it is observed that gas-phase flame propagation occurred (causing flashover), it may be possible, based on estimates of fuel supply rate and air entrainment rate to the fire, to conclude that fuel rich conditions did indeed develop. On the other hand, if spontaneous ignition of another item were observed, it should be possible to analyze this process and identify its causative factors. In this way, mechanisms of flashover might be identified and analyzed.

From observations of fire development and appropriate material data, it is also possible to analyze a particular furnishing component in terms of its contribution to flashover. For wall and ceiling materials it is expected that measurements of their ignition, flame spread properties, and mass loss and energy release rate should completely characterize their contribution. Various laboratory test apparatuses exist to perform these measurements. Although it is not yet possible to develop predictive methods for fire growth in terms of laboratory test data, it may be fruitful to analyze and ultimately correlate full-scale results in terms of these data. Also, such material test data reveal the individual combustion characteristics of a material. Thus, if ignition is assessed to be critical in a particular fire scenario, then ignition characteristics alone will serve to evaluate a material's performance. In this fashion, experiments can be analyzed to seek clues in developing correlations with test data.

DISCUSSION

GENERAL.

The first area of this investigation centered on analyses related to the involvement of aircraft paneling in the FAA post-crash cabin fire scenario. The second area centered on the derivation of experimental data for the selected series of fire aircraft panel materials. These areas were subdivided into specific tasks based on the scope and apparatus requirements of the task. In each of the tasks a specific individual was responsible for its conduct. Their results are reported in each of the subsequent chapters.

The chapters present a logical sequence of starting with a specific fire hazard analysis for aircraft paneling in a post-crash fire context. The exposure conditions for a ceiling panel are estimated and a computational procedure is developed for estimating its response and potential ignition. No effort was made to predict subsequent flame spread on the panel, nor to predict fire growth within the cabin for other furnishings. Although such predictions are not feasible, it was felt that panel ignition is critical. Extensive regions of the ceiling would be quickly involved following ignition and ceiling flame radiation and its general failure would lead to the involvement of other furnishings. While ceiling ignition may not be a necessary condition for cabin flashover, it is certainly sufficient. Thus chapters 1 and 2 address the heating conditions and prediction of ceiling ignition in a post-crash fire scenario. Of course other fire scenarios that are plausible must be considered in a comprehensive hazard analysis for aircraft panels.

Data for specific aircraft panel materials are presented in chapters 3, 4 and 5. The materials constituted a set of five specially fabricated panels supplied by the FAA Technical Center. These materials are described in table 1. In the chapters to follow, the materials are referred to by number or sample name.

TABLE 1. AIRCRAFT PANEL DESCRIPTIONS*

Aircraft Panel Item Number	Sample Name	Description*	Lot No.
1 (A)	Epoxy fiberglass	Epoxy glass facings, face and back 1 ply 7781 style woven fiberglass impregnated with epoxy resin, fire retardant, and co-cured to 1/8 cell Nomex® honeycomb. One surface to be covered with 2 mil white Tedlar®.	051283
2 (B)	Phenolic fiberglass	Phenolic glass facings, face and back 1 ply 7781 style woven fiberglass impregnated with a modified phenolic resin, and co-cured to 1/8 cell Nomex honeycomb. One surface to be covered with 2 mil white Tedlar.	070583
3 (C)	Epoxy Kevlar®	Epoxy Kevlar facings, face and back 1 ply 285 style woven Kevlar impregnated with epoxy resin fire retardant, and co-cured to 1/8 cell Nomex honeycomb. One surface to be covered with 2 mil white Tedlar.	051683
4 (D)	Phenolic Kevlar	Phenolic Kevlar facings, face and back 1 ply 285 style woven kevlar impregnated with a modified phenolic resin and co-cured to 1/8 cell Nomex honeycomb. One surface to be covered with 2 mil white Tedlar.	092283
5 (E)	Phenolic graphite	Phenolic graphite facings, 1 ply 8 harness satin, 3 K fiber T-300 woven graphite impregnated with a modified phenolic resin, and co-cured to 1/8 cell Nomex honeycomb. One surface to be covered with 2 mil white Tedlar.	090983

*The use of trade names are for descriptive purposes only, and should not be construed as endorsement by the National Bureau of Standards or the Federal Aviation Administration.

Chapter 3 addresses the performance of the materials under piloted ignition as a function of external radiation. The results are given in terms of ignition temperatures and thermal properties. These values are effective properties of the composite panel structure and do not elucidate the effect of each component of the composite. Parameters governing downward and upward spread on a vertical orientation are also presented. A full theory for upward spread is not yet developed, therefore its results are preliminary and inconclusive.

In chapter 4, energy release results are presented for vertically and horizontally oriented samples under exposure conditions of 2.5 to 7.5 W/cm^2. These are derived from the NBS "cone calorimeter" apparatus. Ignition data are also presented.

Similar but more extensive results are derived from the FMRC flammability apparatus and presented in chapter 5. However, only peak values are given and no time resolutions of these data are given in this report. Ignition results are also given along with generation rates of chemical species. The range of exposure conditions were 1 to 6.1 W/cm^2 and approximately 2 to 21 percent oxygen in the atmosphere.

Data in the last three chapters are extensive and their complete application to the hazard analysis may not be obvious. It mainly provides a resource of information to be used to explain and perhaps be used in part to correlate full-scale results. Also the common elements of the data set among the three apparatuses provides a means of assessing the universality of the combustion data obtained from the three devices. Such comparisons will be presented for ignition and energy release rate data common or derivable from the three apparatuses.

CHAPTER 1. CABIN FIRE ENERGY RELEASE RATES IN A POST CRASH FIRE.

A series of full-scale tests discussed in reference 1.1 was conducted by FAA to assess the effect of seat fire-blocking layers on the conditions within an aircraft cabin following the development of a post-crash fire. Specifically, the experiments simulated the ignition of a large external fuel spill adjacent to a door-like opening in the fuselage and the subsequent ignition of cabin seats and linings. The tests were conducted in the FAA C-133 test article shown in figure 1.1. Gas temperatures and concentrations, heat flux levels, and smoke concentrations were measured at various locations throughout the cabin in order to characterize the environment. Also, movies of the cabin interior were made from one or more vantage points.

The current work involves an analysis of these test data with the objective of gaining insight into the roles of the combustible seats, floor, and wall materials in contributing to the extremely hazardous condition known as "flashover". Flashover occurs when enough thermal energy is present to almost instantaneously ignite most, if not all, the combustibles within the cabin. This energy comes from the pool fire outside the cabin, as well as from items burning inside. This report presents estimates of the overall heat release rate from burning cabin materials as a function of time for two tests, each configured as shown in figure 1.1. The first (test 35 of reference 1*) involved 21 "regular" seats composed of fire retarded (FR) polyurethane foam covered with wool-nylon fabric. The second (test 34) was similar except that a Vonar-3®† (polyester scrim) blocking layer was included in the seats.

In chapter 2, this heat release information is used in an analysis of the combined effects of interior and exterior heat sources on cabin ceiling temperatures. These temperatures are critical in that ceiling involvement is a key factor in determining the time to flashover.

APPROACH TO MAKING ENERGY RELEASE ESTIMATES. Limitations in the available test data and the lack of theoretical or empirical models of the burning of relatively complex structures such as aircraft seats preclude an accurate determination of heat release by any single technique. Nevertheless, if independent, although approximate techniques for estimating heat release rates would lead to consistent results, then confidence in such techniques would be enhanced. Along this line the following techniques of data analysis will be used:

- estimate area of involvement from visual recordings and combine with OSU calorimeter heat release data.
- estimate flame heights from visual recordings and apply flame height verses heat release correlations.

---

*All test numbers refer to test numbers reported in reference 1.1.

†The use of trade names are for descriptive purposes only, and should not be construed as endorsement by the National Bureau of Standards or the Federal Aviation Administration.

- utilize FAA mass-loss data from subsidiary experiments involving single aircraft seats and apply heat of combustion data.

- utilize cabin oxygen concentration and gas temperature data in conjunction with oxygen-depletion method for determining heat release rate.

ESTIMATES OF HEAT RELEASE RATE FROM AN INDIVIDUAL SEAT. Figure 1.2 shows a plan view (not to scale) of the C-133 test article. Seat locations are numbered to facilitate the following discussion.

The visual recordings of the tests of interest (tests 34 and 35) do not provide a clear view of the involvement of each seat. At best, one can see that some specific portion of a seat is burning. However, visual results from two supplementary tests (tests 1 and 4, table 1.1), run with only two seats in the cabin, clearly show the involvement of the seats. These seats were located in positions 2 and 5 in figure 1.2 and were subjected to the external pool fire. Other supplementary tests (tests 110 and 107, table 1.1) were run with one seat in position 2 exposed to the external pool fire. This seat was instrumented to measure mass loss. Unfortunately, the exact combinations of seat materials of interest -- FR foam with no blocking layer and FR foam with a Vonar-3 blocking layer -- were not tested in this manner. Nevertheless, tests 110 and 107 represent non-FR-foam analogs to these combinations and can serve as first order approximations.

TABLE 1.1 TEST DESCRIPTIONS

Test No.	
1	One double seat frame constructed from steel angle having a sheet metal back and open bottom. Fire retarded (FR) polyurethane foam cushions on the frame. Cushions covered with wool (90%) - nylon (10%) fabric. No blocking layer. No other combustibles in cabin.
4	Same as test 1 except Vonar-3 (5 mm polyester scrim) blocking layers included in cushions.
34	Six double and three triple standard aircraft assemblies. FR polyurethane seat cushions covered with wool (90%) - nylon (10%) fabric. Vonar-3 blocking layers included in cushions. Honeycomb composite ceiling and wall panels. Honeycomb composite overhead storage bins. Wool pile carpet.
35	Same as test 34 except no blocking layers in cushions.
107	Single seat frame constructed from steel angle with open back and bottom. Non-FR polyurethane cushions with Vonar-3 blocking layers covered with wool (90%) - nylon (10%) fabric. No other combustibles in cabin.
110	Same as test 107 except no blocking layer in cushions.

The results of these supplementary tests provide a means for estimating the heat release rate for a single seat. Later this information will be combined with estimates of seat involvement as judged from the visual records of multi-seat tests 34 and 35.

Regular Seats. Supplementary test 1 was conducted with a simulated double aircraft seat consisting of a metal double-seat frame with "regular" cushions (FR polyurethane foam covered with wool-nylon fabric), sheet metal back, and open bottom. Approximate seat dimensions are shown in figure 1.3. Area-of-involvement was judged as a function of time from the visual recording. The OSU heat release data (reference 1.2) shown in figure 1.4 were then applied to obtain the heat release rate for the double seat as a function of time. This result is shown as the solid lines in figure 1.5.

Flame height above the double seat at what appeared to be the time of peak burning rate (~ 210 seconds) was visually judged to be approximately 1.65 m. Correlations between flame height and heat release rate do not exist for seat geometries. Nevertheless, as a first approximation, the seat fire can be viewed as a free pool fire or a pool fire against a wall. Zukoski's correlation (reference 1.3) for free pool fires is

$$\frac{L_f}{D} = 3.30\ \dot{Q}^{*2/3} \tag{1}$$

where

$$\dot{Q}^* = \frac{\dot{Q}}{\rho_\infty T_\infty C_p \sqrt{g}\ D^{5/2}} > 1 \tag{2}$$

L_f is the flame height above the top face of the horizontal cushion, m

$\dot{Q}$ is the heat release rate, kW

ρ_∞ is the density of ambient air, kg/m^3

T_∞ is the temperature of ambient air, K

c_p is the specific heat of ambient air, KJ/kg-K

g is gravitational acceleration, m/s^2

D is the diameter of the pool, m.

Solving Eqs. (1) and (2) for $\dot{Q}$ and inserting appropriate values for the parameters yields

$$\dot{Q} = 184\ DL_f^{3/2} \tag{3}$$

Hasemi's correlation (reference 1.4) for a square burner against a wall is

$$\frac{L_f}{D_H} = 4\ \dot{Q}_H^{*2/5}\ ;\ \dot{Q}_H^* > 0.4 \tag{4}$$

where $\dot{Q}^*_H$ is defined as the $\dot{Q}^*$ of eq. (2) but D now being taken as D_H, the length of the burner edge, m.

In this case

$$\dot{Q} = 34.5\ L_f^{5/2} \qquad (5)$$

and there is no dependence on D.

An effective D of 0.7 m was taken for the horizontal portion of the double seat. Inserting this value and L_f = 1.65 m into eqs. (2) and (3) yields $\dot{Q}^*$ = 0.60 and $\dot{Q}$ = 273 kW. Inserting the same values into eqs. (4) and (5) yields $\dot{Q}^*_H$ = 0.26 and $\dot{Q}$ = 121 kW. Since the value of $\dot{Q}^*_H$ is outside the range of the correlation, the corresponding $\dot{Q}$ represents an extrapolation. These two values of $\dot{Q}$ are plotted in figure 1.5 at 210 seconds. It is interesting to note that they bracket the peak result of the area-of-involvement calculation. Indeed, their average value of 197 kW closely agrees with the peak result of 175 kW from the analysis based on energy release rate per unit area and the area-of-involvement.

Supplementary test 110 was conducted in the C-133 test using a single-seat mock-up consisting of non-FR polyurethane foam cushions without a blocking layer. The rear surface of the upright cushion was exposed in this case (no sheet metal) and the entire assembly was placed on a load cell. The seat was positioned next to the fire door (No. 2 position, figure 1.2), subjected to the pool fire, its mass recorded for 120 seconds, and then extinguished. Unfortunately, the erratic nature of the instantaneous mass results precluded a reliable determination of instantaneous mass loss rates. Nevertheless, a reliable average mass loss rate based on the initial and final mass values was available. This was found to be 6.8 g/s. In other experiments, Walton and Twilley (reference 1.5) measured the heats of combustion, ΔH, of various aircraft materials, providing a value of 19000 kJ/kg for flexible polyurethane foam (Custom Products Inc., HD54CA low density*). Assuming this value for the foam used in test 110, the average heat release rate over the 120 second period becomes 130 kW. Since the back of this seat was not covered, the exposed area is equivalent to 1.44 times the area of one of the seats used in test 1. Consequently, for comparison purposes, an average value of 130/1.44 or 90 kW is shown in figure 1.5. In this case the meaningful comparison is between the total heats released during the initial 120 second period. These are represented by the areas beneath the curves. Good agreement is shown.

On the basis of the results displayed in figure 1.5, it is concluded that the heat release rate from a single fully-involved "regular" aircraft seat is 90 kW. It is important to note that this value does not account for the contribution from the rear face of the upright portion of the seat. Based on the above mass-loss calculation, the rear face contributes an additional 40 kW (average), i.e., 90 + 40 = 130 kW. Based on the area-of-involvement calculation, this face contributes 90 x 0.44 = 40 kW (peak). These 40 kW values for the rear face of the upright are somewhat supported by a calculation based on Hasemi's flame-height correlation for wall fires (reference 1.6)

---

*Use of trade names implies no endorsement by the National Bureau of Standards.

$$L_f = 6\ \dot{Q}_W^{*2/3}\ D_W \tag{6}$$

where

$$\dot{Q}_W^* = \frac{\dot{Q}/\ell}{\rho_\infty T_\infty c_p \sqrt{g}\ D_W^{3/2}} > 1 \tag{7}$$

L_f is the flame height above the base of the pyrolyzing surface, m

D_W is the height of the pyrolyzing surface, m

ℓ is the width of the pyrolyzing surface, m

Equations (6) and (7) reduce to

$$\dot{Q} = 75\ \ell\ L_f^{3/2} \tag{8}$$

The visual records from test 35 (Regular FR aircraft seats with no blocking layer) show the rear face of the upright portion of seat No. 4 burning with a flame height of approximately 1.14 m relative to the bottom of the upright. For ℓ = 0.45 m, eq. (8) yields $\dot{Q}$ = 41 kW and eq. (7) produces $\dot{Q}_W^*$ = 0.12. Although $\dot{Q}_W^*$ is outside the range of the correlation, the value of 41 kW predicted by the correlation agrees with the 40 kW (peak) estimate obtained previously.

In summary, estimates of heat release rate based on flame height and on OSU calorimeter data together with the actual area of involvement produce consistent results. The horizontal cushion and forward face of the upright cushion of a single aircraft seat produce a peak heat release rate of approximately 90 kW. The rear face of the upright produces a peak heat release rate of approximately 40 kW.

Seats With Vonar-3 Layer. Supplementary test 4 was similar to test 1 except that Vonar-3 blocking layers with polyester scrim were included in the cushions. Again, area of involvement was judged as a function of time and the average calorimeter data (reference 1.2), shown in figure 1.6*, were applied to obtain heat release rate as a function of time. This result is shown as the lower solid line in figure 1.7. The peak heat release rate, which occurs at about 60 seconds, is 43 kW. The burning behavior exibited in this figure is considerably different from that shown in figure 1.5 for the regular seats. Indeed, essentially only one of the two Vonar-3 seats became involved. Flames spread rapidly over this entire seat, died back to the outboard edge, and then slowly spread back over a fraction of the previously involved area. Owing to the rapid development of the peak burning rate, the peak OSU value (figure 1.6) rather than the average value over the first 60 seconds may be more appropriate in describing the early burning behavior. This peak result, based on the peak OSU value, is 118 kW and is shown as the upper solid line in figure 1.7.

---

*These data represent Vonar-3 with cotton scrim over FR polyurethane foam. Nevertheless, they are essentially the same as results for polyester scrim in the same configuration (reference 1.7).

The visual record of test 4 showed a peak flame height of approximately 1.14 m. Inserting this value and D = 0.51 m (effective diameter for one seat) into eq. (3) yields $\dot{Q}$ = 114 kW. A similar calculation using eq. (5) yields 49 kW. These results are also plotted in figure 1.7 and are consistent with the bounds established by the calorimeter-data calculations.

Test 107 was similar to test 110 except that Vonar-3 blocking layers were included in the cushions. Again, the erratic nature of the instantaneous mass measurements precluded the determination of reliable instantaneous mass loss rates. Nevertheless, the average mass loss rate was found to be 2.1 g/s. Assuming ΔH = 19000 kJ/kg, the corresponding average heat release rate over 120 seconds is 40 kW. Since this value includes the contribution from the back surface of the upright, a value of 40/1.44 = 28 kW is plotted in figure 1.7. Total heat releases up to 120 seconds (areas beneath the curves) are in reasonable agreement.

Based on the above estimate obtained from the mass-loss data, the rear surface of the upright contributes an average of 12 kW (the difference of 40 and 28 kW). On the basis of the area-of-involvement calculation - using average and peak OSU data - this surface contributes between 19 and 52 kW (peak). Visual records of test 34 show the rear surface of seat No. 4 producing a flame height of 1.22 m relative to the base of the upright. Equation (8) yields $\dot{Q}$ = 46 kW (peak) in this case.

In summary, the horizontal cushion and forward face the upright cushion of a single Vonar-3 seat produce a peak heat release rate of approximately 43-118 kW. The rear face of the upright produces a peak heat release rate of approximately 19-52 kW.

ESTIMATE OF TOTAL HEAT RELEASE RATE FROM CABIN MATERIALS DURING MULTI-SEAT TESTS 35 AND 34. Table 1.2 lists the fire growth scenario as judged from the visual records from test 35 (21 regular seats). Included are estimates of the heat release rates from specific seats and wall and floor linings. The ceiling was obscured by the smoke layer and its involved area could not be judged. Indeed, the ignition of the ceiling is the subject of the subsequent chapter by Cooper. Heat release rates from seats were obtained from estimates of areas of involvement and OSU calorimeter data and/or flame heights (eqs. (3), (5), and (8)) as described in previous sections. Heat release rate from the wall lining was estimated from the involved area and a calorimeter value of 16 W/cm^2 for aircraft panels previously reported by Walton and Twilley (reference 1.5). Although the floor was covered with a wool carpet, it was clear from the films that much of the burning material was actually drippings from the seats. For this reason the heat release rate per unit of floor area was assumed equal to that of the seat. This was set at 10 W/cm^2, which is the average value of the seat data over the first 180 seconds (see figure 1.4).

The information in table 1.2 was interpolated and tallied to yield the individual heat release rates due to the seats, wall, and floor. These results are shown in table 1.3 and plotted in figure 1.8 along with their sum, the total heat release rate from these items.

The corresponding results for test 34 (21 Vonar-3 seats) are shown in tables 1.4 and 1.5 and figure 1.9. In this case, a value of 6.5 W/cm^2 was assumed for the floor material. This is the average value for the Vonar-3 seat material over the first 180 seconds (see figure 1.7). The dip in the seats curve in figure 1.9 is a result of the decrease and subsequent increase in the burning rates of seats Nos. 2 and 5 during the 120-140 second period.

TABLE 1.2. TEST 35 (REGULAR SEATS); SEQUENCE OF EVENTS AS JUDGED FROM FILMS AND ESTIMATES OF HEAT RELEASE RATES

Brackets [ ] denote estimates based on calorimeter data and areas of involvement

Parentheses ( ) denote estimates based on flame heights†

Time (seconds)	
0	Fuel pan is ignited.
35	Seat No. 2 is burning. Presumably the upper face of the horizontal cushion and the forward face of the upright are involved [90 kW]. Flames extend to approximately 38 cm above the top of the upright (48-114 kW).
50	Still only seat No. 2 is burning [90 kW]. Flame extension is unchanged (48-114 kW). Approximately 2700 cm^2 of floor area outboard of seat No. 2 is burning [34 kW].
55	Wall panel at the forward edge of the large opening ignites.
65	Rear face of seat No. 1 upright ignites [40 kW]. Flames extend to approximately 38 cm above the top of the upright (41 kW). Approximately 5100 cm^2 of floor area outboard of and beneath seat No. 2 is burning [64 kW].
80	Rear face of seat No. 4 upright ignites.
90	Most of horizontal cushion and forward face of upright on seat No. 5 are involved [90 kW]. Flames extend to approximately 51 cm above top of upright (63-134 kW). Items previously burning continue to burn. Rear faces of uprights on seats No. 1 and 4 are involved [40 kW each] producing flame heights of 51 cm (48 kW) in both cases. Approximately 1300 cm^2 of wall panel area forward of the large opening is burning [20 kW]. Approximately 900 cm^2 of the wall panel to the rear of the large opening is burning [14 kW].
95	Approximately 7500 cm of floor area is involved [94 kW].
100	Seats No. 2 and 5 continue burning [90 kW each]. Flame heights above uprights are approximately 76 cm (98-176 kW) and 57 cm (70-144 kW), respectively. Seats No. 3 and 6 are involved. Presumably the horizontal cushions and forward faces of the uprights are involved [90 kW each]. Flame heights relative to the tops of the uprights are approximately 51 cm (63-134 kW) and 76 cm (98-176 kW), respectively. Presumably, the rear faces of seats No. 2 and 5 are also involved [40 kW each].

†Listed flame heights are relative to the top of the seat upright. The height of the upright (76 cm) was added in making the $\dot{Q}$ calculations.

110 Approximately 1750 cm^2 of the wall panel forward of the large opening is involved [28 kW]. Approximately 12500 cm^2 of the floor area is burning [156 kW].

120 The wall panel area above the second window to the rear of the large opening is burning. A total wall area of approximately 1300 cm^2 is involved aft of the large opening [21 kW].

130 Approximately 2000 cm^2 of wall area forward of the large opening is burning [32 kW]. Seats No. 3 and 6 are producing flame heights of approximately 76 cm (98-176 kW) each.

140 Approximately 37500 cm^2 of floor area is burning [469 kW].

140+ Flashover occurs.

TABLE 1.3. ESTIMATES OF HEAT RELEASE RATES DURING TEST 35

Heat Release Rates* in kW

Time, t [s]	Seats										Floor	Wall
	Individual Seats									Total		
	No. 1	No. 2	No. 3	No. 4	No. 5	No. 6	No. 8	No. 11	No. 14			
35		[90] (48-114)								[90] (48-114)		
50		[90] (48-114)								[90] (48-114)	[27]	
65	[40] (41)	[90] (48-114)								[130] (89-155)	[51]	
90	[40] (48)	[90] (48-114)		[40] (48)	[90] (63-134)					[260] (207-344)		[34]
95											[76]	
100	[40] (18)	[130] (68-176)	[90] (63-134)	[40] (48)	[130] (70-144)	[90] (98-176)				[520] (425-726)		
110											[125]	[47]
120												[51]
130	[40] (48)	[130] (98-176)	[90] (98-176)	[40] (48)	[130] (70-144)	[90] (98-176)				[520] (460-768)		
140											[374]	

*Brackets [] denote estimates based on calorimeter data and areas of involvement. Parentheses () denote estimates based on flame height.

TABLE 1.4 TEST 34 (VONAR-3 SEATS); SEQUENCE OF EVENTS AS JUDGED FROM FILMS AND ESTIMATES OF HEAT RELEASE RATES

Brackets [ ] denote estimates based on calorimeter data and areas of involvement

Parentheses ( ) denote estimates based on flame heights[†]

Time (seconds)	
0	Fuel pan is ignited.
40	Seat No. 2 is burning. Possibly only left edge is involved [4-12 kW]. Flame height relative to the top of the seat upright (back) is approximately 25 cm (35-95 kW).
60	Approximately 5100 cm^2 of the floor area outboard of and beneath seat No. 2 is burning [32 kW].
70	The horizontal cushion and forward face of upright on seat No. 2 appear to be nearly fully involved [43-118 kW]. Flame height above top of the upright is approximately 45 cm (56-125 kW). Forward edge of first wall panel located aft of large opening is ignited.
75	Burning rate of seat No. 2 appears to be diminishing [37-100 kW].
80	Wall panel forward of large opening ignites.
85	Flames appear on forward face of upright on seat No. 5 [22-59 kW].
90	Tops and/or rear faces of uprights on seats No. 1 and 4 are burning [19-52 kW each]. Flame heights above tops of these uprights are approximately 46 cm (45 kW each). Approximately 1300 cm^2 of the wall area forward of the large opening is burning [21 kW]. Flame heights above tops of uprights of seats No. 2 and 5 are approximately 38 cm (48-114 kW) and 25 cm (35-95 kW), respectively.
95	Approximately 1500 cm^2 of the wall area forward of the large opening is involved [24 kW]. First flashes appear in the upper gas layer.
105	Approximately 7600 cm^2 of floor area is burning [48 kW].

[†]Listed flame heights are relative to the top of the seat upright. The height of the upright (76 cm) was added in making the $\dot{Q}$ calculations.

120 Burning rate of seat No. 5 appears to be diminishing [9 kW]. Burning area of wall forward of the large opening is now less than it was at 90 seconds [< 24 kW]. Approximately 900 cm^2 of wall area to the rear of the large opening is involved [14 kW].

125 Flashing is again observed in the upper gas layer.

150 Burning rates of seats No. 2 and 5 appear to be increasing. It is unclear whether this increase is due to the horizontal cushions and forward faces of the uprights or the involvement of the rear faces of the uprights of these seats. The former will be assumed [43-118 kW each]. Flame heights above the rear faces of uprights on seats No. 1 and 4 reduce to approximately 25 cm (34 kW) each. Approximately 12500 cm^2 of floor area is burning [79 kW]. Only a very small portion of wall area forward of the large opening is burning.

155 Flashing continues in the upper gas layer.

160 Center-section aisle seat No. 8 ignites [43-118 kW]. Flame height above top of upright is approximately 40 cm (50-117 kW). Rear faces of uprights on seats No. 1 and 4 [19-52 kW each] are producing flame heights of approximately 25 cm each relative to the tops of the uprights (34 kW each). Seats No. 3 and 6 ignite [43-118 kW each] and produce a single merged flame which extends to approximately 76 cm above the top of the uprights (98-241 kW). Presumably, the rear faces of the upright sections of seats No. 2 and 5 are also burning [19-52 kW each]. Approximately 1300 cm^2 of wall area to the rear of the large opening is involved [21 kW].

170 Center-section seat No. 11 ignites [43-118 kW] producing a flame height of approximately 25 cm (35-95 kW). Center-section seat No. 8 [43-118 kW] is producing a flame height of approximately 41 cm (51-119 kW). Showering of burning wall material through the upper layer occurs.

180 Center-section seat No. 14 ignites [43-118 kW] producing a flame height of approximately 25 cm (35-95 kW). Center-section seats No. 8 and 11 [43-118 kW each] are each producing flame heights of approximately 57 cm (70-144 kW each). Approximately 18000 cm^2 of floor area is involved [113 kW].

210 Ceiling is falling.

210+ Flashover occurs.

TABLE 1.5. ESTIMATES OF HEAT RELEASE RATES DURING TEST 34

Heat Release Rates* in kW

Time, t [s]	Seats										Floor	Wall
	Individual Seats									Total		
	No. 1	No. 2	No. 3	No. 4	No. 5	No. 6	No. 8	No. 11	No. 14			
40		[4-12] (35-95)								[4-12] (35-95)		
60											[33]	
70		[43-118] (56-125)								[43-118] (56-125)		
75		[37-100]								[37-100]		
85		[26-64]			[22-59]					[48-123]		
90	[19-52] (45)	[20-45] (48-114)		[19-52] (45)	[43-118] (35-95)					[101-267] (173-299)		[21]
95												[24]
100	[19-52]	[9]		[19-52]	[32-82]					[79-195]		
105											[49]	
120	[19-52]	[4]		[19-52]	[9]					[51-117]		[34]
150	[19-52] (34)	[43-118] (56-125)		[19-52] (34)	[43-118] (56-125)					[124-340] (180-318)	[81]	[19]
160	[19-52] (34)	[62-170] (56-125)	[43-118] (49-120)	[19-52] (34)	[62-170] (56-125)	[43-118] (49-120)	[43-118] (50-117)			[291-798] (328-675)		[21]
170	[19-52] (34)	[62-170] (56-125)	[43-118] (49-120)	[19-52] (34)	[62-170] (56-125)	[43-118] (49-120)	[43-118] (51-119)	[43-118] (35-95)		[334-916] (364-772)		
180	[19-52] (34)	[62-170] (56-125)	[43-118] (49-120)	[19-52] (34)	[62-170] (56-125)	[43-118] (49-120)	[43-118] (70-144)	[43-118] (70-144)	[43-118] (35-95)	[377-1034] (453-941)	[116]	

*Brackets [] denote estimates based on calorimeter data and area of involvement. Parentheses () denote estimates based on flame height.

The oxygen depletion technique (reference 1.8) provided another means for independently estimating the total heat release rate within the cabin. The relationship between heat release rate and oxygen concentration of the combustion gases is

$$\dot{Q} = \dot{m}_g \left(Y_{ox\infty} - Y_{ox}\right) \left(13 \times 10^3 \text{ kJ/kg } (O_2)\right) \qquad (9)$$

where $\dot{m}_g$ is the mass flow rate of the combustion products, kg/s

$Y_{ox\infty}$ is the ambient oxygen mass fraction

Y_{ox} is the mass fraction of oxygen in the gas stream

Oxygen and gas temperature data recorded in the outflow stream at the rear door of the cabin were used in this calculation. Implicit in using these data to estimate total heat release rate within the cabin are the assumptions that 1) all the combustion gases within the cabin left through the rear door opening and 2) these gases are produced only by materials burning within the cabin. In reality, some gas left the cabin through the fire door and some of the combustion gases from the external pool fire entered at the same location. Earlier analyses by Quintiere and Tanaka (reference 1.9) and Emmons (reference 1.10) addressed these phenomena. Applying such analyses, however, was beyond the scope of the present effort. As a first approximation, the net flow through the fire door was taken as zero. Cabin gases also exited through two small window-like hatch openings in the rear of the cabin. In order to compensate for these losses, the calculation was made assuming a uniform Y_{ox} vertical profile, with Y_{ox} set equal to Y_{ox} (maximum) measured near the top of the opening. This leads to a maximum value of $\dot{Q}$ since the actual profile was statified (similar to the gas temperature profile within the opening).

The gas mass outflow rate through the opening ($\dot{m}_g$) was estimated using the "two-layer" vent model (reference 1.11)

$$\dot{m}_g = \frac{2}{3} \sqrt{2g}\, C \rho_\infty A_o \sqrt{H_o} \left[\left(T_\infty/T\right)\left(1 - T_\infty/T\right)\right]^{1/2} \left(1 - N/H_o\right)^{3/2} \qquad (10)$$

where g is gravitational acceleration, m/s^2

C is the orifice coefficient, (C = 0.73)

ρ_∞ is the density of ambient air, kg/m^3

A_o is the area of the opening, m^2

H_o is the height of the opening ,m

T_∞ is ambient temperature, K

T is the temperature of the upper gas layer, K

N is the height of the neutral plane within the opening, m.

The neutral plane height, N, was taken as 0.5 H_o. The time scales of the heat release rates so determined were adjusted to account for the time required for

the gases to traverse the 19 m distance between the burning section and the rear door. This time was computed using an average gas velocity based on the mass flow rate and density at the rear door opening and an average hot-layer depth equal to one-half the height of the cabin.

The heat release rates based on oxygen depletion are shown in figure 1.10 where they are compared with the total heat release rates obtained by the other techniques. Symbols in this figure denote heat release rates based on the measured Y_{ox} values. The attached bars account for time lag associated with gas transit time between the measuring probe and analyzer (~ 1 second) and the response time of the analyzer (~ 20 seconds for 90% response to a step change). The latter correction was made using the inversion-integral technique reported by Croce (reference 1.12) and Evans and Breden (reference 1.13). In general, good agreement is shown. The outlying point at 115 seconds is based on a depletion value less than 0.5% and is probably unreliable.

SUMMARY. Total heat release rates from cabin materials during two full-scale fire tests were estimated from available test data. Estimates based on involved area, calorimeter heat release data, flame heights, and oxygen levels are shown to be in good agreement. These results will be used by Cooper in a subsequent analysis of the combined effect of internal and external heat sources on cabin ceiling temperatures.

REFERENCES.

1.1 Hill, R. G., Johnson, G. R., and Sarkos, C. P., Postcrash Fuel Fire Hazard Measurements in a Wide-Body Aircraft Cabin, Report No. FAA-NA-79-42, U.S. Department of Transportation, Federal Aviation Administration, FAA Tech. Center, Atlantic City, NJ, December 1979.

1.2 Brown, L. J. and Johnson, R. M., Correlation of Laboratory Scale Fire Test Methods for Seat Blocking Layer Material with Large-Scale Test Results, DOT/FAA/CT-83/29, U.S. Department of Transportation, Federal Aviation Administration, FAA Tech. Center, Atlantic City, NJ, June 1983.

1.3 Zukoski, E. E., Kubota, T., and Cetegen, B., Entrainment in Fire Plumes, Fire Safety Journal 3, 107 (1981).

1.4 Hasemi, Y. and Tokunaya, T., Some Experimental Aspects of Turbulent Diffusion Flames and Buoyant Plumes from Fire Sources against a Wall and in a Corner, Annual Conference on Fire Research in Honor of H. W. Emmons, Center for Fire Research, National Bureau of Standards (U.S.), August 1983. (Submitted to Combustion Science and Technology).

1.5 Walton, W. D. and Twilley, W. H., Heat Release and Mass Loss Rate Measurements for Selected Materials, NBSIR, National Bureau of Standards (U.S.), in review.

1.6 Hasemi, Y., personal communication.

1.7 Hill, R.G., personal communication.

1.8 Sensenig, D. L., An Oxygen Consumption Technique for Determining the Contribution of Interior Wall Finishes to Room Fires, NBS Technical Note 1128, National Bureau of Standards (U.S.), July 1980.

1.9 Quintiere, J. G. and Tanaka, T., Some Analyses of the FAA Post Crash Aircraft Fire Scenario, Fire and Technology 19, 77 (1983).

1.10 Emmons, H. W., The Ingestion of Flames and Fire Gases into a Hole in an Aircraft Cabin for Tilt Angles and Low Wind Speeds, Harvard University, Home Fire Project Technical Report No. 49, October 1981.

1.11 Rockett, J. A., Fire Induced Gas Flow in an Enclosure, Combustion Science and Technology 12, 165 (1976).

1.12 Croce, P. A., A Method for Improved Measurement of Gas Concentration Histories in Rapidly Developing Fires, Combustion Science and Technology 14, 221 (1976).

1.13 Evans, D. D., and Breden, L. H., Time Delay Correction for Heat Release Rate Data, Fire Technology 14, 85 (1978).

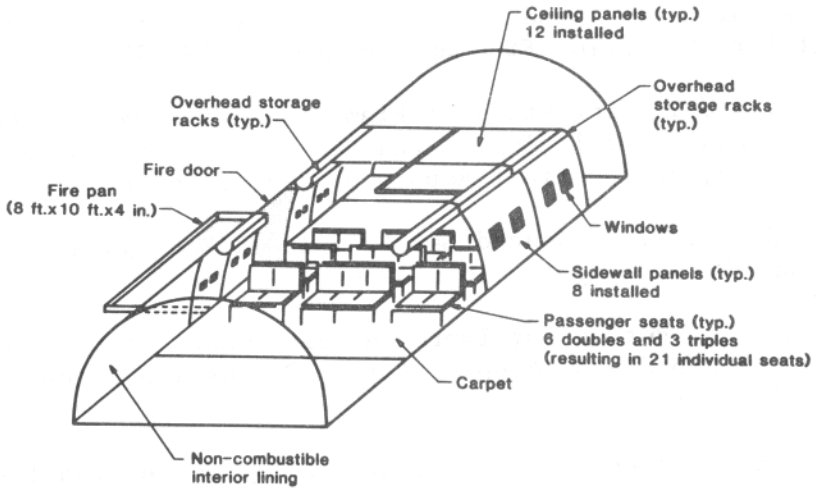

FIGURE 1.1. C-133 FULL-SCALE TEST FACILITY.

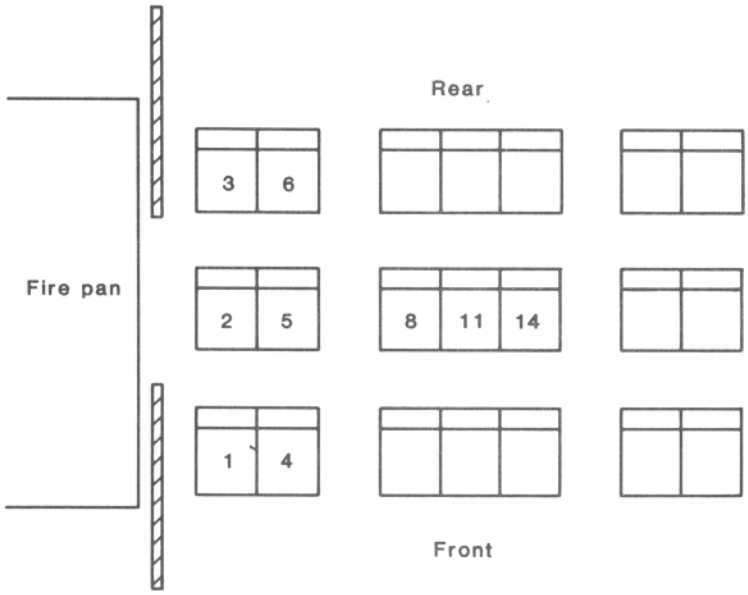

FIGURE 1.2. SKETCH OF C-133 PLAN (NOT TO SCALE) WITH SEAT POSITION IDENTIFIED.

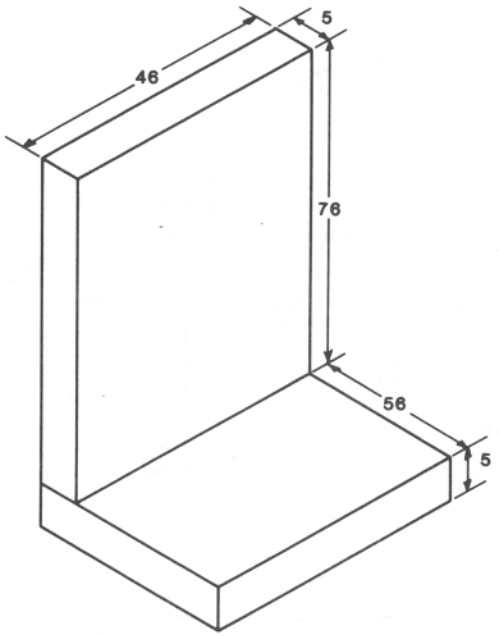

FIGURE 1.3. APPROXIMATE DIMENSIONS OF A SINGLE SEAT IN CM.

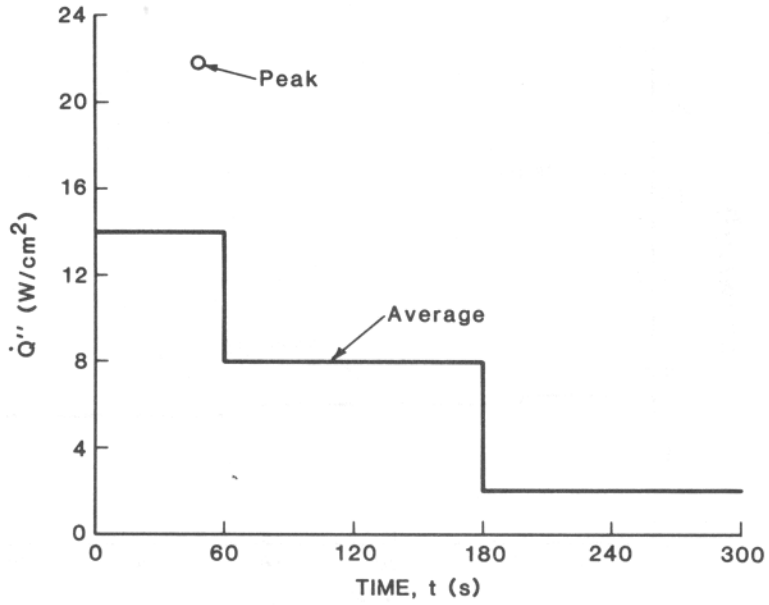

FIGURE 1.4. OSU AVERAGE AND PEAK HEAT RELEASE RATES PER UNIT AREA FOR REGULAR SEAT MATERIAL AT 7.5 W/CM^2 INCIDENT FLUX (REFERENCE 1.2).

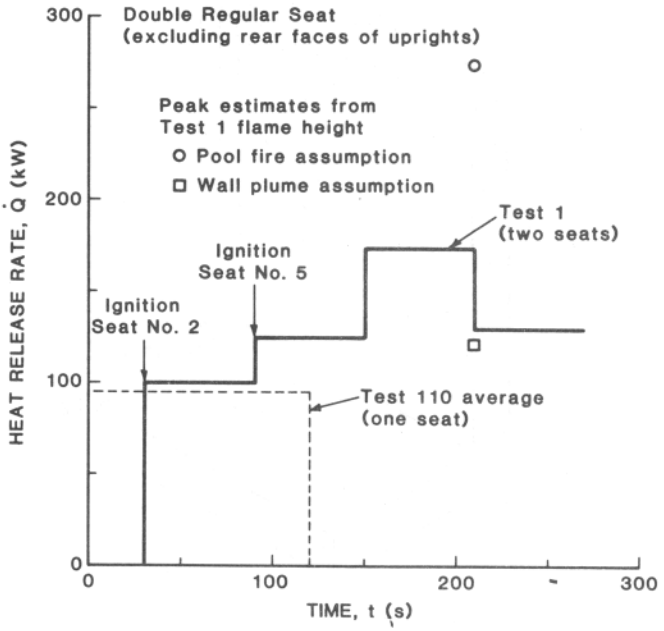

FIGURE 1.5. HEAT RELEASE RATE FROM DOUBLE REGULAR SEAT (EXCLUDING REAR FACES OF UPRIGHTS) BASED ON: ——, CALORIMETER DATA AND AREA-OF-INVOLVEMENT DATA FROM TEST 1: O - □, FLAME HEIGHT DATA FROM TEST 1; ----, MASS LOSS DATA FROM TEST 110.

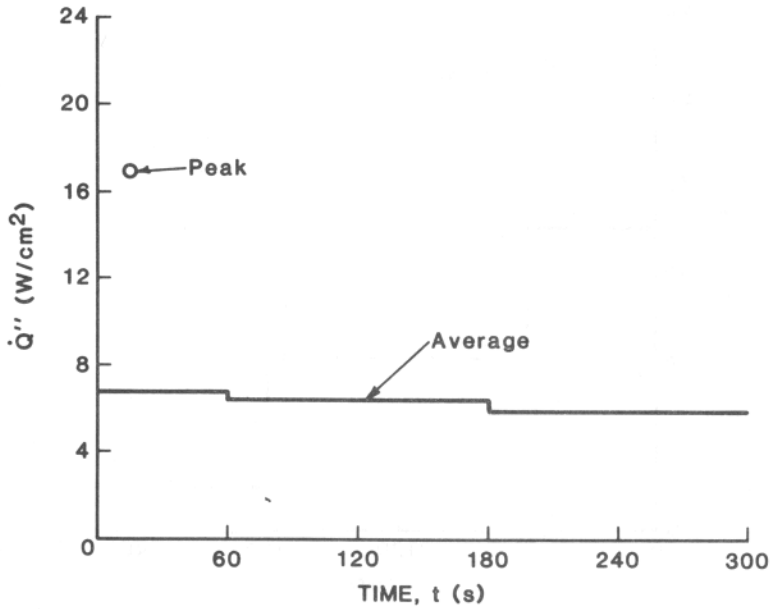

FIGURE 1.6. OSU AVERAGE AND PEAK HEAT RELEASE RATES PER UNIT AREA FOR VONAR-3 WITH COTTON SCRIM OVER FR POLYURETHANE FOAM AT 7.5 W/CM^2 INCIDENT FLUX (REFERENCE 1.2).

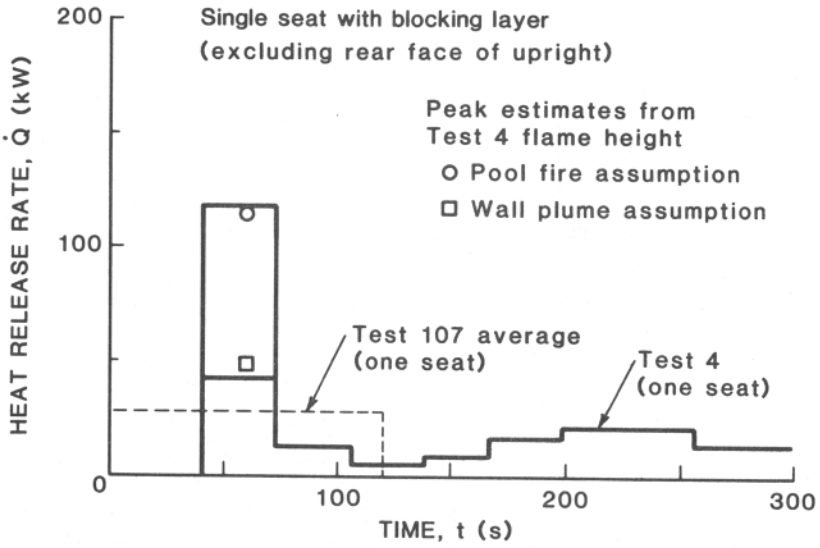

FIGURE 1.7. HEAT RELEASE RATE FROM SINGLE VONAR-3 SEAT (EXCLUDING REAR FACE OF UPRIGHT) BASED ON:———, CALORIMETER DATA AND AREA-OF-INVOLVEMENT DATA FROM TEST 4; O, □, FLAME HEIGHT DATA FROM TEST 4; ----, MASS LOSS DATA FROM TEST 107.

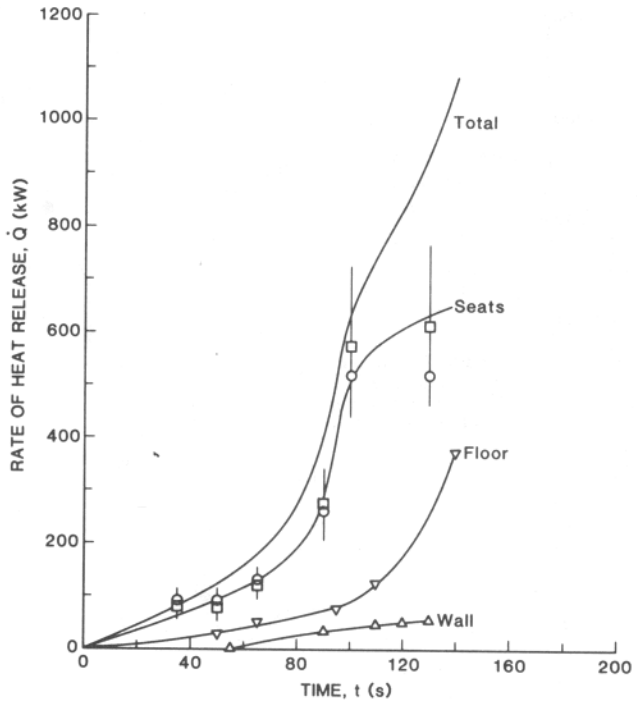

FIGURE 1.8. ESTIMATES OF HEAT RELEASE RATES DURING TEST 35 (REGULAR SEATS). SYMBOLS: O, ▽, △ - BASED ON AREA-OF-INVOLVEMENT AND CALORIMETER HEAT RELEASE DATA; □ - BASED ON FLAME HEIGHT DATA.

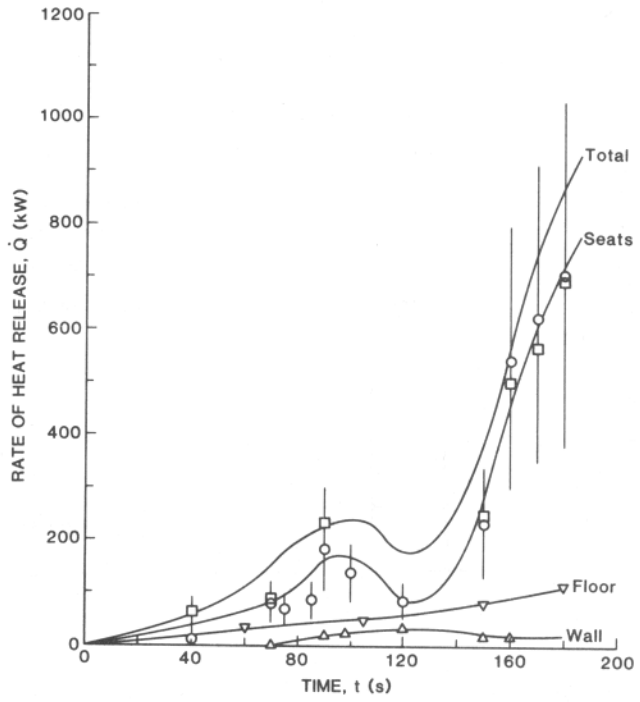

FIGURE 1.9. ESTIMATES OF HEAT RELEASE RATES DURING TEST 34 (VONAR-3 SEATS). SYMBOLS: O, ▽, Δ - BASED ON AREA-OF-INVOLVEMENT AND CALORIMETER HEAT RELEASE DATA: □ - BASED ON FLAME HEIGHT DATA.

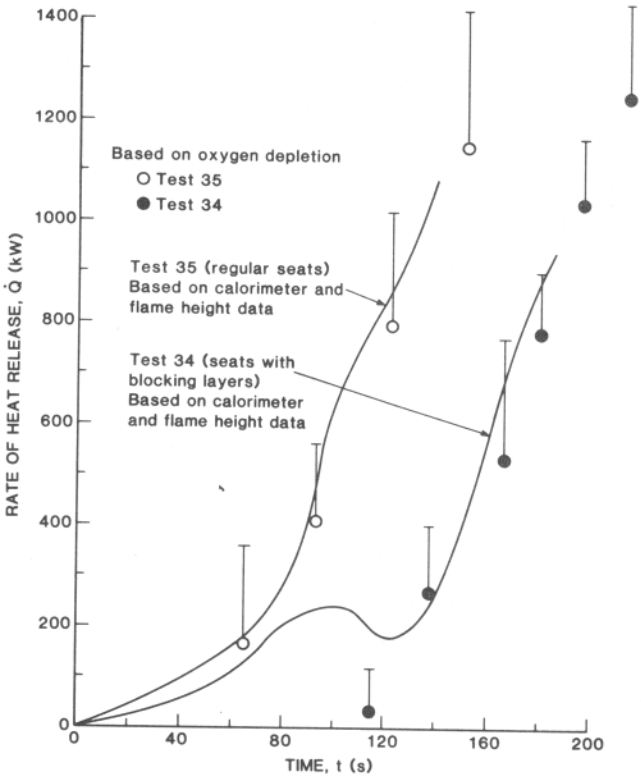

FIGURE 1.10. TOTAL HEAT RELEASE RATES DURING MULTI-SEAT TESTS.

CHAPTER 2. THE THERMAL RESPONSE OF AIRCRAFT CABIN CEILING MATERIALS DURING A POST-CRASH, EXTERNAL FUEL-SPILL, FIRE SCENARIO.

The purpose of this investigation is to analyze aircraft cabin ceiling surface temperature data recently acquired during full-scale test simulations of post-crash fires. The analysis is carried out with a view toward the development of a procedure for estimating the temperature histories of overhead aircraft cabin materials subsequent to the ignition of exterior, fuel-spill fires. With such a capability it would be possible to estimate the time for such materials to reach ignition temperatures. This would result in a rational means of ranking the fire safety of candidate overhead aircraft cabin materials.

All tests described here were carried out by staff of the United States (U.S.) Department of Transportation Federal Aviation Administration (FAA) at the FAA Technical Center, Atlantic City, New Jersey.

DESCRIPTION OF THE TESTS. The experiments involved wide-body aircraft cabin post-crash fire test simulations similar to those reported previously in reference 2.1. The test setup simulated a wide-body aircraft with two open doorways where the fuselage at one of the doorways is engulfed by fire of a large, burning, external fuel spill. The fuel-spill fire is simulated by a fire in a 2.44 m x 3.05 m pan of jet fuel (JP-4). The threat to the cabin which would be generated by this external test fire configuration has been shown in (reference 2.1) to be representative of the threat which would be generated by real, large, external fuel-spill fires. No-wind conditions were simulated during the tests. The actual test article was a surplus U.S. Air Force C133A cargo aircraft with wings and tail surfaces removed.

The ceiling of the test cabin was made up of panels of 0.0127 m thick rigid Kaowool® ceramic fiber board. In the analysis to follow, the thermal properties of this material are assumed not to vary with temperature. Consistent with information from the manufacturer, they are taken to be

$$\text{thermal conductivity} = k = 0.045 \text{ W/mK}$$
$$\text{thermal diffusivity} = \alpha = 2.67\ (10^{-7})\ \text{m}^2/\text{s} \qquad (1)$$

A mockup seat made up of cushions placed on a steel frame was placed in the cabin directly in front of the open doorway which was exposed to the fuel spill fire. The placement was likely to lead to the most rapid ignition of the cushion material. In the present study, data from only eight tests, designated as test numbers 104-111, are considered. The only parameter which was varied from test to test was the seat cushion/fabric construction. One test, test 111, is designated as the background test since it involved the seat frame with no cushioning.

A schematic of the test set up is presented in figure 2.1.

During the tests, the radiant heat flux near the doorway was measured with fluxmeters facing outward toward the pan fire. Measurements were taken at two elevations, 0.30 m and 0.91 m above the floor. At all times during each of the tests the flux measured by the two gages were substantially similar. An example of this can be seen in figure 2.2 where plots of the two fluxmeter

measurements, acquired during the background test, are presented. In the analysis to follow it will be assumed that the radiant flux from the pan fire is uniform and isotropic across the entire doorway. This flux will be taken to be the flux measured by the lower of the two near-doorway fluxmeters. The measured flux history at this elevation for all eight tests are plotted together in figure 2.3. This figure provides support for the assumption that the exposure fire was closely reproduced in each of the tests of the series.

This study will consider near-ceiling temperature measurements which were acquired from three thermocouples placed in the line which traverses the width of the cabin and which is directly above the center of the doorway. As noted in figure 2.1, one of these thermocouples, at designated position 1, was directly above the center of the seat. The other two were 0.91 m (position 2) and 1.83 m (position 3) from the first. The thermocouples were constructed from 24 gage (0.000584 m diameter) chromel/alumel wire. The wire from each of the three thermocouples was supported several centimeters from its bead, and there was an attempt to position the bead close to the ceiling surface with the hope that the bead temperatures would be substantially similar to the respective, nearby, ceiling surface temperatures. Although there was no attempt to measure them, bead-to-ceiling distances were probably of the order of a millimeter. It is noteworthy that the placement of near-ceiling thermocouples in the present test series is different than in previous test series where thermocouple bead-to-ceiling distances were of the order of a few centimeters.

Except for the background test, data for all tests were available only until 120 s after ignition of the pan fire. The Test 111, background test data were available for 240 s.

The measured temperatures, up to 120 s after ignition, for all eight tests are presented in figures 2.4-2.6. Plots of measured temperature vs time at position 1, above the seat, are presented in figure 2.4. Plots of measured temperature histories at positions 2 and 3 are presented in figures 2.5 and 2.6, respectively. As can be seen from these three figures, at each thermocouple location the measured temperature histories are substantially similar for each test. Based on this observation, it is reasonable to assume that, for the threat scenario being simulated and up to the 120 s time mark, fire development in a single, mockup seat would not add significantly to the ceiling surface material fire threat. For this reason, in the analysis of the present test series, it is assumed to be adequate to study the thermal response of the ceiling only during the background test. Plots of the temperature histories measured by the three, near-ceiling thermocouples during the background test are presented in figure 2.7.

AN ANALYSIS OF THE THERMAL RESPONSE OF THE CABIN CEILING MATERIAL. During post-crash fires of the type simulated in the test series there are two major phenomena which can lead to relatively prompt lower surface heating of the cabin ceiling.

The first of these phenomena involves the thick flames and copious products of combustion which engulf the exterior of the fuselage in the vicinity of the threatened, open, cabin doorway. These lead to significant components of both radiant and convective heat flux to the cabin ceiling.

The convective component comes about from the hot, buoyant gases of the fuel spill fire which are captured by the open doorway. Upon entering the cabin, these gases are driven upward toward the ceiling, forming an outward (i.e., away from the doorway and toward the cabin interior) moving ceiling jet. After spreading radially from the doorway, this ceiling jet is redirected away from the general location of the doorway and toward the front and rear of the cabin. Eventually the hot, captured, products of combustion start to fill the cabin. They then participate in venting from the second open doorway and in complicated entrainment processes which develop at the fire-threatened/exposed open doorway itself. (It is noteworthy that a global analysis of the external, fuel spill fire and the captured cabin flow under rather general wind conditions has been presented previously in reference 2.2.)

The second phenomenon which leads to heat flux to the lower ceiling surface involves the growing fire which spreads in the cabin seating. As mentioned earlier, the limited, single-seat scenario of the present tests appears to result in only marginally important levels of ceiling heat flux. Yet, as will be discussed later, fire spread in a fully outfitted cabin could indeed lead to a significant additional threat to the cabin ceiling. The seating fire leads to both radiative and convective heating of the ceiling. The radiation would be primarily from the fire's combustion zone, and the convection would result from the fire's plume-driven ceiling jet. This latter ceiling jet would augment the previously mentioned, captured-gas-driven ceiling jet.

Other components of heat flux to/from both the upper and lower ceiling surfaces are radiation from relatively cool, far-field surfaces and reradiation from the ceiling surfaces themselves. Finally, in an analysis of the ceiling heating it is reasonable to account for natural convection cooling of the upper ceiling surface.

For the purpose of analysis the geometry of figure 2.8, which is somewhat simpler than the actual cabin geometry, will be adopted.

Quantitative estimates for the above components of ceiling heat transfer are developed below. Using these estimates, the boundary value problem for the transient temperature distribution of the ceiling material is then formulated and solved.

Radiation from the Doorway. The entire doorway opening is assumed to be a source of uniform diffuse radiation. The radiant flux emitted from this doorway is assumed to have an amplitude, $\dot{q}''_{rad\text{-}door}(t)$, identical to that measured by the lower of the doorway flux calorimeters mentioned earlier.

Any line-of-sight interference by the seats of doorway-to-ceiling radiation will be neglected.

Referring to figure 2.8. and using a well-known view-factor result given, e.g., in reference 2.3, the view-factor, $F_{A\text{-}dA}$, between the area of the doorway opening, A, and a horizontal element of lower ceiling surface, dA, lying on a line normal to the plane of the doorway is given by

$$F_{A\text{-}dA} = \frac{1}{\pi}\frac{c}{b}\left(\Gamma_2 \tan^{-1}(\Gamma_2) - \Gamma_1 \tan^{-1}(\Gamma_1)\right) \qquad (2)$$

where

$$\Gamma_1 = b/(a_1^2 + c^2)^{1/2};\ \Gamma_2 = b/(a_2^2 + c^2)^{1/2} \tag{3}$$

and where the dimensions a_1, a_2, b and c are defined in figure 2.9. Thus, the thermal radiant flux from the outside, fuel-spill fire, through the door, and to the ceiling element is taken to be

$$\dot{q}''_{door\text{-}ceiling} = \dot{q}''_{rad\text{-}door}\ F_{A\text{-}dA} \tag{4}$$

Captured External Fire Product Gases - An Equivalent Buoyant Source. The products of combustion of the external, simulated, fuel-spill fire which are captured at the open cabin doorway rise in a plume to the ceiling of the cabin, entraining far-field cabin air during their ascent. In the present analysis the "captured gas" plume will be modeled by a nonradiating, equivalent, point source of buoyancy located at the center of the horizontal surface of the mockup seat, and identified in figure 2.8. Note that all radiation transfer from the exterior fuel spill fire to the cabin ceiling is assumed to be taken account of in eq. (4). The strength of the equivalent source, $\dot{Q}_{equiv}$, will be assumed to be directly proportional to $\dot{q}''_{rad\text{-}door}$. Thus

$$\dot{Q}_{equiv} = \beta \dot{q}''_{rad\text{-}door}\ (\beta \text{ in } m^2) \tag{5}$$

and β is an, as yet undetermined, constant.

As the captured-gas plume impinges on the ceiling near (thermocouple) position 1, it forms an outward moving ceiling jet. As will be described below, estimates of convective heat transfer from this jet to the ceiling surface will make use of the results of reference 2.4.

Radiation and Convection for the Seating Fire. During the first 120 s of the post-crash fire, cabin ceiling heat transfer contributions from the burning single mockup cabin seat did not appear to be significant. However, in fully outfitted cabins, it is anticipated that this situation would be changed especially after the first minute or two subsequent to ignition. This is the case since, by these times, fires in FAA, multiple-seat, cabin test configurations have been observed to grow and spread beyond single seat involvement. Since the present analysis will be extended to fully outfitted cabin scenarios, ceiling heat transfer with an important contribution from the seating fire will be included here at the outset.

The seating fire is simulated by a time-dependent point source of energy release rate, $\dot{Q}_{seat}$, which is assumed to be located, together with the nonradiating source, $\dot{Q}_{equiv}$, at the center of the horizontal surface of the outer, external-fire-exposed, doorway seat. In contrast to $\dot{Q}_{equiv}$, a nonzero fraction, $\lambda_{r,seat}$, of $\dot{Q}_{seat}$ is assumed to be radiated uniformly over a sphere surrounding the combustion zone, and to the far field. The remaining rate-of-energy release, $(1 - \lambda_{r,seat})\ \dot{Q}_{seat}$, drives the buoyant fire plume upward. Thus, the radiation from the seating fire which is incident on the ceiling at a distance r from the plume impingement point leads to a radiant flux which is assumed to be

$$\dot{q}''_{rad-seat} = \lambda_{r,seat}\ \dot{Q}_{seat}/[4\pi H^2\ (1 + r^2/H^2)^{3/2}] \qquad (6)$$

where, as defined in figure 2.8, H is the source-to-ceiling distance and r is the radial distance from the souce as measured along the ceiling. In the above, $(r^2 + H^2)^{1/2}$ is the source-to-ceiling element distance and $H/(T^2 + H^2)^{1/2}$ is the cosine of the angle which the ceiling normal makes with the source-to-ceiling ray (see figure 2.8).

$\dot{Q}_{seat}$ would vary from one seat cushion construction to another. $\dot{Q}_{seat}$ would typically have to be estimated from test data, and then specified in the present analysis. $\lambda_{r,seat}$ would also vary somewhat from one construction to another, although it is reasonable to choose the value $\lambda_{r,seat} = 0.35$, a value which characterizes the radiation from flaming combustion zones of many practical fuel assemblies (reference 2.5). In all calculations to be presented here, the 0.35 value will be adopted.

Convective Heat Transfer from a Combined, Equivalent Source of Buoyancy. A single point source of buoyancy, $\dot{Q}$, is used to describe the total generation of upward moving combustion gases which are driven by a combination of the equivalent, captured-gas-buoyancy source, $\dot{Q}_{equiv}$, and the seating-fire-buoyancy source, $(1 - \lambda_{r,seat})\ \dot{Q}_{seat}$. Thus

$$\dot{Q} = \dot{Q}_{equiv} + (1 - \lambda_{r,seat})\ \dot{Q}_{seat} \qquad (7)$$

All convective heat transfer to the cabin ceiling will be modeled by a $\dot{Q}$-generated, plume-driven, ceiling jet. This heat transfer will be estimated with the use of the algorithm, reproduced below, which was developed in reference 2.4, and used in reference 2.6. Thus, the convective rate of heat transfer to the ceiling surface will be estimated from

$$\dot{q}''_{conv,L} = h_L\ (T_{ad} - T_{s,L}) \qquad (8)$$

In the above, $T_{s,L}$ is the instantaneous, absolute temperature of the lower ceiling surface, T_{ad} is the absolute temperature that would be attained by the lower surface of an adiabatic ceiling,

$$\frac{(T_{ad} - T_{amb})}{T_{amb}\ \dot{Q}^{*2/3}} = \begin{cases} 10.22\ \exp\ (-1.77\ r/H),\ 0 \leq r/H \leq 0.75 \\ 2.10\ (r/H)^{-0.88},\ 0.75 \leq r/H \end{cases} \qquad (9)$$

$\dot{Q}^*$ is a dimensionless buoyant source strength,

$$\dot{Q}^* = \dot{Q}/(\rho_{amb} C_p T_{amb}\ g^{1/2}\ H^{3/2}) \qquad (10)$$

g is the acceleration of gravity, and ρ_{amb}, T_{amb} and C_p are the density, absolute temperature and specific heat, respectively, of the ambient air. Also, h_L is the heat transfer coefficient

$$h_L/\tilde{h} = \begin{cases} 7.75\ Re^{-0.5}\ [1 - (5.0 - 0.390\ Re^{0.2})(r/H)],\ 0 \leq r/H \leq 0.2 \\ 0.213\ Re^{-0.3}\ (r/H)^{-0.65},\ 0.2 \leq r/H \leq 1.03 \\ 0.217\ Re^{-0.3}\ (r/H)^{-1.2},\ 1.03 \leq r/H \end{cases} \quad (11)$$

where

$$\tilde{h} = \rho_{amb}\ C_p\ g^{1/2}\ H^{1/2}\ \dot{Q}^{*1/3}$$

$$Re = g^{1/2}\ H^{3/2}\ Q^{*1/3}/\nu \quad (12)$$

and ν is the kinematic viscosity of the ambient air.

The above algorithm will be used in the present calculations. In doing so, two major assumptions are made; namely 1) effects of the inevitable, growing, upper-cabin smoke layer are relatively weak during the early times of interest, and 2) the interactions of the ceiling jet and lateral cabin wall surfaces, especially surfaces immediate to the doorway side of the plume-ceiling impingement point will not lead to total, instantaneous, heat transfer flux amplitudes which are significantly larger than peak, instantaneous values that will be estimated with their neglect.

Radiation Between the Lower Ceiling Surface and the Far-Field Cabin Surfaces. At all times subsequent to ignition, the lower ceiling surface at temperature $T_{s,L}$ is assumed to diffusely radiate to the initially ambient temperature, illuminated surfaces of the cabin and its furnishings. In response to this radiation, the temperatures of those lower surfaces outside of the seating combustion zone also increase with time. However, for times of interest here, it is assumed that these latter temperature increases above T_{amb} are always relatively small compared to the characteristic increases of $T_{s,L}$. Accordingly, at a given radial position of the lower ceiling surface, the net radiation exchange between the ceiling and the nonburning surfaces below can be approximated by a net reradiation flux

$$\dot{q}''_{rerad,L} = \varepsilon_L \sigma\ (T^4_{s,L} - T^4_{amb}) \quad (13)$$

where σ is the Stephan-Boltzmann constant, and ε_L is the emittance/absorptance of the assumed grey, lower ceiling surface.

Heat Transfer from the Upper Ceiling Surface. Heat is transferred through the ceiling, and eventually the temperature of its upper surface, which is also assumed to be exposed to a constant T_{amb} environment, begins to rise.

The rate of heat transfer from the upper ceiling surface has convective and radiative components, $\dot{q}''_{conv,U}$ and $\dot{q}''_{rerad,U}$, respectively. These can be estimated from

$$\dot{q}''_{conv,U} = h_U\ (T_{s,U} - T_{amb})$$

$$\dot{q}''_{rerad,U} = \varepsilon_U \sigma\ (T^4_{s,U} - T^4_{amb}) \quad (14)$$

where $T_{s,U}$ is the instantaneous upper surface temperature, h_U is an effective heat transfer coefficient, and ε_U is the emittance/absorptance of the assumed grey, upper ceiling surface. The value for h_U to be used in the present calculations will be reference 2.7

$$h_U = 1.675 \left| T_{s,U} - T_{amb} \right|^{1/3} \text{ W/m}^2 \quad (T \text{ in K}) \tag{15}$$

The Boundary Value Problem for the Ceiling, and the Method of Its Solution. The absolute temperature field of the ceiling material is assumed to be governed by the Fourier heat conduction equation. Initially, the ceiling is taken to be of uniform temperature, T_{amb}. The net rates of heat transfer to the lower and upper surfaces, $\dot{q}''_L$ and $\dot{q}''_U$, respectively, are given by

$$\begin{aligned} \dot{q}''_L &= \dot{q}''_{\text{door-ceiling}} + \dot{q}''_{\text{rad-seat}} + \dot{q}''_{\text{conv,L}} - \dot{q}''_{\text{rerad,L}} \\ \dot{q}''_U &= - \dot{q}''_{\text{conv,U}} - \dot{q}''_{\text{rerad,U}} \end{aligned} \tag{16}$$

For times of interest here, radial gradients of variables of the problem are assumed to be small enough so that conduction in the ceiling is quasi-one dimensional in space, i.e., $T = T(Z, t; r)$, where Z is the indepth ceiling coordinate.

An illustration of the final, idealized, post-crash fire scenario to be analyzed here is presented in figure 2.10.

A computer program for solving the above problem was developed. The solution to the heat conduction equation for the ceiling at every radial position of interest is by finite differences. The algorithm for this was taken from reference 2.8 and 2.9. For a given calculation, $N \leq 20$ equally spaced points are positioned at the surfaces and through the thickness of the ceiling. The spacing of these, δZ, is selected to be large enough (based on a maximum time step) to insure stability of the calculation. Throughout a calculation, the change in time for all time steps is made small enough so that, at a given lower surface node, the temperature increase from time step to time step never exceeds one percent of the current value of T at that node.

CALCULATION OF THE RESPONSE OF THE CEILING IN THE POST-CRASH TEST SIMULATION. The algorithm described in the last section was used to predict the ceiling response during the first 240 s of the Test 111, post-crash simulation.

Eq. (1) values of k and α were used for the 0.0127 m thick Kaowool® ceiling. The ceiling surfaces were assumed to absorb and radiate as black bodies ($\varepsilon_U = \varepsilon_L = 1$). Consistent with previous discussion, for this test $\dot{Q}_{seat}$ of eq. (6) was taken to be identically zero, and $\dot{q}''_{rad\text{-}door}(t)$ of eq. (5) was taken to be identical to the Test 111, underseat fluxmeter measurements. Ceiling temperatures at positions 1, 2 and 3 were computed for different β's in the range $0 \leq \beta \leq 6.0$ m^2. (This range of β leads to the approximate $\dot{Q}_{equiv}$ range $0 \leq \dot{Q}_{equiv} \leq 300$ kW.)

The computed lower ceiling histories for $\beta = 0.$ and 3.0 m^2 are plotted in figure 2.11 together with the corresponding, measured, near-ceiling temperatures of figure 2.7.

The Importance of $\dot{Q}_{equiv}$. If convective ceiling heating from doorway-captured products of combustion is equivalent to a near-seat buoyancy source of the order of a few hundred kW, then the calculated results plotted in figure 2.11 indicate that such heating is not significant compared to doorway radiation. (Note that β = 0. and 3.0 m^2 of figure 2.11 leads to a $\dot{Q}_{equiv}$ of zero and approximately 150 kW, respectively. Also, except for the very earliest few seconds subsequent to ignition, convection from the relatively weak source associated with β = 3.0 m^2 is seen to lead to net cooling of the strongly irradiated ceiling surface.) This result is consistent with earlier observations where variations in single seat cushion construction (peak energy release rates likely never exceeding the few hundred kW level) did not lead to significant differences in near-ceiling temperature measurements (see figures 2.4-2.6).

Comparisons Between Computed and Measured Temperatures. As can be seen in figure 2.11 the peak computed values of ceiling temperature compare favorably with the corresponding peak temperatures measured by the near-ceiling thermocouples. However, the basic qualitative characteristics of the computed and measured transient thermal responses are significantly different. In particular, the measured temperatures of the thermocouples do not have the same type of rapid response which the numerical solution properly predicts for the lower ceiling surface temperatures. Also, the close tracking of the position 2 and 3 thermocouples at early times does not compare favorably with a like tracking of the computed, lower ceiling temperatures at these two positions.

Two conclusions result from these observations; namely, the thermocouples are not measuring the temperature of the near-by ceiling surface, and, therefore, data to support the validity of the analysis are not evident. As a result of these conclusions an analysis of the response of the thermocouples was carried out. This analysis, to be reported in the next section, had a two-fold purpose; first, to explain the measured thermocouple responses, and second, to bring a measure of experimental validation, albeit indirect, for the predicted ceiling response.

AN ANALYSIS OF THE THERMAL RESPONSE OF THE NEAR-CEILING THERMOCOUPLES. The objective of the present analysis is to predict the thermal response of the thermocouples when appropriately placed within the figure 2.10 scenario, near, but not touching the ceiling. The procedure for positioning these devices prior to testing was such that the thermocouple wires were essentially parallel to the lower ceiling surface and at a distance, d, of the order of 0.001 m. The actual orientation of the 24 gage (diameter = 0.000584 m) wire relative to the doorway plane is unknown. As depicted in figure 2.12, the analysis will consider two extreme configurations for the wire, viz., normal and parallel to the doorway.

The characteristic time for conductive heat transfer through the wire thickness is relatively small, of the order of tenths of a second. The analysis will therefore assume that throughout the experiment the wire is spatially uniform in temperature.

The density and specific heat of the chromel/alumel wire (a 95 percent Nickel alloy) will be taken to be identical to that of Nickel, viz.,

density = ρ = 8800 kg/m^3

specific heat = C_p = 460 Ws/(kgK)

From references 2.4 and 2.10 or from reference 2.11 it is possible to conclude that the thickness of the ceiling jet within which the thermocouples are submerged are of the order of several centimeters. With a characteristic thermocouple-to-ceiling separation distance, d, of the order of 0.001 m, it is therefore reasonable to assume that gas velocities local to the thermocouple wire are so small that forced convection heating compared to radiative heating of the wire is negligible. On account of the fineness of the wire, the characteristic Grashoff numbers would be relatively small, and any natural convection heat transfer would be reduced to a conduction limit. This would be dependent on the unknown thermocouple wire-to-ceiling separation distance.

At early times radiant flux from the doorway drives the rate-of-rise of the thermocouple temperature. Also, a steady-state analysis which balances doorway heating and radiation exchanges between thermocouple, ceiling and ambient (i.e., which ignores conduction) leads to a result which is consistent with late-time, figure 2.11, measured and computed temperatures of thermocouple and ceiling, respectively.

The thermal analysis which emerges from the above discussion leads to the following equation for the temperature, T_w, of the thermocouple wire

$$\frac{\pi}{4}\rho C_p D^2 \frac{dT_w}{dt} = \dot{Q}'_{door-wire} + \dot{Q}'_{ceiling-wire} + \dot{Q}'_{amb-wire} - \dot{Q}'_{wire} \qquad (17)$$

where

$$\dot{Q}'_{wire} = \text{reradiation from the wire, per unit length of wire} = \pi D \sigma T_w^4 \qquad (18)$$

$$\dot{Q}'_{amb-wire} = \text{radiation from lower ambient temperature surfaces to the wire, per unit length of wire} = \frac{\pi D}{2}\sigma T_{amb}^4 \qquad (19)$$

$$\dot{Q}'_{ceiling-wire} = \text{radiation from the ceiling to the wire, per unit length of wire} = \frac{\pi D}{2}\sigma T_{s,L}^4 \qquad (20)$$

$$\dot{Q}'_{door-wire} = \text{radiation from the doorway to the wire, per unit length of wire} = \alpha D \dot{q}''_{door-ceiling} \qquad (21)$$

In eq. (21), $\dot{q}''_{door-ceiling}$ is given in eq. (4), and, depending on the wire configuration,

α = 1 for wire normal to the door plane, i.e., configuration 2 of figure 2.12.

$\alpha = 1/\sin\theta$ (see figure 2.9 for definition of θ) for wire parallel to the door plane, i.e., configuration 1 of figure 2.12. (22)

In the above, all surfaces are assumed to radiate and absorb as black surfaces.

To obtain a solution for the T_w of a thermocouple at a given position along the cabin ceiling one would specify α and $T_{s,L}(t)$ at that position, use the measured values of $\dot{q}''_{rad\text{-}door}$ to obtain $\dot{q}''_{door\text{-}ceiling}$, and solve eq. (17) subject to the initial condition $T_w(t = 0) = T_{amb}$.

Solutions for T_w in the Test 111 Scenario. The above procedure for predicting $T_w(t)$ was applied to the Test 111 scenario. The analysis was carried out numerically for a thermocouple in position 1, 2 or 3 and in configuration 1 or 2. In each case, the history for $T_{s,L}(t)$, which was required in the analysis, was taken from the ceiling temperature calculations described earlier.

The results of the T_w calculations are presented in figures 2.13, 2.14, and 2.15 for β values of 2.0 m^2, 3.0 m^2, and 4.0 m^2, respectively. Also included in these figures are plots of the measured T_w values previously presented in figures 2.7 and 2.8.

Comparison Between Computed and Measured Temperatures - An Optimum Choice for the Value of β. As can be seen in figures 2.13-2.15, the computed and measured thermocouple temperatures compare as favorably as one could reasonably hope for in an analysis of the kind of experimental fire scenario under investigation.

Perhaps of greatest significance is the early-time thermocouple temperature predictions, which were of particular concern in the previous ceiling temperature - thermocouple temperature comparisons of figure 2.11. Here, the simulations of the early, near-linear responses of the thermocouples are noteworthy.

Of further significance is the fact that the results of the calculations reveal a possible explanation for the previously noted, close tracking of the response of the thermocouples at positions 2 and 3. As can be observed in each of the three figures, the present analysis predicts such behavior if the thermocouple wire at position 2 was normal to the door plane (configuration 2), and the thermocouple wire at position 3 was parallel to the door plane (configuration 1).

Figures 2.13-2.15 provide a basis for selecting the "best" value for β with which to carry out the ceiling temperature calculation in the context of the post-crash cabin fire scenario under investigation. In this regard, the β predicting a ceiling response which, in turn, yields the most favorable comparisons between calculated and measured values of T_w would be the obvious choice. As is evident from the figures, the T_w predictions are not very sensitive to β variations in the appropriate range 2.0-4.0 m^2. Furthermore, of the values β = 2.0 m^2, 3.0 m^2, and 4.0 m^2, all yield reasonable T_w predictions, and no one of these values clearly yields more favorable T_w predictions than the others. β = 3.0 m^2 will be chosen as the "best" value.

PREDICTING THE POST-CRASH TIME-TO-IGNITION OF CEILING CONSTRUCTIONS IN A FULLY SEATED CABIN. The results of the previous section provide some confidence in the post-crash ceiling thermal response algorithm. To use the algorithm in a manner that would simulate the post-crash fire exposure of a fully seated cabin, it is necessary to include the effects of fire spread in an array of seating adjacent to the exposed, open doorway. As was discussed earlier, this would be done by inputing appropriate, nonzero, $\lambda_{r,seat}$ and $\dot{Q}_{seat}$ terms in eqns. (6) and (7). Then, using the k and α of a candidate ceiling material, the algorithm would calculate the ceiling's time-dependent, post-crash, thermal response.

In the most likely case of a combustible ceiling material, one could, for example, predict the time for the lower surface to reach a characteristic ignition temperature. Results of the FAA experimental program described in reference 2.1 indicate that away from the combustion zone tenable conditions are maintained throughout the cabin prior to ceiling ignition. With these ceiling materials the time-to-ceiling ignition would therefore provide a reasonable measure of post-crash cabin fire safety, viz., the minimum time available for passengers to evacuate the cabin or the Available Safe Egress Time (ASET) (reference 2.12). Hopefully, evaluations of practical cabin ceiling material candidates would lead to associated ignition times, or minimum ASET's, which exceed the time required for cabin evacuation. In any event, the greater the time-to-ignition of a material the better.

In the case of a noncombustible ceiling, time-to-ignition in the above discussion would be replaced by time to reach some agreed upon ceiling temperature (e.g., 600°C), which would typically be associated with cabin flashover.

Estimates of Post-Crash Fire Growth in Arrays of Cabin Seats. The objective of reference 2.13 was to obtain estimates of the energy release rate of post-crash fires growing through arrays of cabin seats. Based on FAA, full-scale, 21 seat tests which were similar to Tests 104-111, estimates of fire growth in two types of seat construction were obtained. The first type of seats, designated as "regular" seats were made of fire retarded polyurethane foam covered with wool-nylon fabric. The second seat construction was similar to the first, except that it included a blocking layer constructed of a 0.0048 m thick sheet of neoprene with a polyester scrim.

The estimates of $\dot{Q}_{seat}(t)$ for the two types of seats are plotted in figure 2.16. The plots terminate at 140 s and 185 s, at which times video-tape recordings of the tests indicated the initiation of either flashover (the 140 s time) or of rapid development of total obscuration (the 185 s time).

The $\dot{Q}_{seat}$ estimates of figure 2.16 will be used below to evaluate the post-crash response of a specific, honeycomb ceiling material.

POST-CRASH RESPONSE OF A HONEYCOMB CEILING MATERIAL - ESTIMATES OF TIME-TO-IGNITION. The algorithm developed here was used to estimate the post-crash thermal response of a 0.0254 m thick, honeycomb composite, aircraft lining material with an epoxy fiberite covering. The effective thermal properties of the composite were measured, and found to be (reference 2.14)

$$k = 5.9\ (10^{-5})\ kW/(mK)$$

$$\alpha = 4.8\ (10^{-7})\ m^2/s \qquad (23)$$

$$\rho = 110.\ kg/m^3$$

$$C_p = 1.11\ kJ/(kgK)$$

$\lambda_{r,seat}$ of eq. (7) was taken to be 0.35 and $\dot{Q}_{seat}$ was simulated by the plots of figure 2.16. The computer program written to exercise the algorithm was actually designed to accept pairs of [t, $\dot{Q}_{seat}(t)$] data points as input, and then to linearly interpolate between these to obtain $\dot{Q}_{seat}$ at any arbitrary time during the calculation. β of eq. (5) was taken to be 3.0 m^2. ε_L and ε_U were taken to be 1.

The predicted history of the lower surface of the honeycomb ceiling directly above the doorway seat is plotted in figure 2.17 for both "regular" seating and "blocked" seating.

The ignition temperature, T_{ign}, of the honeycomb material had been measured previously, and was found to be (reference 2.15)

$$T_{ign} = 536^0C \qquad (24)$$

As can be seen in figure 2.17 the calculation predicts onset of ceiling ignition at 148 and 204 s for "regular" and "blocked" seating, respectively. For cabins outfitted with ceilings of the honeycomb material, the use of the blocked rather than the unblocked seating construction would lead to a 56 s advantage in time available for post-crash cabin evacuation.

SUMMARY AND CONCLUSIONS. An algorithm was developed to predict the thermal response of aircraft ceiling materials during a specific, post-crash, external fuel-spill, fire scenario. Experimental measurements of near-ceiling temperatures in a series of eight, full-scale, post-crash, single seat, test simulations provided indirect validation of the algorithm. Two other full-scale tests, each of which involved fire spread through arrays of seating with different types of seat construction (fire retarded polyurethane foam covered with a wool-nylon fabric, with and without a neoprene sheet-polyester scrim blocking layer) provided the input data required to exercise the algorithm.

The post-crash, time-to-ignition of a ceiling construction, which can be associated with the time available for passengers to safely evacuate an aircraft, was recommended as one possible measure of the fire safety of the cabin ceiling-seat construction system (i.e., changing either the ceiling or the seat-construction has an impact on cabin fire safety).

Relative to the post-crash fire scenario considered here, the algorithm was used to predict the response of a candidate honeycomb ceiling material when used in a wide-body aircraft, with and without seat blocking. Times-to-ceiling ignition were estimated to be 148 and 204 s with and without seat blocking, respectively.

In a similar way, the algorithm developed here could be used to estimate the time-to-ignition of any other candidate ceiling material which would be used in cabins having either blocked or unblocked seating. Required inputs are the thickness and the effective thermal conductivity and diffusivity of the material.

REFERENCES.

2.1 Hill, R.G., Johnson, G.R. and Sarkos, C.P., Postcrash Fuel Fire Hazard Measurements in a Wide-Body Aircraft Cabin, FAA-NA-79-42, Federal Aviation Admin., NAFEC, Atlantic City, NJ, 1979.

2.2 Emmons, H.W., The Ingestion of Flames and Fire Gases Into a Hole in an Aircraft Cabin for Arbitrary Tilt Angles and Wind Speed, Home Fire Proj. Rpt. 52, Harvard Univ. Div. Appl. Sciences, Cambridge, MA, 1982.

2.3 Eckert, E.R.G. and Drake, R.M., Heat and Mass Transfer, McGraw-Hill, 2nd Ed., 1959.

2.4 Cooper, L.Y., Heat Transfer from a Buoyant Plume to an Unconfined Ceiling, J. Heat Transfer, 104, p. 446, 1982.

2.5 Cooper, L.Y., A Mathematical Model for Estimating Available Safe Egress Time in Fires, Fire and Materials, 6, p. 135, 1982.

2.6 Cooper, L.Y., Thermal Response of Unconfined Ceilings Above Growing Fires and the Importance of Convective Heat Transfer, 22nd National Heat Transfer Conf., ASME Paper 84-HT-105, 1984 and NBSIR 84-2856, National Bureau of Standards, Washington, DC, 1984.

2.7 Yousef, W.W., Tarasuk, J.D. and McKeen, W.J., Free Convection Heat Transfer from Upward-Facing, Isothermal, Horizontal Surfaces, J. Heat Transfer, 104, p. 493, 1982.

2.8 Emmons, H.W., The Prediction of Fires in Buildings, 17th Symp. (Inter.) on Combustion, p. 1101, 1979.

2.9 Mitler, H.E. and Emmons, H.W., Documentation for the Fifth Harvard Computer Fire Code, Home Fire Project Tech. Rpt. 45, Harvard Univ., Cambridge, MA, 1981.

2.10 Poreh, M., Tsuei, Y.G. and Cermak, J.E., Investigation of a Turbulent Radial Wall Jet, ASME Journal of Applied Mechanics, p. 457, 1967.

2.11 Alpert, R.L., Turbulent Ceiling-Jet Induced by Large-Scale Fires, Combustion Science and Technology, Vol. 11, p. 197, 1975.

2.12 Cooper, L.Y., A Concept of Estimating Safe Available Egress Time, Fire Safety Journal, Vol. 5, p. 135, 1983.

2.13 Steckler, K., National Bureau of Standards, private communication (see Chapter 1).

2.14 Parker, W., National Bureau of Standards, private communication.

2.15 Harkleroad, M., Quintiere, J. and Walton, W., Radiative Ignition and Opposed Flame Spread Measurements on Materials, DOT/FAA/CT-83/28 (National Bureau of Standards Rpt. to) Federal Aviation Admin., Atlantic City, NJ, 1983.

NOMENCLATURE.

a_1, a_2, b, c	dimensions, Fig. 9
C_p	specific heat
D	wire diameter
F_{A-dA}	view factor, Eq. (2)
g	acceleration of gravity
H	seat fire-to-ceiling distance
h_L, h_U	lower/upper surface heat transfer coefficient
$\tilde{h}$	dimensionless heat transfer coefficient, Eq. (12)
k	thermal conductivity
N	number of grid points in ceiling analysis
$\dot{Q}$	enthalpy flux in plume, Eq. (7)
$\dot{Q}^*$	dimensionless $\dot{Q}$, Eq. (10)
$\dot{Q}_{equiv}$	equivalent fire strength
$\dot{Q}_{seat}$	strength of seat fire
$\dot{Q}'_i$	radiant heat transfer to wire per unit length
$\dot{Q}'_{amb-wire}$	radiation from ambient to wire
$\dot{Q}'_{ceiling-wire}$	radiation from ceiling to wire
$\dot{Q}'_{door-wire}$	radiation from doorway to wire
$\dot{Q}_{wire}$	radiation from wire
$\dot{q}''_i$	rates of heat transfer per unit area
$\dot{q}''_{conv,U}$, $q_{conv,L}$	convection to upper/lower ceiling
$\dot{q}''_{door-ceiling}$	radiation from doorway to ceiling
$\dot{q}''_{rad-door}$	radiation from doorway
$\dot{q}''_{rad-seat}$	radiation from seat fire to ceiling
$\dot{q}''_{rerad,U}$, $\dot{q}''_{rerad,L}$	radiation from upper/lower ceiling

$\dot{q}''_U$, $\dot{q}''_L$	net heat transfer to upper/lower ceiling
Re	Reynold's number, Eq. (12)
r	distance from plume impingement point
T_{ad}	adiabatic ceiling temperature, Eq. (9)
T_{amb}	ambient temperature
T_{ign}	ignition temperature
$T_{s,U}$, $T_{s,L}$	upper/lower surface ceiling temperature
T_w	thermocouple wire temperature
t	time
α	thermal diffusivity/wire configuration constant, Eq. (22)
β	a constant
Γ_1, Γ_2	constants, Eq. (3)
δZ	indepth spacing of ceiling grid points
ε_U, ε_L	lower/upper ceiling emissivity
θ	configuration angle, Fig. 9
$\lambda_{r,seat}$	fraction of $\dot{Q}_{seat}$ radiated
ν	kinematic viscosity
ρ	density
ρ_{amb}	density of ambient
σ	Stefan-Boltzmann constant

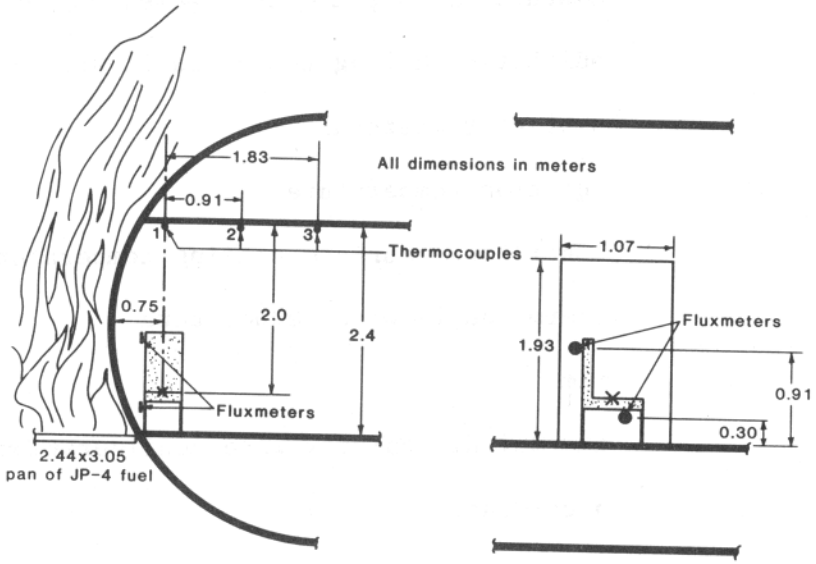

FIGURE 2.1. A SCHEMATIC OF THE TEST SETUP.

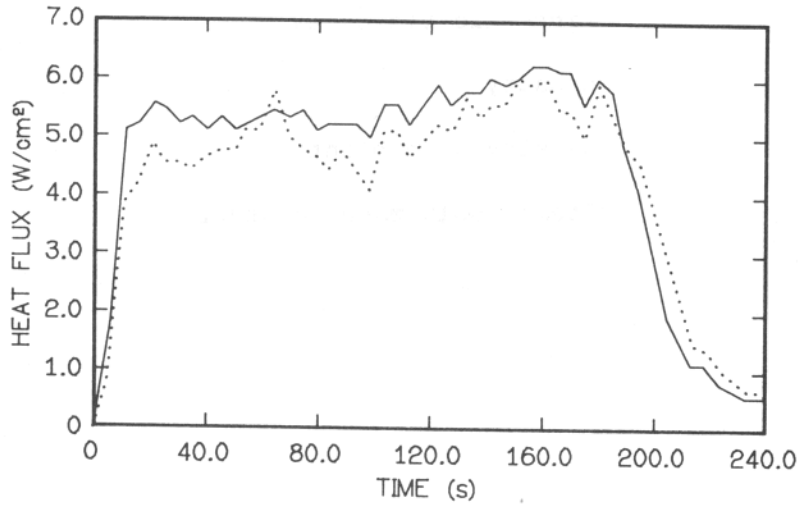

FIGURE 2.2. MEASURED DOORWAY HEAT FLUX VS TIME (LOWER FLUXMETER ....; UPPER FLUXMETER ——); TEST 111 (BACKGROUND).

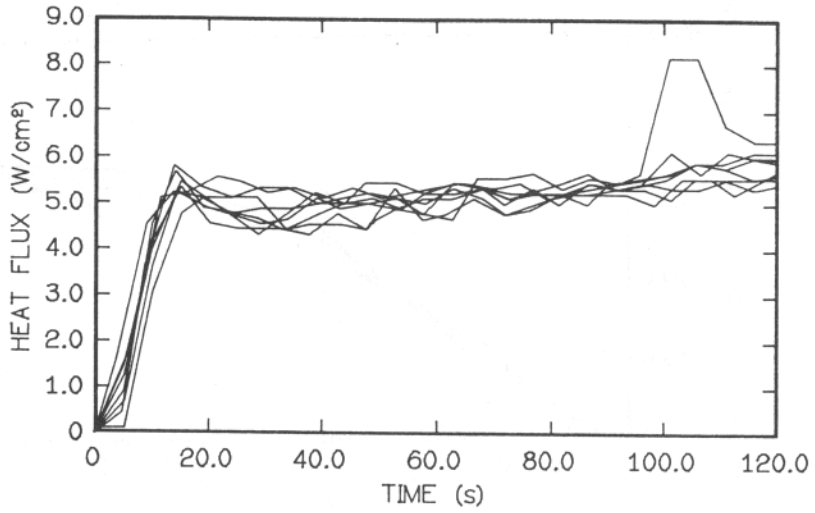

FIGURE 2.3. MEASURED DOORWAY HEAT FLUX VS TIME (LOWER FLUXMETER; TESTS 104-111).

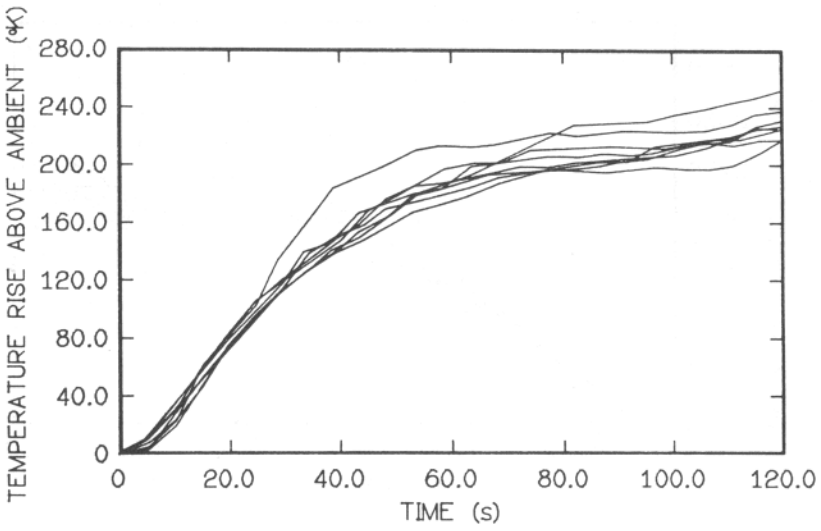

FIGURE 2.4. MEASURED TEMPERATURE VS TIME AT POSITION 1; TESTS 104-111.

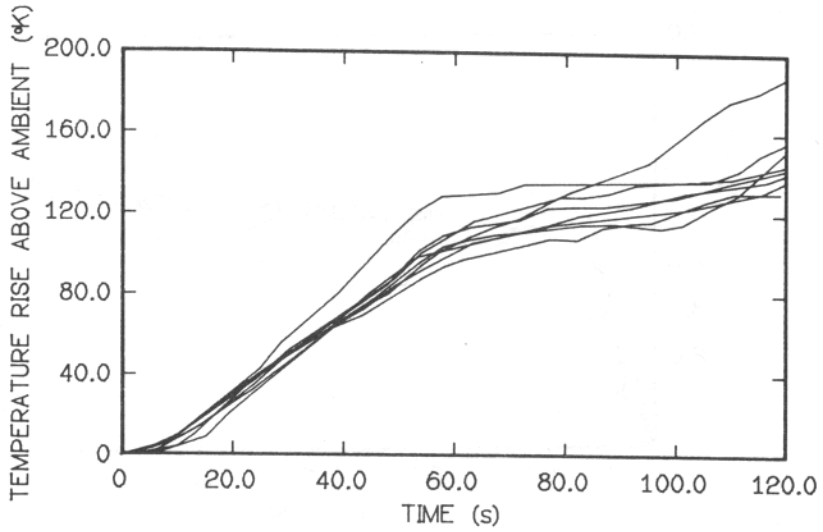

FIGURE 2.5. MEASURED TEMPERATURE VS TIME AT POSITION 2; TESTS 104-111.

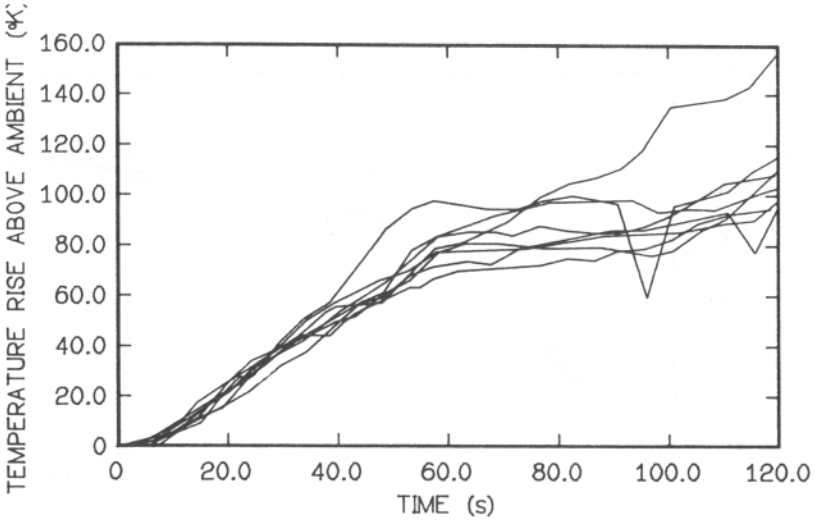

FIGURE 2.6. MEASURED TEMPERATURE VS TIME AT POSITION 3; TESTS 104-111.

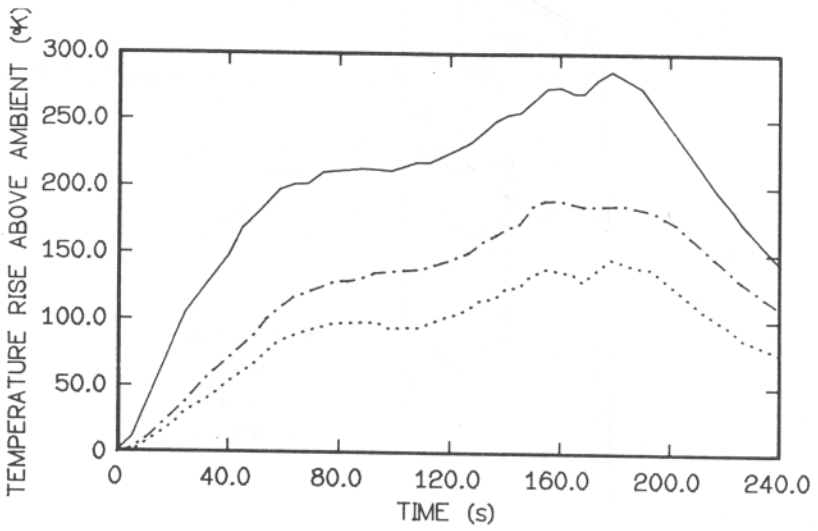

FIGURE 2.7. MEASURED TEMPERATURE VS TIME AT POSITIONS 1 (——), 2 (——•——•——), AND 3 (....); TEST 111.

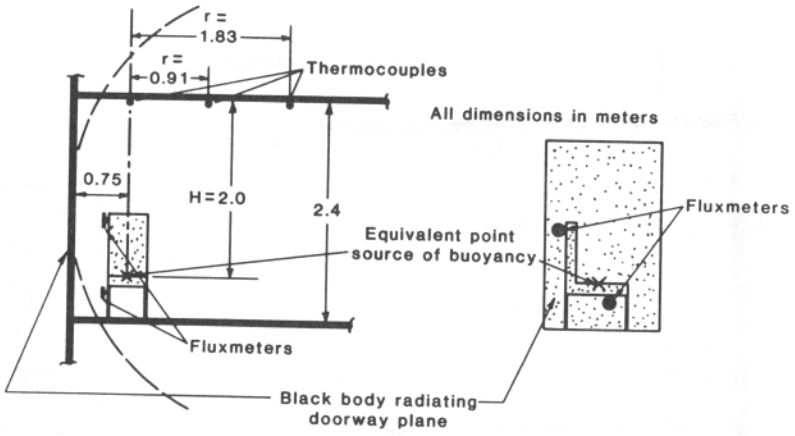

FIGURE 2.8. A SIMPLIFIED VERSION OF THE POST-CRASH FIRE SCENARIO.

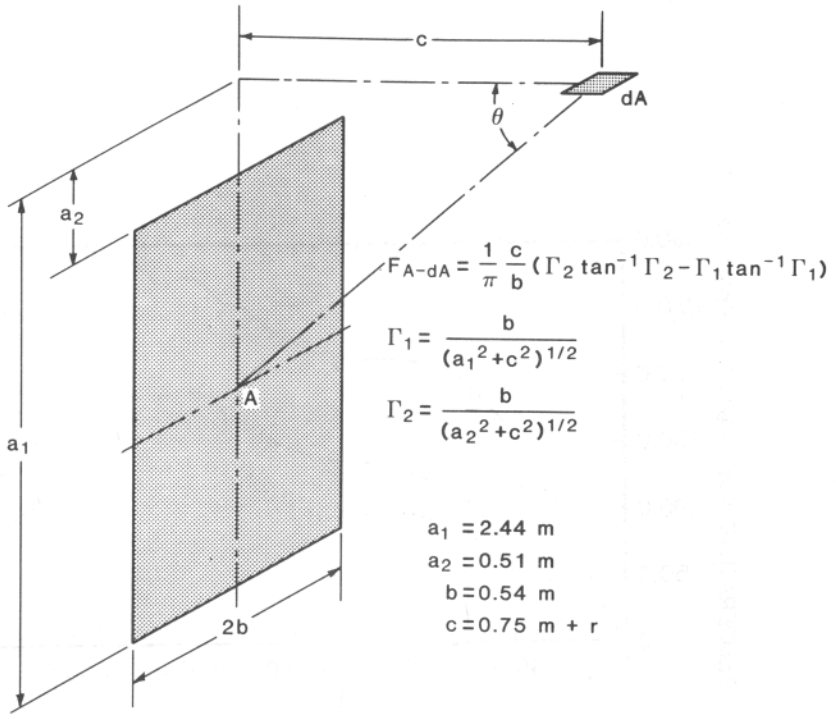

FIGURE 2.9. THE VIEWFACTOR BETWEEN THE DOORWAY AND A CEILING ELEMENT.

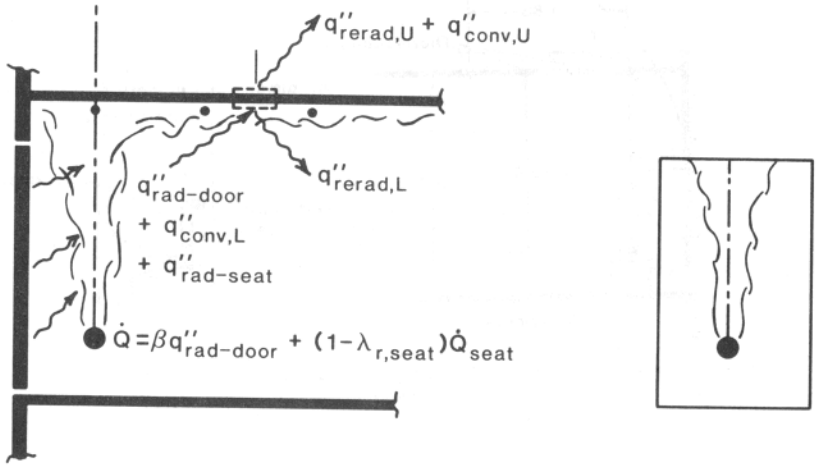

FIGURE 2.10. THE IDEALIZED POST-CRASH FIRE SCENARIO.

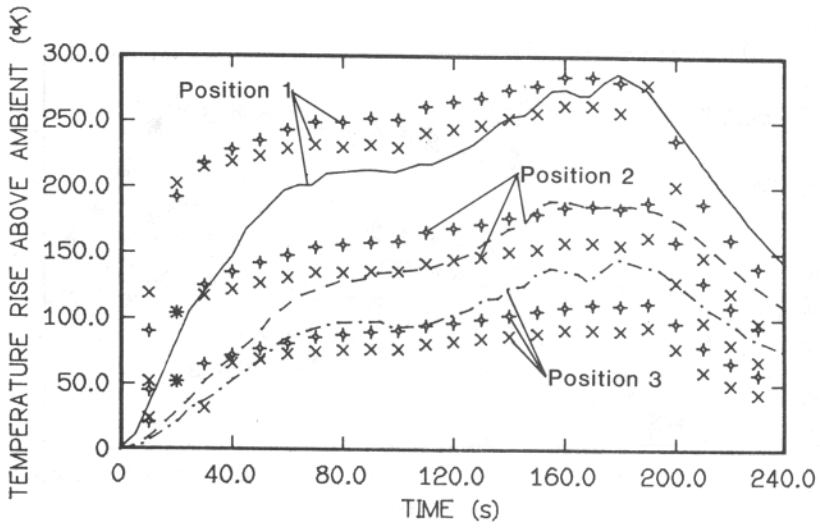

FIGURE 2.11. COMPUTED TEST 111, LOWER CEILING SURFACE TEMPERATURE (+:β=0.; x:β=3.0m^2) AND CORRESPONDING MEASURED NEAR-CEILING TEMPERATURES AT POSITIONS 1, 2, and 3.

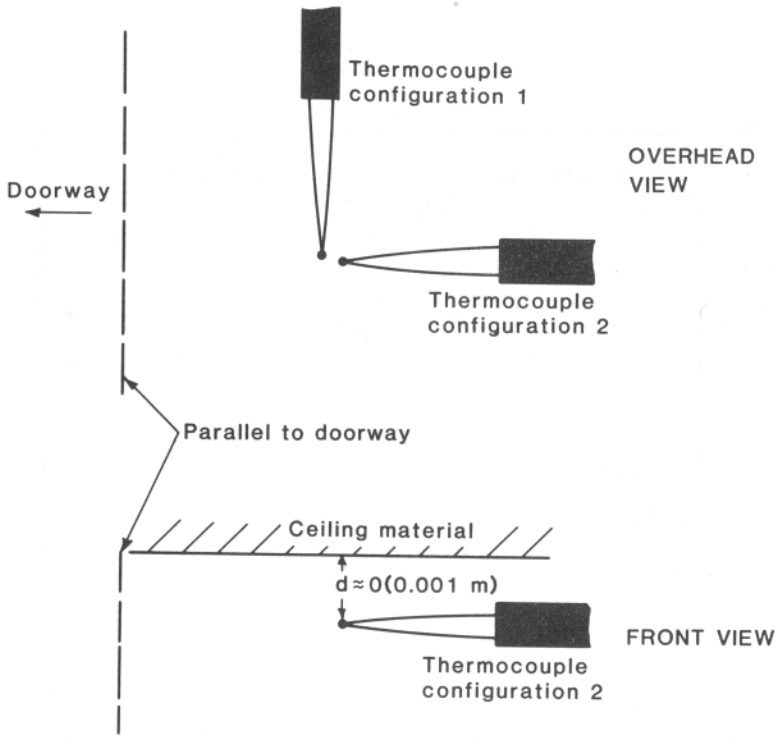

FIGURE 2.12. TWO EXTREME CONFIGURATIONS FOR PLACEMENT OF THE NEAR-CEILING THERMOCOUPLES.

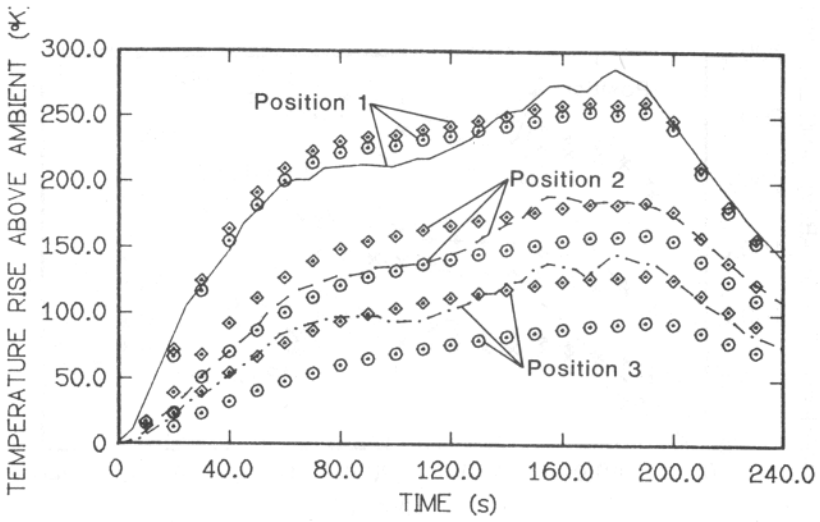

FIGURE 2.13 PREDICTED AND MEASURED TEST 111 THERMOCOUPLE TEMPERATURES (β= 2.0 m^2).
◇: PREDICTED T_w, CONFIGURATION 1
⊙: PREDICTED T_w, CONFIGURATION 2
____, __ __ __, __: MEASURED T_w

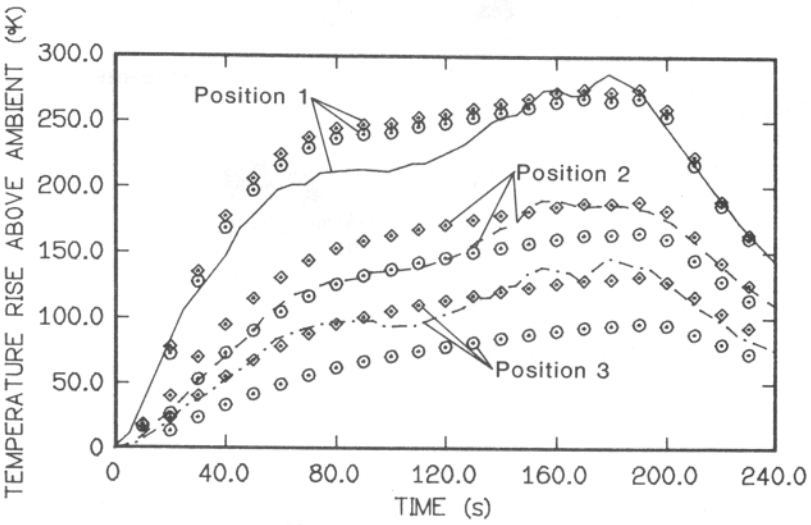

FIGURE 2.14. PREDICTED AND MEASURED TEST 111 THERMOCOUPLE TEMPERATURES (β= 3.0 m^2).
◇: PREDICTED T_w, CONFIGURATION 1
⊙: PREDICTED T_w, CONFIGURATION 2
____, __ __ __, __ . __: MEASURED T_w

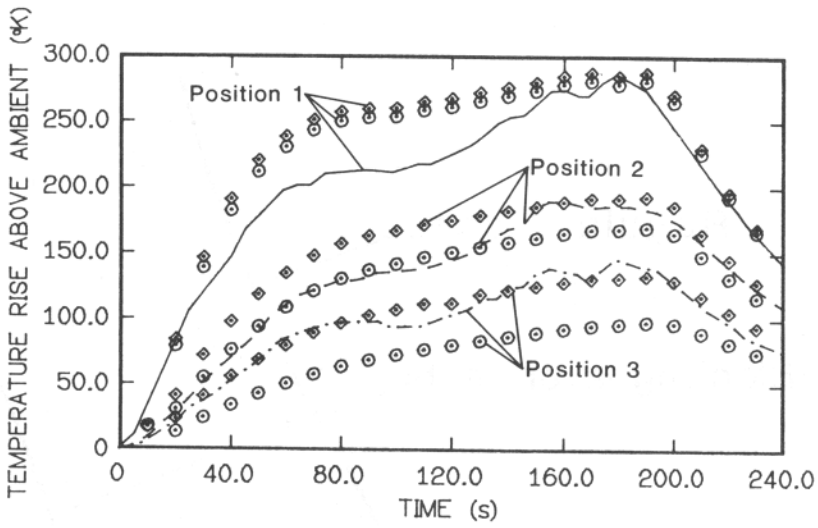

FIGURE 2.15. PREDICTED AND MEASURED TEST 111 THERMOCOUPLE TEMPERATURES (β = 4.0 m^2).
◇: PREDICTED T_w, CONFIGURATION 1
⊙: PREDICTED T_w, CONFIGURATION 2
____, __ __ __, __ . __; MEASURED T_w

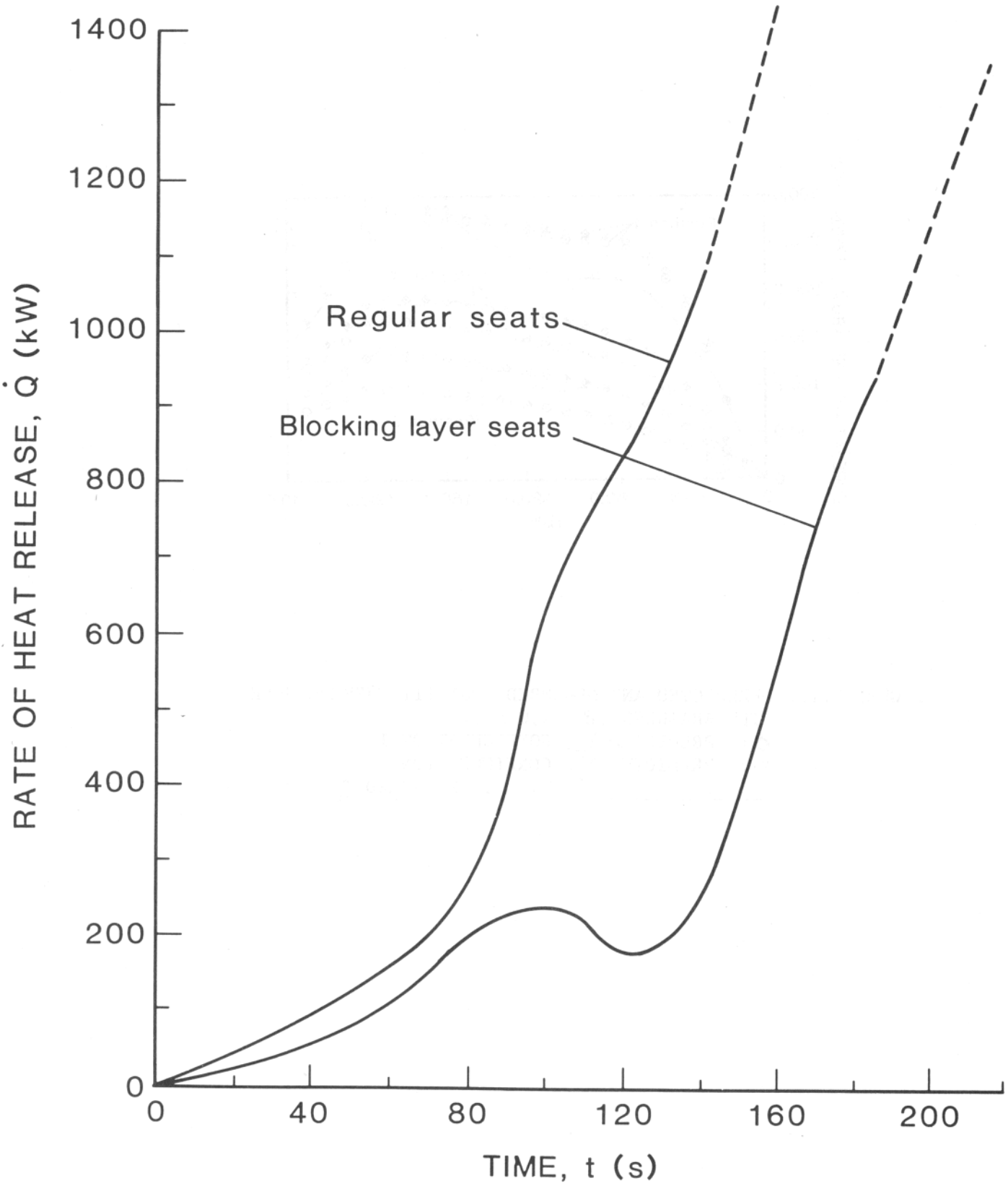

FIGURE 2.16. ESTIMATE FOR $\dot{Q}_{seat}$ FOR ARRAYS OF POLYURETHANE SEATS WITH AND WITHOUT BLOCKING LAYERS [13] (__ __ __ EXTRAPOLATED FROM CURVES OF [13]).

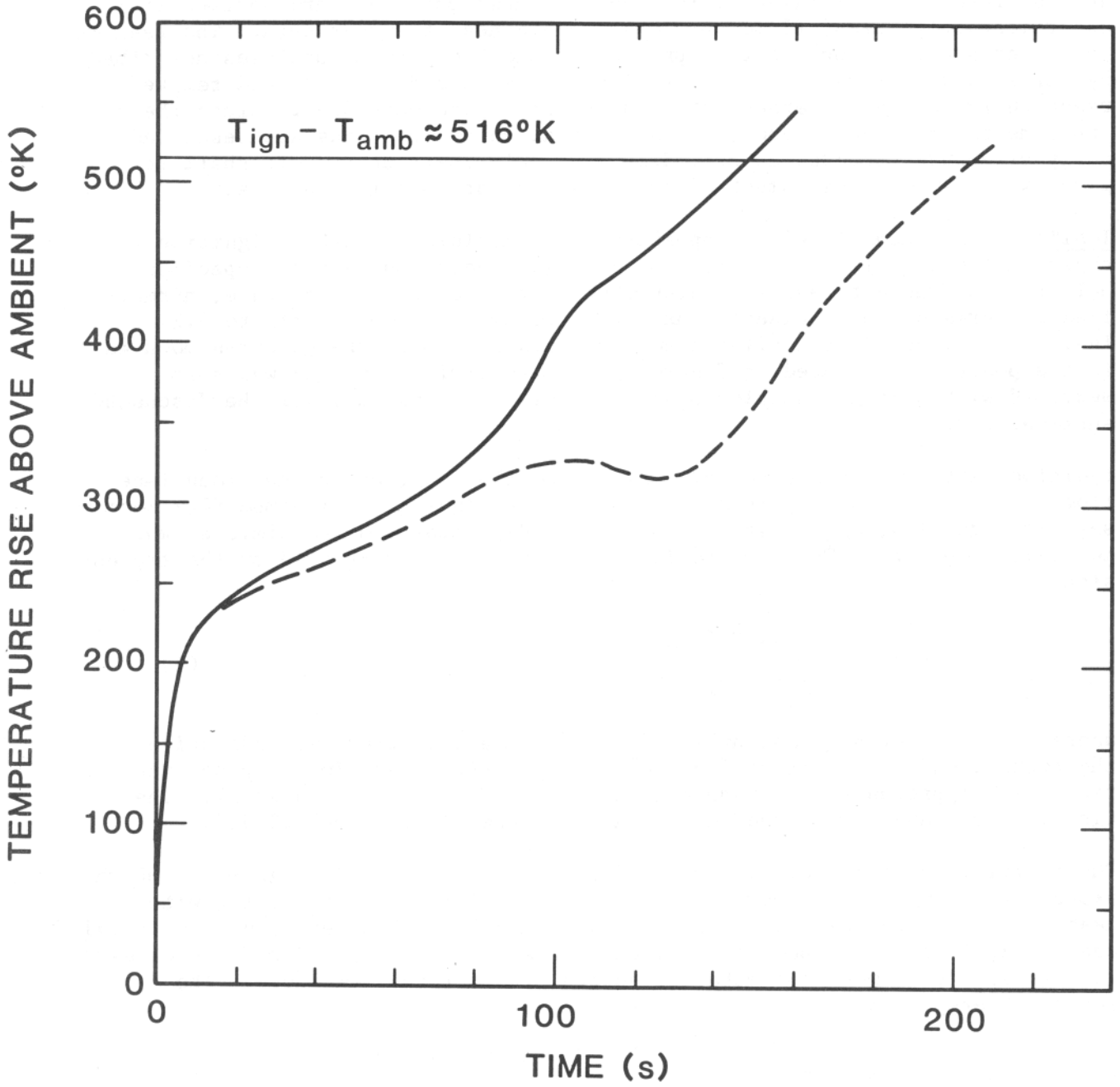

FIGURE 2.17. PREDICATED LOWER SURFACE, POST-CRASH, TEMPERATURE OF THE HONEYCOMB CEILING MATERIAL IN A CABIN OUTFITTED WITH POLYURETHANE SEAT CUSHIONS: WITH (—— ——) AND WITHOUT (——) BLOCKING LAYERS.

CHAPTER 3. FLAME SPREAD AND IGNITION CHARACTERISTICS OF AIRCRAFT PANELS.

Five aircraft paneling materials were examined for their ignition and flame spread properties. Parameters relevant to these phenomena are derived from experimental ignition, flame spread and flame heat transfer data. The results presented are based on the test procedures and theoretical analyses described by Harkleroad (reference 3.1), Quintiere (reference 3.2, 3.3), and related research by Walton (reference 3.4) and Hasemi (reference 3.5). Since these experimental procedures and their analytical interpretations are described fully elsewhere (references 3.1, 3.2, 3.3) only their end result shall be given below in the assessment of the five aircraft panel materials.

IGNITION. A schematic of the apparatus for examining radiative ignition is shown in figure 3.1. It consists of a radiant heat source and a specimen holder. The radiant heat flux distribution to the specimen surface, normalized in terms of the incident flux at x = 50 mm, is shown in figure 3.2. Ignition, triggered by a pilot flame, was measured with the specimen mounted in the position indicated in figure 3.1. Lateral flame spread was also measured with a larger sample mounted in this apparatus and will be discussed subsequently.

Ignition tests were conducted by varying the flux, $\dot{q}''_e$, on the specimen face from 1.5 to 6.5 W/cm^2 and recording the time to ignite. A minimum flux necessary for ignition, $\dot{q}''_{o,ig}$, is experimentally determined as the limit at which no ignition occurs. The time to ignite (t) data are correlated by the expression

$$\frac{\dot{q}''_{o,ig}}{\dot{q}''_e} = F(t) = \begin{cases} b\sqrt{t}, & t \leq t_m \\ 1, & t \geq t_m \end{cases} \qquad (1)$$

where b is a material constant and t_m is a characteristic time indicative of the thermal equilibrium time (reference 3.2). F(t) is a time-response function which represents the transient thermal response of the material. The ignition data and correlated results are included in figures 3.3-3.7.

The ignition temperature, T_{ig} can be found from the curve in figure 3.8 which expresses a surface heat balance based on natural convective cooling with no heat transfer into the solid (references 3.1, 3.2). This represents the ideal case of ignition described for an inert blackbody solid of infinite thickness. It corresponds to most non-metallic solids of practical thickness. The surface energy balance is given below:

$$\dot{q}''_{o,ig} = \sigma \left(T_{ig}^4 - T_\infty^4\right) + h_c \left(T_{ig} - T_\infty\right) = h \left(T_{ig} - T_\infty\right) \qquad (2)$$

where h_c is the convective heat loss coefficient and h is a combined radiative-convective coefficient. The results for the five materials based on these ignition correlations are given in table 3.1.

TABLE 3.1. IGNITION PARAMETERS BASED ON EQ. (1)

Material	$\dot{q}''_{o,ig}$ (W/cm^2)	T_{ig} (°C)	b ($s^{-1/2}$)	t_m (s)
Aircraft Panel #1, Epoxy Fiberglass	2.03	438.	0.132	58.
Aircraft Panel #3, Epoxy Kevlar	2.30	465.	0.135	55.
Aircraft Panel #4, Phenolic Kevlar	3.40	558.	0.196	26.
Aircraft Panel #5, Phenolic Graphite	3.60	570.	0.172	34.
Aircraft Panel #2, Phenolic Fiberglass	3.60	570.	0.227	19.

Also from the transient heating of the ideal solid described above an effective conductivity, density, and specific heat product ($k\rho c$) can be derived as follows (references 3.1, 3.2):

$$k\rho c = \frac{4}{\pi}\left(\frac{h}{b}\right)^2 \qquad (3)$$

where h is the radiative and conductive heat transfer given by eq. (2). These $k\rho c$ values are tabulated in table 3.3. Given subsequently, they are effective values that include property variations with temperature, melting, decomposition and solid physical destruction modes which precede ignition.

OPPOSED FLOW FLAME SPREAD ON VERTICAL WALLS. Flame spread experiments were conducted with the specimen mounted in the position indicated in figure 3.1, exposed to a known external irradiance $\dot{q}''_e$, ignited by a pilot flame, and spread then proceded laterally. These results apply to opposed flow flame spread on a vertical surface in which the opposed flow is naturally induced by the sample flame (reference 3.1). A flame spread velocity (V) was determined from the flame front position (x_p) visibly noted on the specimen surface as a function of time. From the external radiant flux distribution curve, figure 3.2, the flux at the flame front position was found so that the flame spread velocity could be represented as a function of external flux ($\dot{q}''_e$) and time:

$$V = \frac{dx_p}{dt} \text{ vs } \dot{q}''_e\left(x_p(t)\right). \qquad (4)$$

Moreover, it has been shown (references 3.1, 3.2) that the velocity can be correlated in terms of the parameters C, a flame heat transfer factor; $\dot{q}''_{o,ig}$, the minimum ignition flux; and F(t), the response factor from Eq. (1) so that

$$V^{-1/2} = C\left[\dot{q}''_{o,ig} - \dot{q}''_e \cdot F(t)\right] \text{ ; for } \dot{q}''_{o,s} \le \dot{q}''_e F(t) < \dot{q}''_{o,ig}. \qquad (5)$$

The minimum flux necessary for spread, $\dot{q}''_{o,s}$, can be derived from the flame propagation limit and figure 3.2 (reference 3.1). These parameters are tabulated in table 3.2. For F(t) = 1, eq. (5) yields the maximum spread velocity as a function of $\dot{q}''_e$. These correlations are plotted for the five materials in figures 3.3-3.7, and the corresponding data are plotted only for conditions in which the tracting time (t) before the arrival of the flame front is greater than t_m, i.e., the spread rate is under condition of surface temperature

equilibrium. Also note that $\dot{q}''_{o,ig}$ of tables 3.1 and 3.2 for each material have been derived from two separate experiments; namely ignition and flame spread. The extent to which the two values agree shows the consistency between these two processes, and suggests the validity of a distinct ignition temperature controlling both spread and ignition.

TABLE 3.2 FLAME SPREAD PARAMETERS IN TERMS OF RADIANT FLUX (EQ. (5))

Material	$\dot{q}''_{o,ig}$ (W/cm^2)	C $\frac{s}{mm}^{1/2} \frac{cm^2}{W}$	$\dot{q}''_{o,s}$ (W/cm^2)
Aircraft Panel #1, Epoxy Fiberglass	2.1	2.50	1.90
Aircraft Panel #3, Epoxy Kevlar	2.4	1.20	1.70
Aircraft Panel #4, Phenolic Kevlar	3.5	1.16	2.80
Aircraft Panel #5, Phenolic Graphite	3.7	0.97	2.80
Aircraft Panel #2, Phenolic Fiberglass	3.8	0.63	2.60

A more general approach to representing flame spread can be represented as

$$V = \frac{\Phi}{k\rho c \left(T_{ig} - T_s\right)^2} \quad \text{for } T_{s,min} \leq T_s < T_{ig} \qquad (6)$$

where Φ is an empirical parameter incorporating gas-phase properties, flame temperature, opposed flow gas velocity and chemical effects usually denoted by a Damkohler number (reference 3.2). In this form, these results should be applicable to any opposed flow natural convection mode on a vertical surface. From the derived $\dot{q}''_{o,s}$, the minimum surface temperature for flame spread ($T_{s,min}$) can be obtained from figure 3.8. Flame spread properties represented by eq. (6) are listed in table 3.3.

FLAME HEIGHT AND FLAME HEAT TRANSFER ON VERTICAL WALLS. The apparatus used to measure flame height and flame heat flux is shown in figure 3.9. The specimen, mounted below a water-cooled instrumented copper plate, is exposed to an irradiant flux, $\dot{q}''_e$, that can be varied from 0.7 to 3.7 W/cm^2. The ignition source is a line burner positioned below the specimen. Water-cooled heat flux sensors embedded in the copper plate record the flux, $\dot{q}''_x$, at six positions above the specimen. Flame heights are determined from video records.

Average peak heat fluxes and flame heights were determined for the time period representing 80 percent of the maximum values recorded. Similarly, peak heat release values were obtained by Walton and Twilley (reference 3.4) in another apparatus for different external radiative heating conditions. The time span that bounds 10 percent of the peak flux is defined as the burn time, t_b.

TABLE 3.3. FLAME SPREAD PROPERTIES (EQ. (6))

	T_{ig} (°C)	$k\rho c$ $\left(\frac{kW}{m^2 K}\right)^2 s$	Φ $\frac{(kW)^2}{m^3}$	$T_{s,min}$ (°C)	$\Phi/k\rho c$ $\frac{m \cdot K^2}{s}$
Aircraft Panel #1, Epoxy Fiberglass	438.	0.174	1.17	425.	7.
Aircraft Panel #3, Epoxy Kevlar	465.	0.188	4.86	400.	26.
Aircraft Panel #4, Phenolic Kevlar	558.	0.133	2.47	510.	18.
Aircraft Panel #5, Phenolic Graphite	570.	0.185	4.58	510.	25.
Aircraft Panel #2, Phenolic Fiberglass	570.	0.106	6.23	490.	58.

Figure 3.10 schematically describes the flame spread problem and from reference 3.3, the approach used for expressing the upward flame spread velocity was

$$V = \frac{(\dot{q}''_f)^2 \ (x_f - x_p)}{k\rho c \ (T_{ig} - T_s)^2} \tag{7}$$

or

$$V = \frac{x_f - x_p}{t_f} \ . \tag{8}$$

Here, $\dot{q}''_f$ represents the flame heat flux; x_f, the flame height; x_p, the pyrolysis height; T_{ig} and T_s, the ignition and surface temperatures, respectively; $k\rho c$, the material thermal property parameter; and t_f, the time for spread over the flame heat transfer region $(x_f - x_p)$ where

$$t_f = k\rho c \ [(T_{ig} - T_s)/\dot{q}''_f]^2 \ . \tag{9}$$

In figure 3.10, x_b represents the length of the region over which pyrolysis has ceased. The time for burnout or the duration of pyrolysis is designated as t_b. This has been determined for each burning condition and sample. It was computed as the duration over which the first heat flux sensor exceeded ten percent of its peak value.

Table 3.4 summarizes these values along with some significant time averaged results. The value selected for $\dot{q}''_f$ was the time-averaged maximum recorded

value over the array of sensors. The time-averaged maximum was computed from the values which exceeded eighty percent of the peak flux reading for that sensor. Similarly this time-averaged maximum was computed for the flame height x_f. A predictive methodology is far from complete for the phenomena of upward flame spread, but these results suggest some tendencies. Indeed the issue of what conditions are necessary for sustained propagation may be more important. Here the ratio t_f/t_b may be significant since the burning time t_b must be long enough relative to t_f to permit spread. It is interesting to observe the nominal spread rates at this scale (ignited height of 28 cm) as computed from the tabulated values assuming spread does occur. These hypothetical upward spread rates are similar in magnitude to the opposed flow maximum spread rates shown in figures 3.3-3.7.

TABLE 3.4. PARAMETERS SIGNIFICANT TO UPWARD FLAME SPREAD

Material	External Flux $\dot{q}''_e$ (W/cm^2)	80% max Flame Flux $\dot{q}''_f$ (W/cm^2)	80% max Flame Length x_f (cm)	Spread Time t_f (s)	Burn Time t_b (s)	Flame Heat Transfer Length $x_f - x_p$ (cm)	Nominal Spread Rate $V = \frac{dx_p}{dt}$ (mm/s)
Aircraft Panel #1	2.5	1.3	58	178	100	30	1.7
Epoxy Fiberglass	3.8	0.9	61	372	29	33	0.9
Aircraft Panel #2 Phenolic Fiberglass	3.8	0.8	90	497	43	62	1.2
Aircraft Panel #3	2.0	1.6	66	144	115	38	2.6
Epoxy Kevlar	2.5	1.1	48	305	115	20	0.6
	3.0	0.9	57	456	115	29	0.6
	3.7	1.7	89	128	101	61	4.8
	3.8	1.6	64	144	115	36	2.5
Aircraft Panel #4	3.0	1.4	66	195	28	38	1.9
Phenolic Kevlar	3.7	2.7	61	52	101	33	6.3
Aircraft Panel #5	2.0	1.0	40	556	29	12	0.2
Phenolic Grahite	3.0	1.1	53	459	29	25	0.5
	3.7	1.0	66	556	29	38	0.7

Wall heat flux distributions are shown in figures 3.11-15. The materials show a decreasing flux with distance measured from the base of the fire (bottom scale). This distance is normalized with the flame height (top scale) and the data are replotted in those figures as an attempt to coalesce the results into a general correlation.

A curve labeled "Hasemi data" depicts a correlation for gaseous fuel heat transfer results along walls (references 3.3, 3.5). A compilation of all the sample heat transfer results are plotted against x/x_f in figure 3.16. It has not yet been generally resolved how to predict this flame heat transfer in terms of underlying parameters. Obviously, sufficient scatter exists in figure 3.16 to preclude its use in accurate quantitative assessments. These data do not corroborate the Hasemi correlation at low x/x_f (i.e. < 0.7 within the flame zone). This is most likely due to just insufficient data in the

region since the flames for these materials are relatively short compared to the first heat flux measurement position at x = 38.6 cm (fig. 3.9). Further study is underway to improve the accuracy and generality of this correlation. More data is needed for these materials to resolve anomalies related to non-monotonic flame height increase with external irradiance for a given material. For reference, the relationship found in reference 3.3 to predict flame height from energy release rate is given below:

$$x_f = k_f (\dot{E}')^{2/3} \qquad (10)$$

where $k_f = 0.0569$ m/(kW/m)$^{2/3}$,

x_f is flame height in m,

and $\dot{E}'$ is energy release rate per unit flame width in kW/m.

For an exposed and fully-involved sample fire area as indicated in figure 3.9, energy release rate per unit sample area ($\dot{E}''$) can be derived from height data. From eq. (10), $\dot{E}' = \dot{E}'' x_p$ where $x_p = 0.284$ m in this case. These energy results were computed and will be reported later in the summary of this report.

CONCLUDING REMARKS. Tables 3.1 and 3.3 present useful results for these five aircraft materials in their prediction of ignition and opposed flow flame spread on vertical surfaces. Table 3.4 gives results to indicate their propensity and properties related to upward flame spread. More research will be needed to more fully resolve the upward spread case to a prescriptive prediction format.

NOMENCLATURE.

b	constant, eq. (1)
c	specific heat
C	flame heat transfer factor, eq. (5)
$\dot{E}$	energy release rate
h	heat transfer coefficient
h_c	convective heat transfer coefficient
k	thermal conductivity
$\dot{q}''$	heat transfer per unit area per unit time
t	time
t_m	characteristic time, eq. (1)
T	temperature
V	spread velocity
x	coordinate
σ	Stefan-Boltzmann constant
ρ	density
Φ	parameter, eq. (6)

Subscripts

e	external
f	flame
ig	ignition
o	minimum
s	surface
p	pyrolysis
∞	ambience

REFERENCES.

3.1 Harkleroad, M., Quintiere, J. and Walton, W., "Radiative Ignition and Opposed Flow Flame Spread Measurements on Materials", U.S. Dept. Trans., Fed. Aviation Admin. Tech. Ctr., DOT/FAA/CT-83/28, August 1983.

3.2 Quintiere, J. and Harkleroad, M., "New Concepts for Measuring Flame Spread", Symp. on Application of Fire Science to Fire Engineering, Amer. Soc. Testing and Materials/Soc. Fire Prot. Engrs., Denver, CO, June 26-27, 1984.

3.3 Quintiere, J., Harkleroad, M. and Hasemi, J., "Wall Flames and Implications for Upward Flame Spread", AIAA Paper No. 85-0456, 1985.

3.4 Walton, W.D. and Twilley, W.H., "Heat Release and Mass Loss Rate Measurements for Selected Materials", NBSIR 84-2960, Nat. Bur. Stand., Dec. 1984.

3.5 Hasemi, Y., personal communications (to be published).

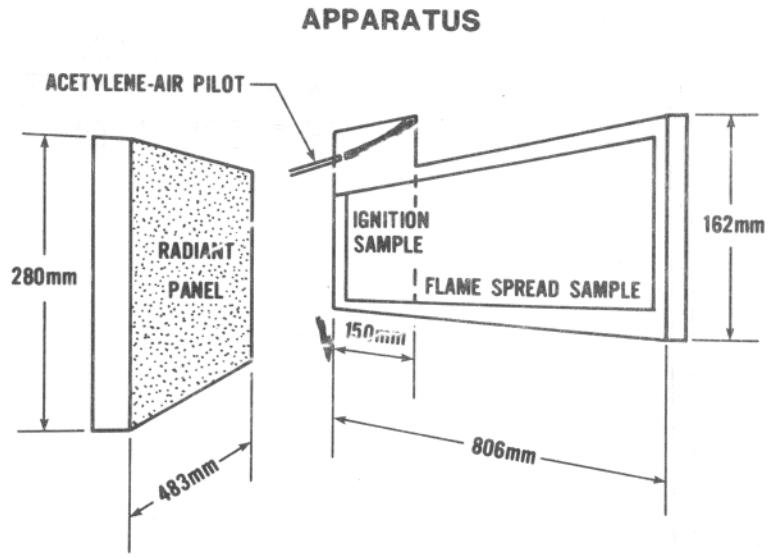

FIGURE 3.1. SCHEMATIC OF IGNITION AND FLAME SPREAD APPARATUS.

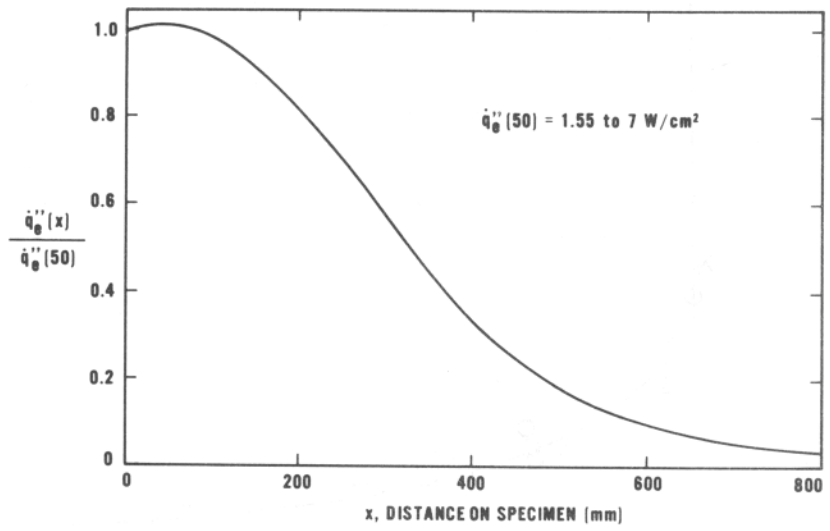

FIGURE 3.2. NORMALIZED IRRADIANCE OVER THE SPECIMEN.

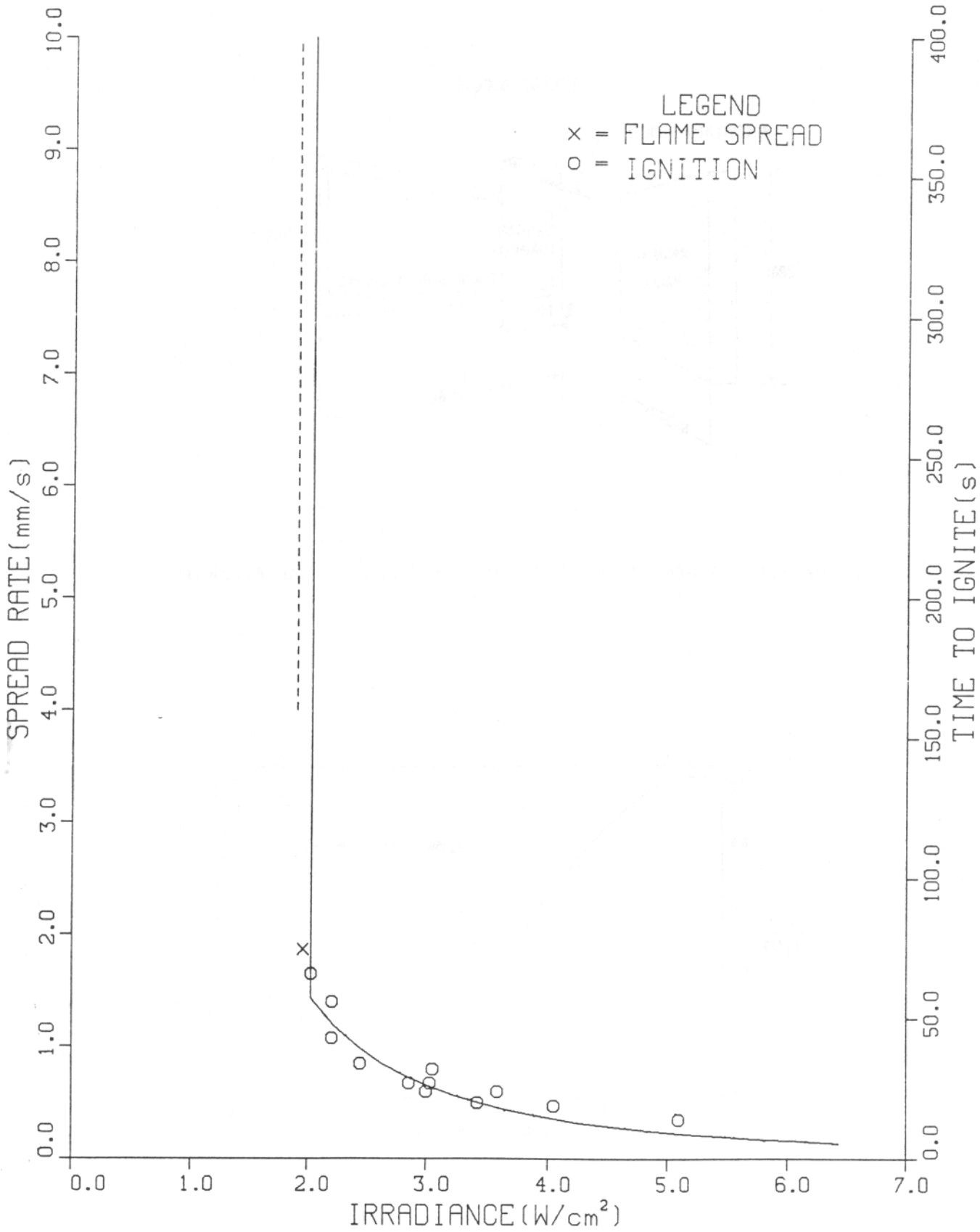

FIGURE 3.3. SPREAD AND IGNITION RESULTS FOR AIRCRAFT PANEL #1, EPOXY FIBERGLASS.

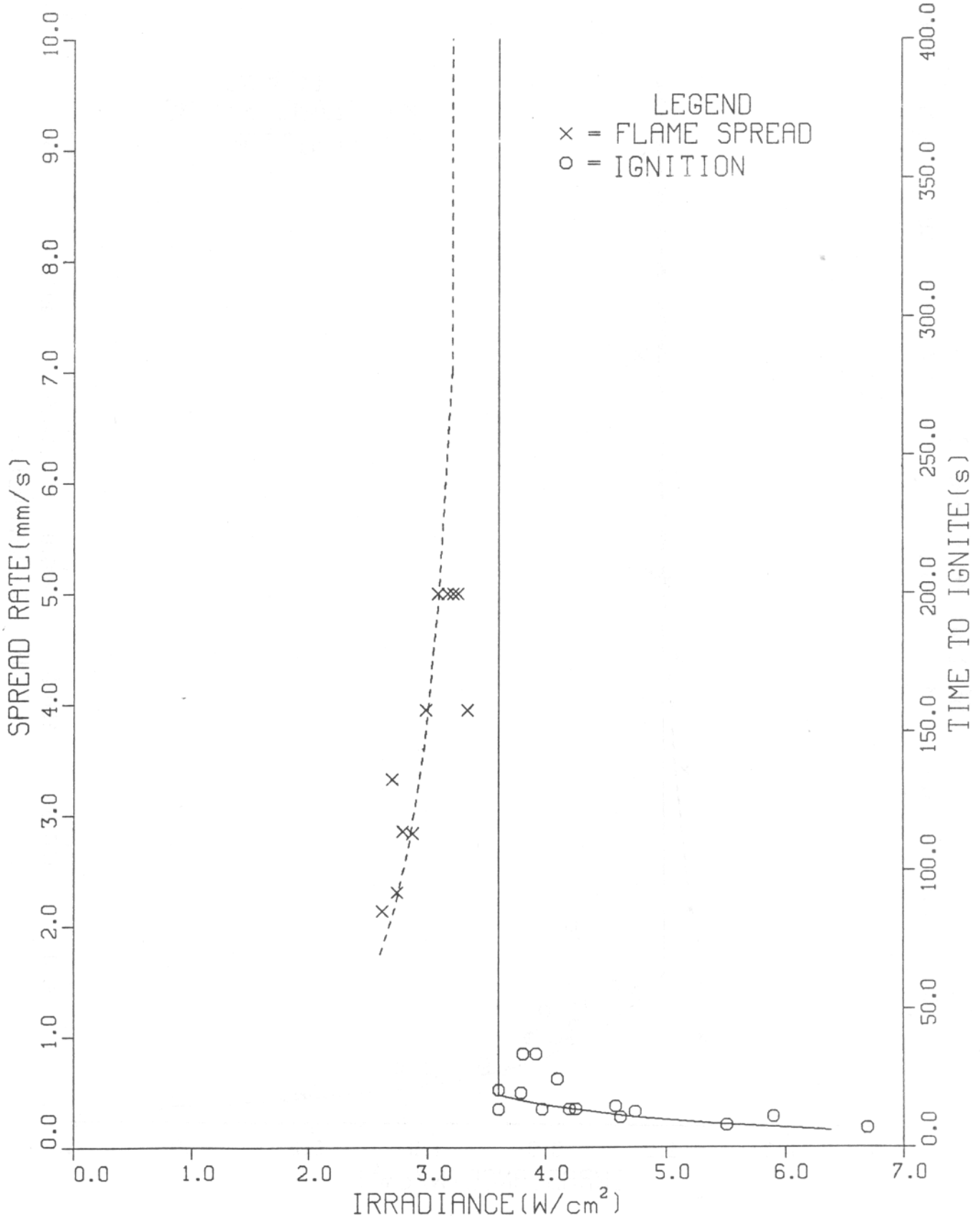

FIGURE 3.4. SPREAD AND IGNITION RESULTS FOR AIRCRAFT PANEL #2, PHENOLIC FIBERGLASS.

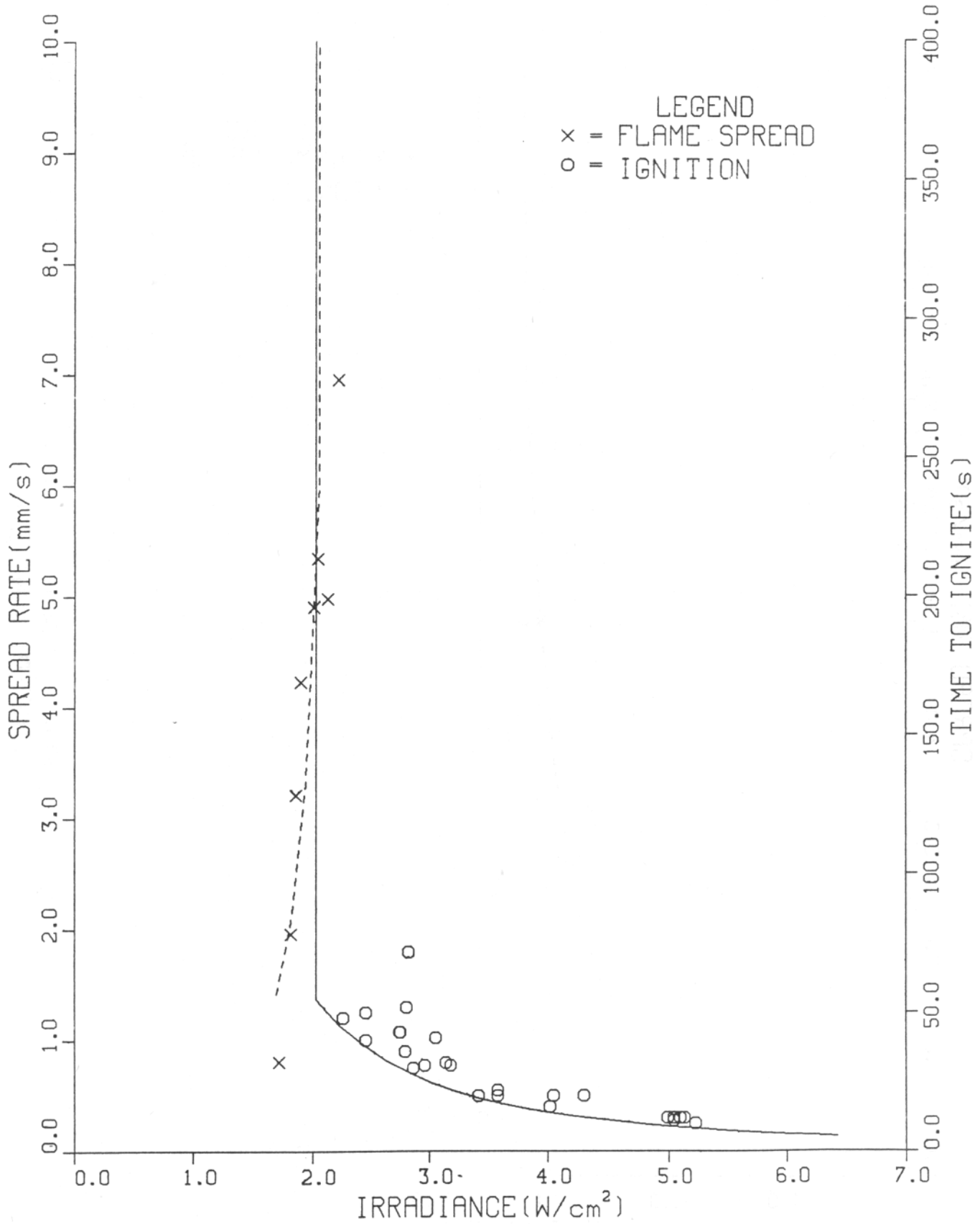

FIGURE 3.5. SPREAD AND IGNITION RESULTS FOR AIRCRAFT PANEL #3, EPOXY KEVLAR.

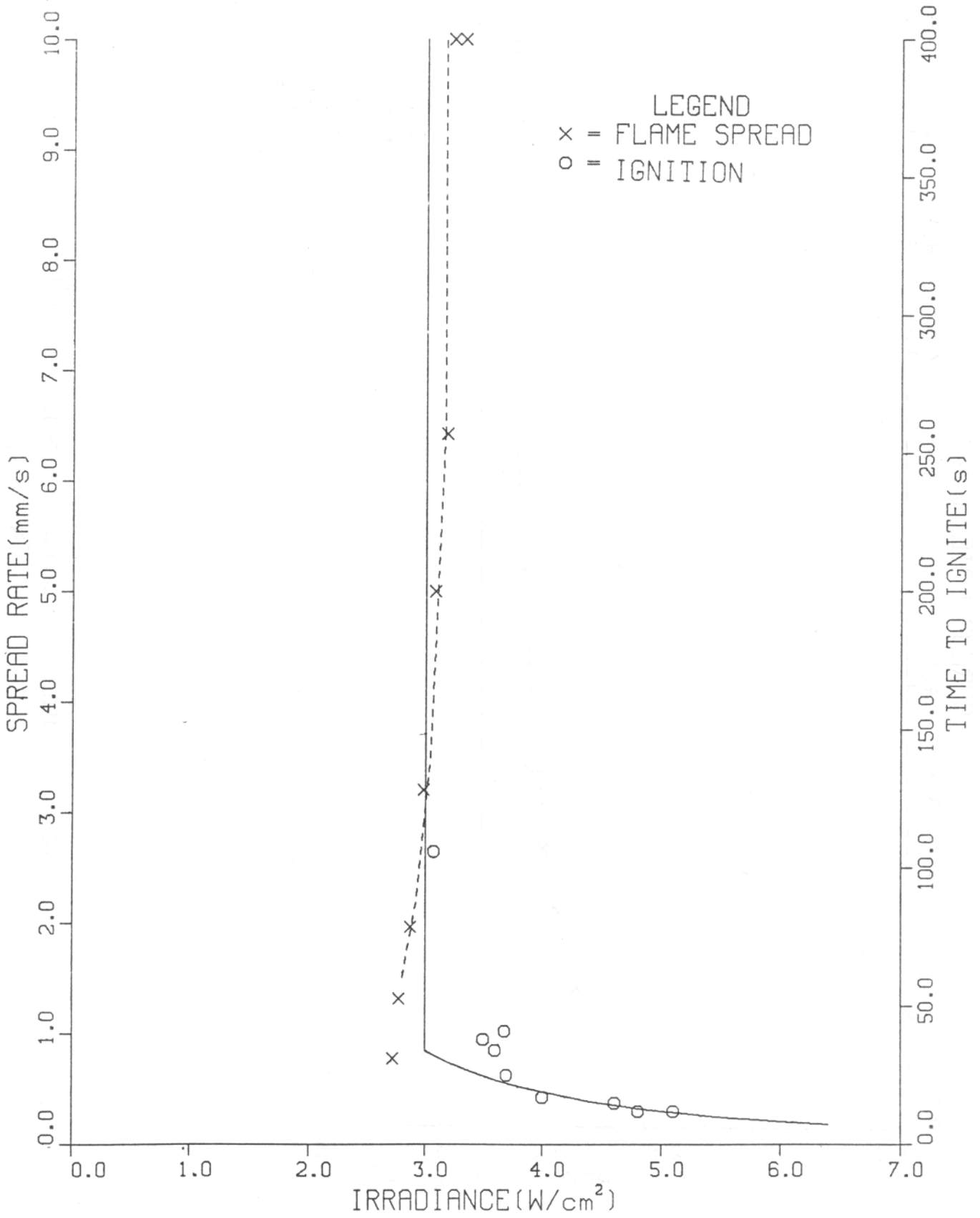

FIGURE 3.6. SPREAD AND IGNITION RESULTS FOR AIRCRAFT PANEL #4, PHENOLIC KEVLAR.

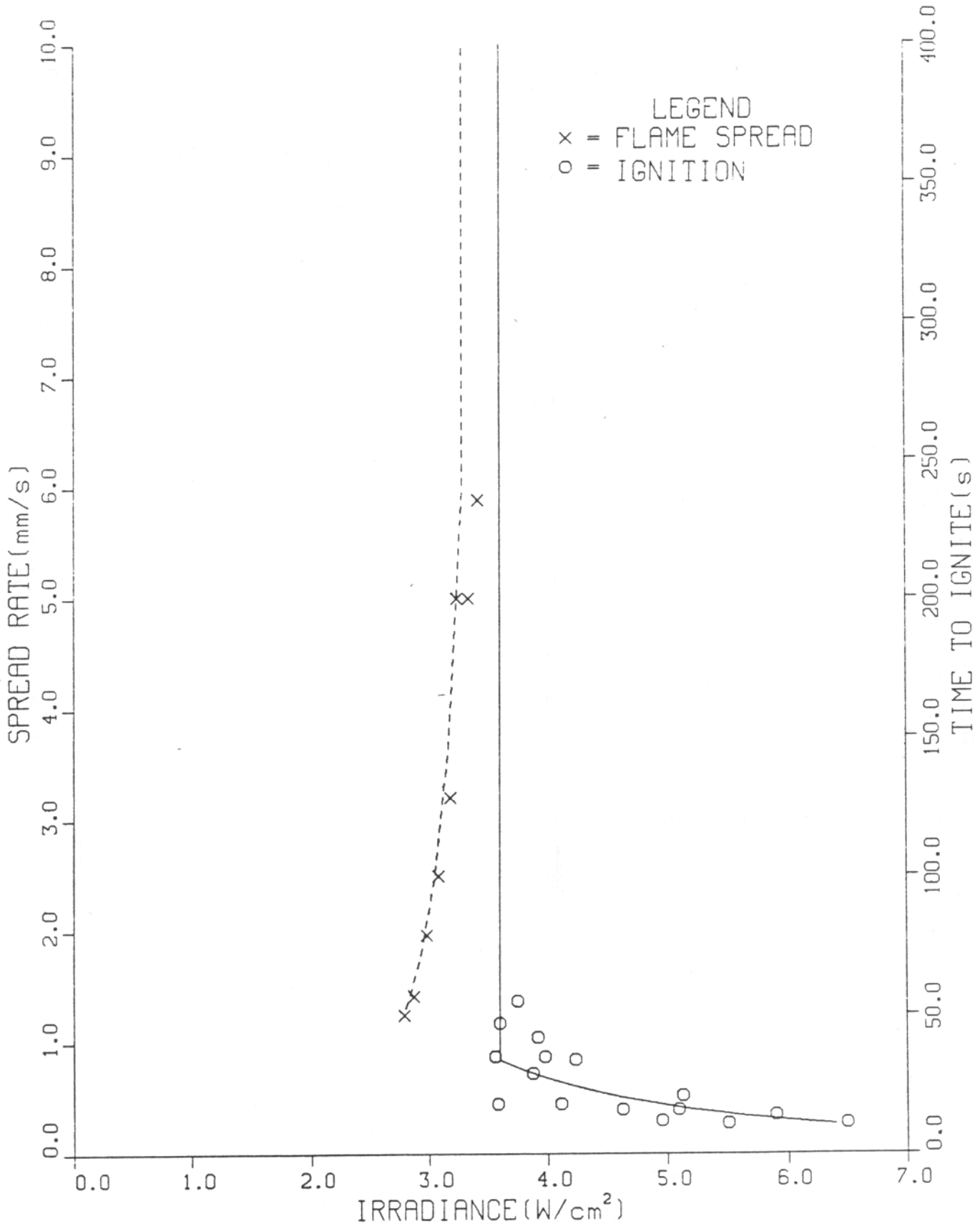

FIGURE 3.7. SPREAD AND IGNITION RESULTS FOR AIRCRAFT PANEL #5, PHENOLIC GRAPHITE.

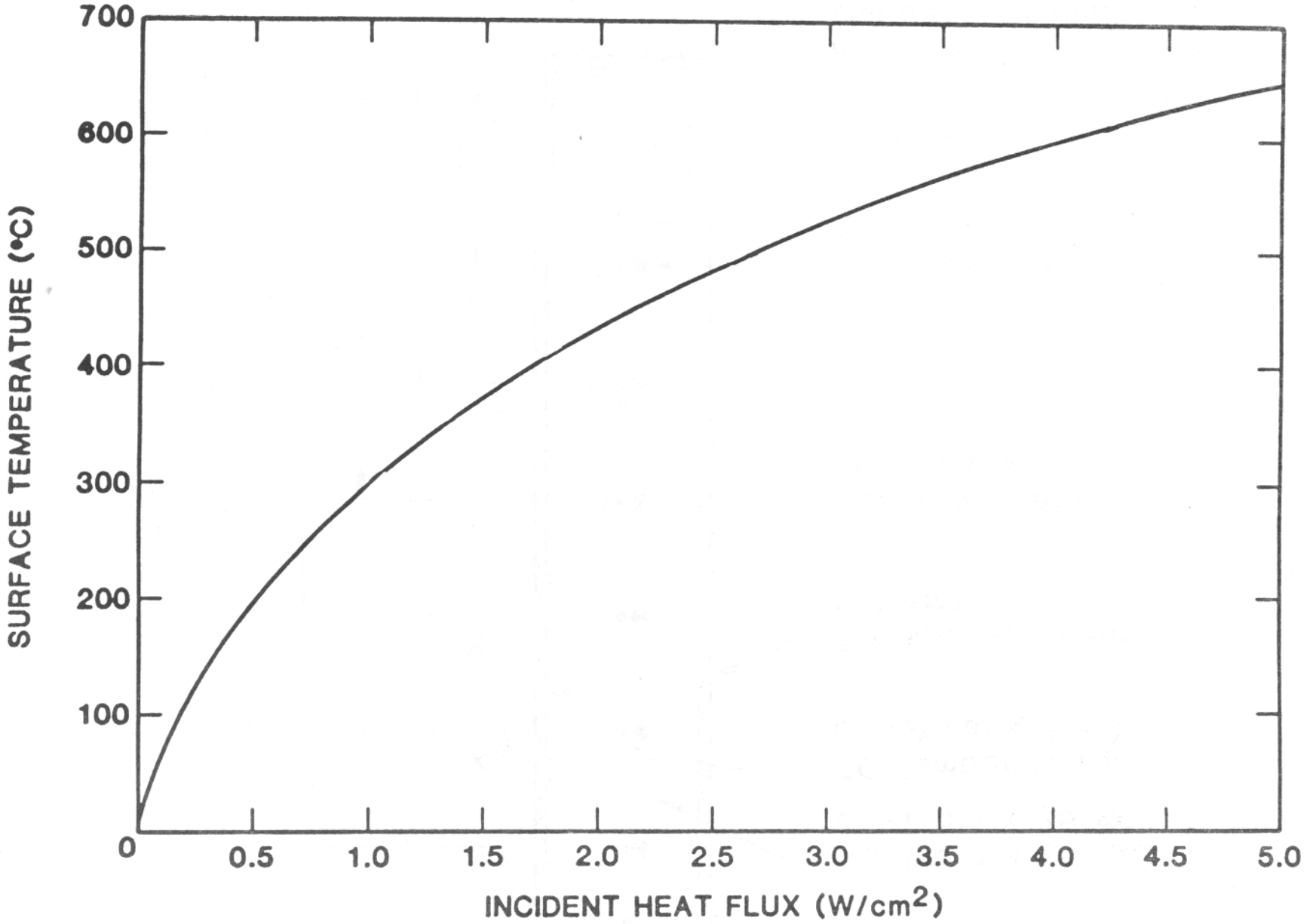

FIGURE 3.8. EQUILIBRIUM SURFACE TEMPERATURE AS A FUNCTION OF EXTERNAL RADIANT HEATING IN A TEST APPARATUS.

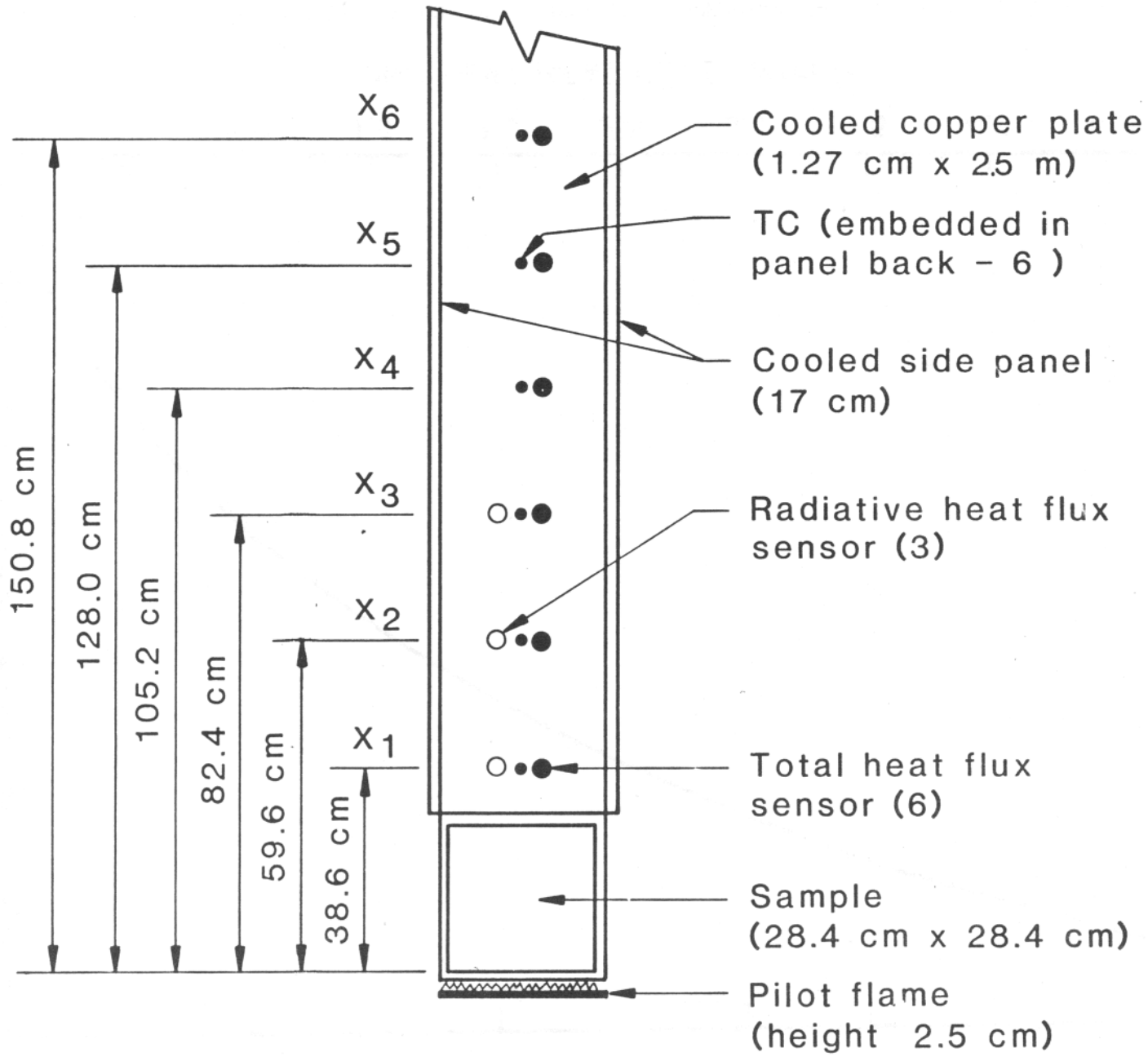

FIGURE 3.9. SCHEMATIC OF FLAME HEIGHT AND HEAT TRANSFER APPARATUS.

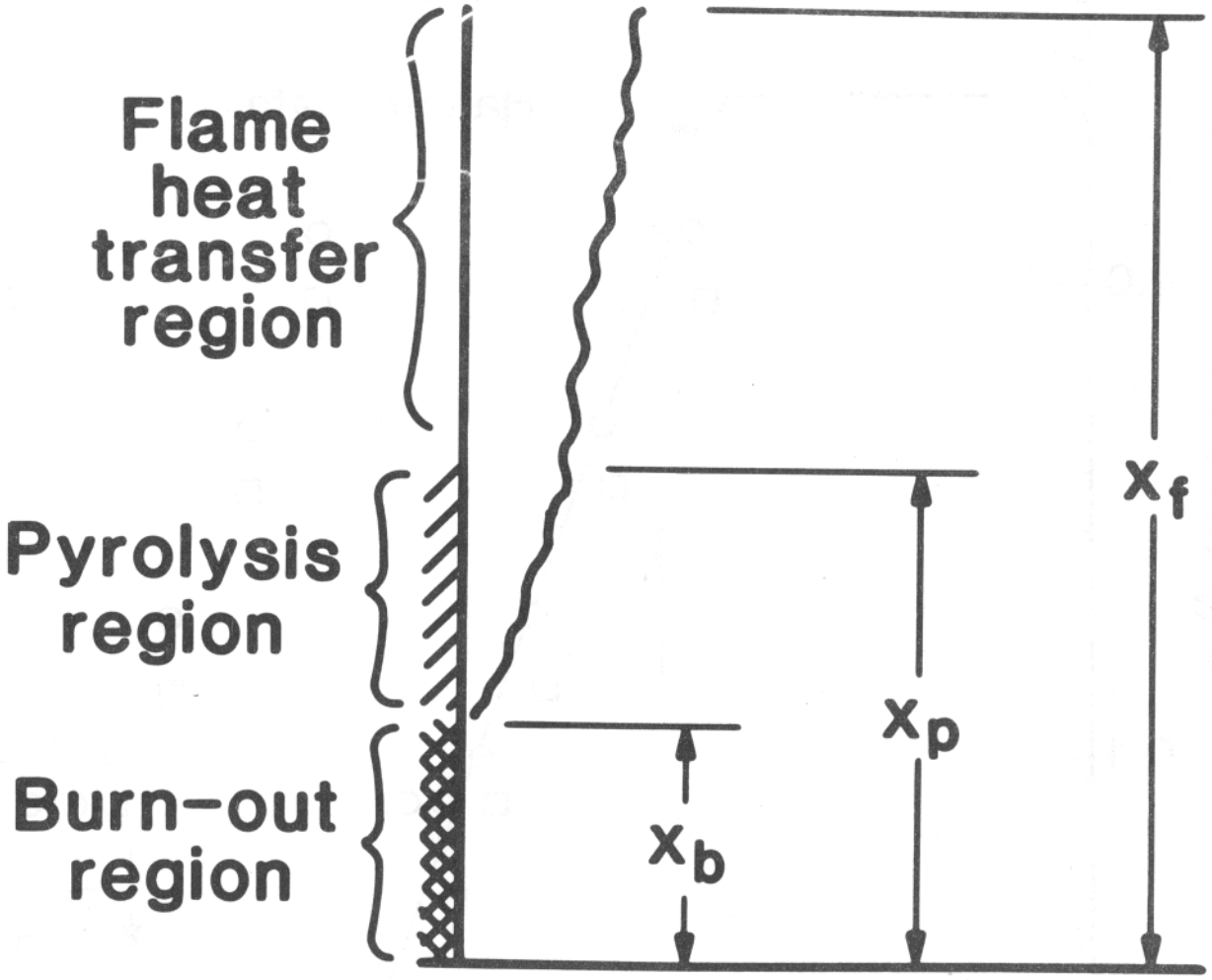

FIGURE 3.10. SCHEMATIC OF FLAME SPREAD PROBLEM.

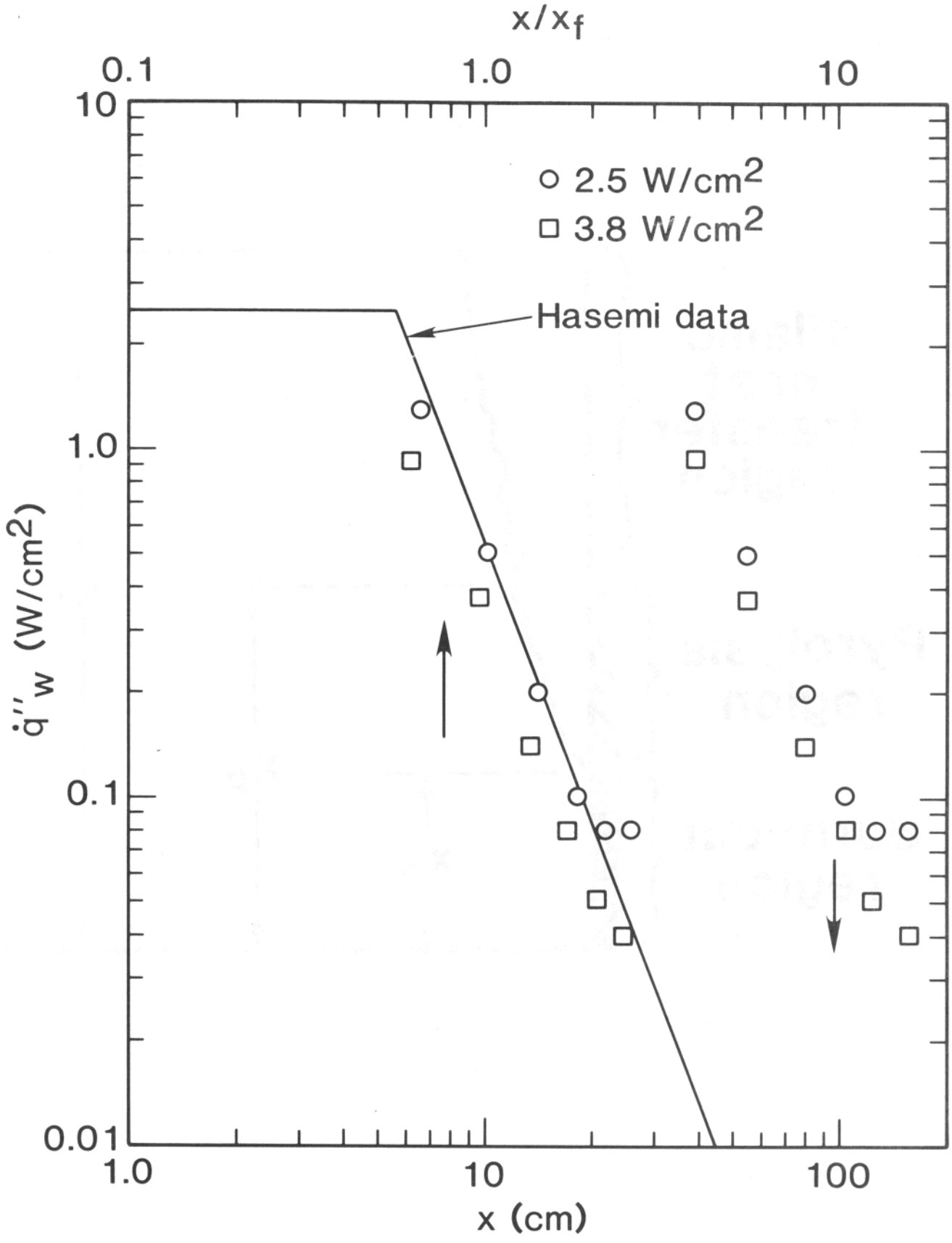

FIGURE 3.11. WALL HEAT FLUX DISTRIBUTION FOR AIRCRAFT PANEL #1, EPOXY FIBERGLASS.

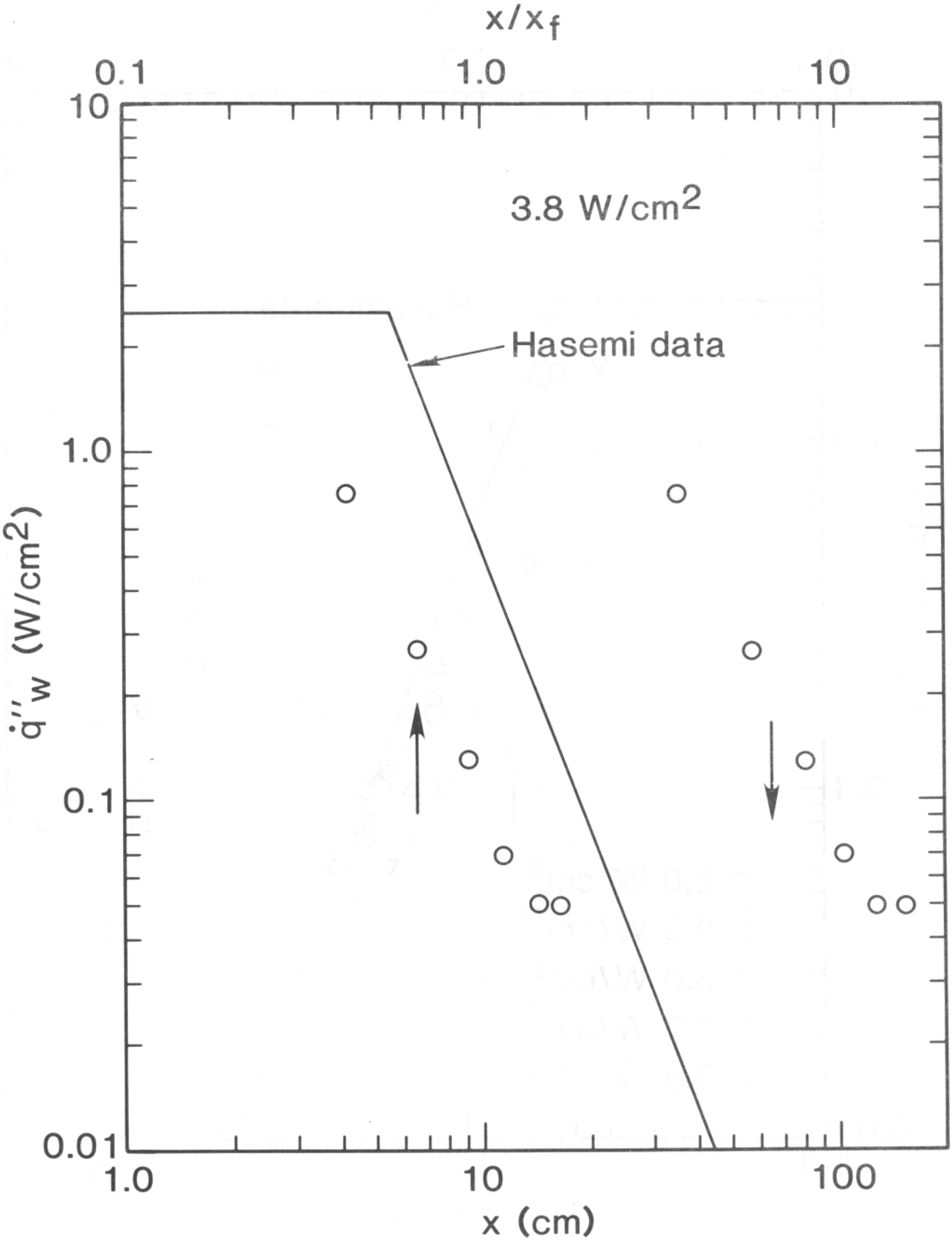

FIGURE 3.12. WALL HEAT FLUX DISTRIBUTION FOR AIRCRAFT PANEL #2, PHENOLIC FIBERGLASS.

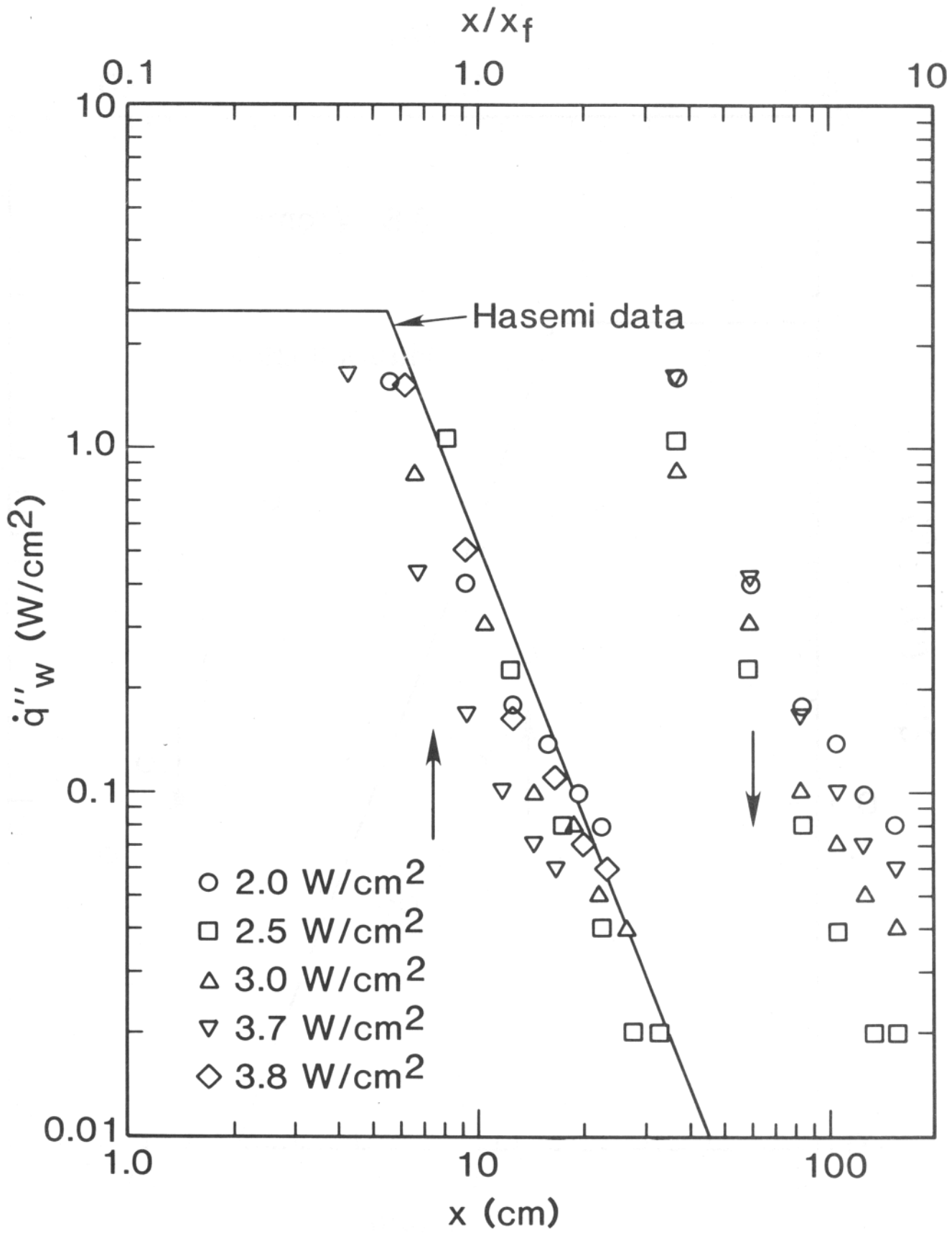

FIGURE 3.13. WALL HEAT FLUX DISTRIBUTION FOR AIRCRAFT PANEL #3, EPOXY KEVLAR.

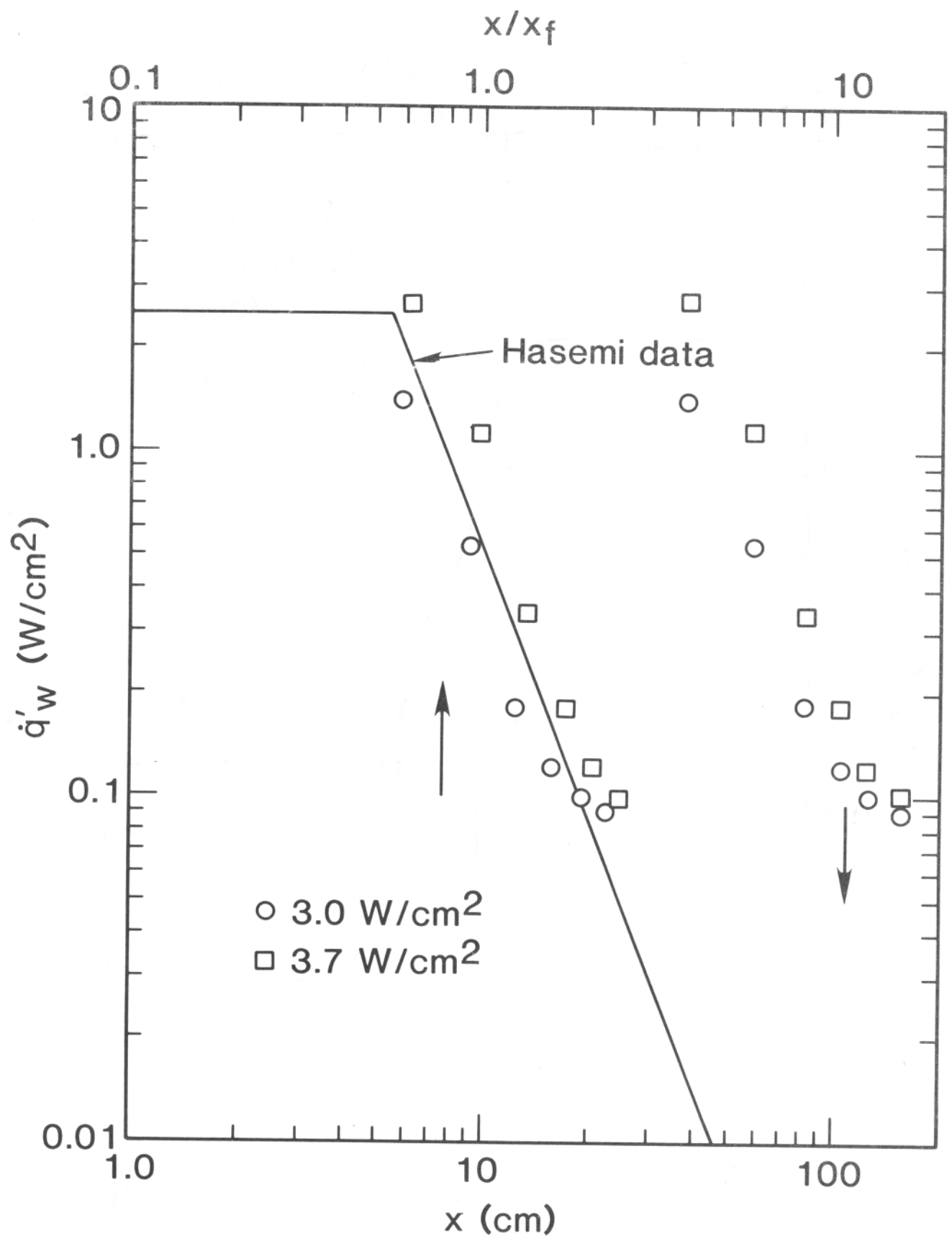

FIGURE 3.14. WALL HEAT FLUX DISTRIBUTION FOR AIRCRAFT PANEL #4, PHENOLIC KEVLAR.

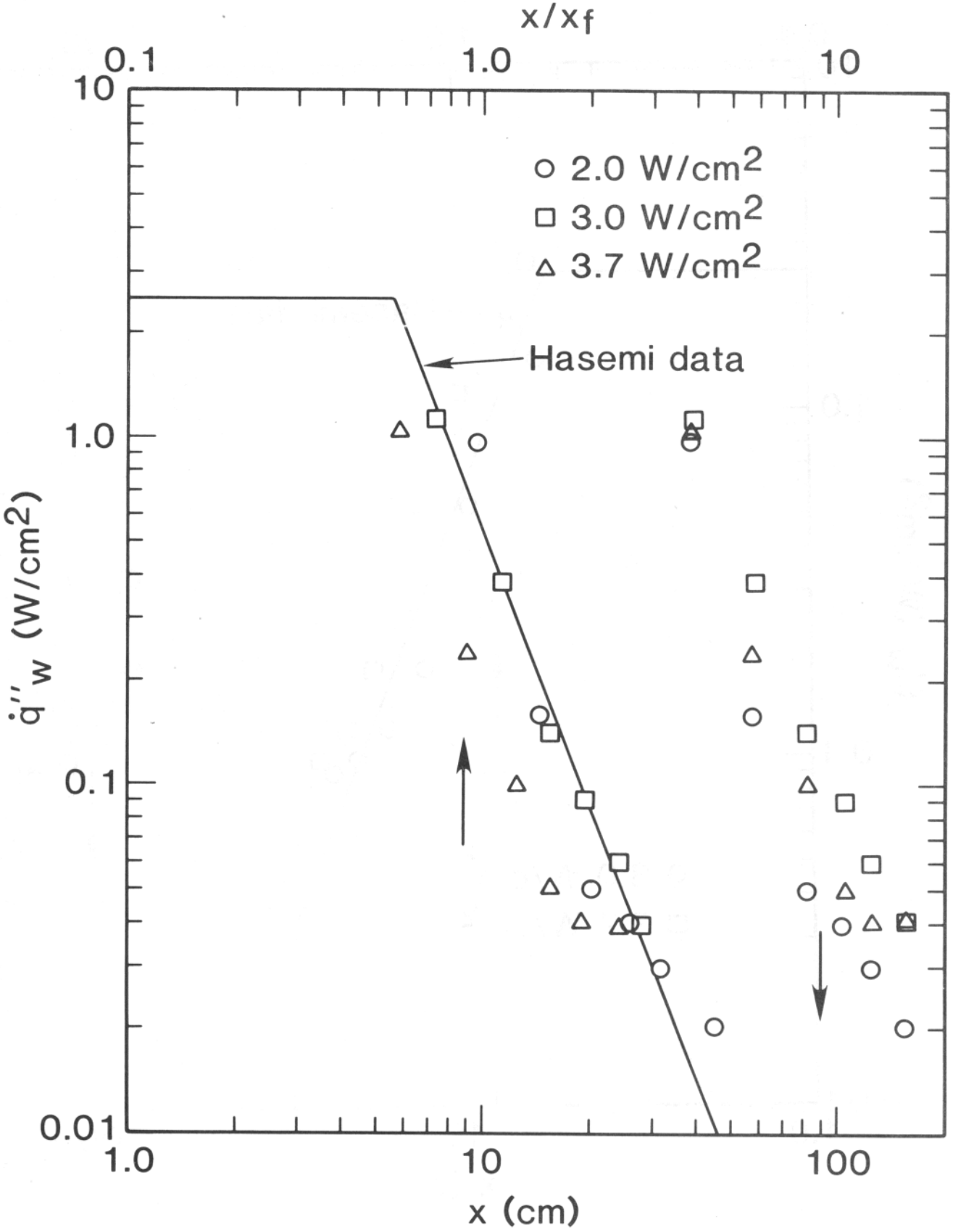

FIGURE 3.15. WALL HEAT FLUX DISTRIBUTION FOR AIRCRAFT PANEL #5, PHENOLIC GRAPHITE.

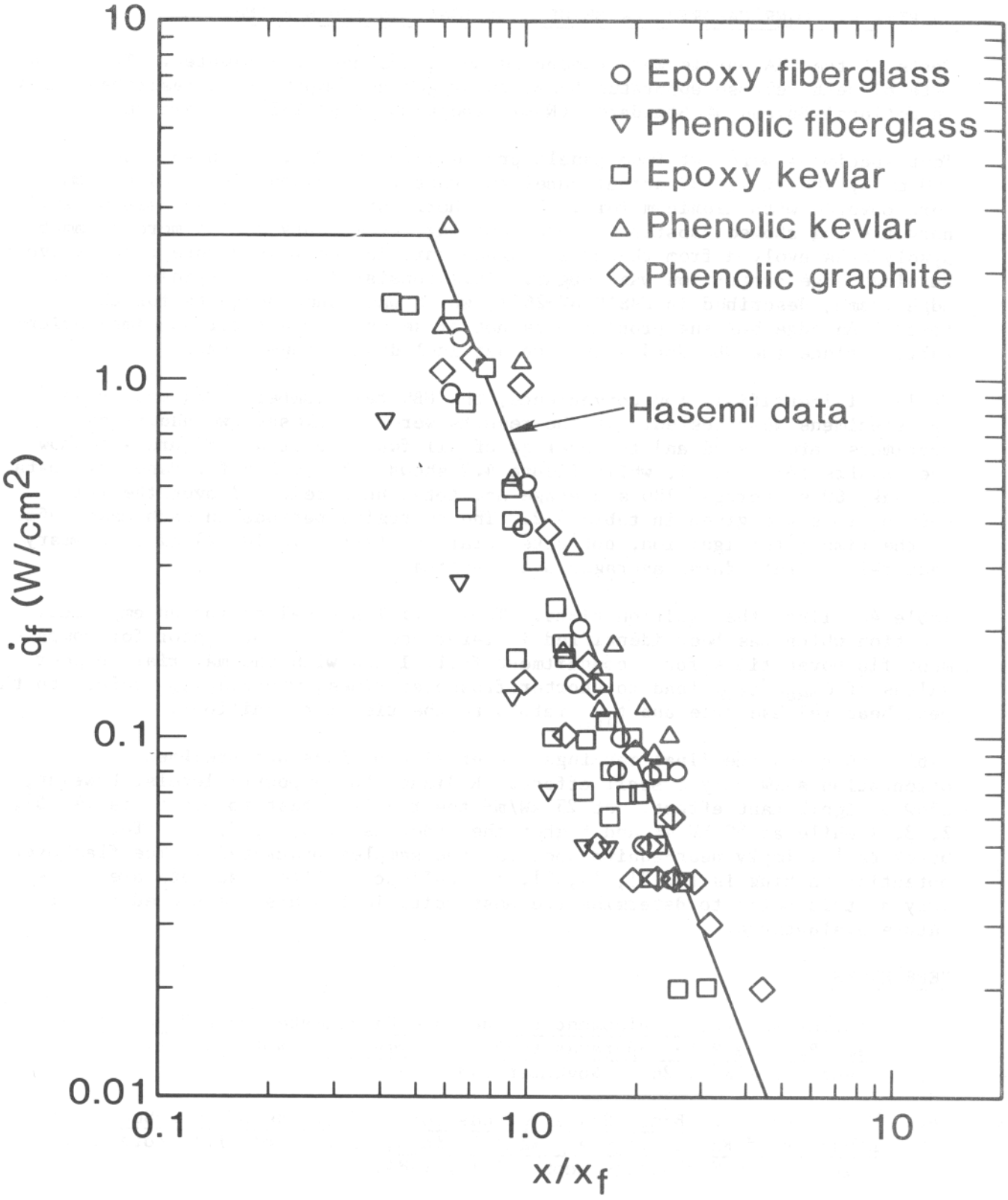

FIGURE 3.16. WALL HEAT FLUX DISTRIBUTION FOR FIVE AIRCRAFT PANELS AT 3.8 W/cm^2 EXTERNAL IRRADIANCE.

CHAPTER 4. CONE CALORIMETER RESULTS ON IGNITION AND BURNING.

Tests of the FAA panels were conducted using the cone calorimeter. This is a rate of heat release apparatus based on oxygen consumption and described fully in National Bureau of Standards (NBS) report NBSIR 82-2611 (reference 4.1).

Test specimens were cut from panels provided by the FAA. Each specimen was 100 mm by 100 mm by the actual panel thickness. Specimen sides and bottom were covered with aluminum foil. In the horizontal orientation, some preliminary testing showed substantial edge burning, presumably due to more flammable pyrolysates evolved from the core. Since this is considered unrepresentative burning, edge protection was sought. This consisted of the stainless steel edge frame, described in NBSIR 82-2611, which was found adequate for these tests. An edge burning problem does not arise in the vertical specimen orientation, since the standard sample holder includes an edge frame.

Table 4.1 identifies, for convenience, the NBS test numbers. In most cases two specimens were tested. If the results were not close, two additional specimens were tested and the average of all four reported. Figure 4.1 shows the results for Panel 1, while figure 4.2 shows the results for Panel 2. Data at peak, 60 s average, 180 s average and total heat released over the full burning time are given in table 4.2. The averaging periods in each case refer to the time after ignition, not after start of test. Table 4.3 gives summary heat release rate data, averaged over replicates.

Table 4.4 lists the ignition times. Table 4.5 lists values for an empirical function which has been identified in reference 4.2 as a predictor for compartment flashover times for a compartment fully lined with the material (higher values of $\dot{q}''_{peak}/t_{ign}$ lead to shorter flashover times, where $\dot{q}''_{peak}$ refers to the peak heat release rate and t_{ign} refers to the time for ignition).

Table 4.6 gives the final rankings. Averaging periods and specimen orientation show only a small effect. Radiant flux exposure levels, however, show a significant effect. At 25 kW/m^2 the ranking, best to worst, is [4, 5], 2, 3, 1 while at 50 kW/m^2 and higher the order is 2, 5, 1, 3, 4. (The brackets [ ] imply near-equivalence for the samples bracketed.) The flashover potential ranking is [2, 5], [4, 3], 1. Full-scale fire test data are necessary at this point to determine the most suitable bench-scale procedure for future evaluations.

REFERENCES.

4.1 Babrauskas, V., Development of the Cone Calorimeter -- A Bench-Scale Heat Release Rate Apparatus Panel on Oxygen Consumption, Nat. Bur. Stand., NBSIR 82-2611, November 1982.

4.2 Babrauskas, V., Bench-Scale Methods for Predictions of Full-Scale Fire Behavior of Furnishings and Wall Linings, Society of Fire Protection Engrs., SFPE Technology Rept. 84-10, 1984.

TABLE 4.1. TEST NUMBERS

	Panel Number				
	1	2	3	4	5
Horizontal					
25	666,667	662,663	664,665	670,671	668,669
50	623,624	629,630	625,626	621,622	627,628
75	613,614	619,620	615,616	610,611	617,618
Vertical					
25	653,654,674,675	651,652,672,673	657,659,676,677	660,661	655,658
50	633,634,678,679	635,636	631,632	637,638	639,640
75	641,642	643,644	649,650	645,646	647,648

TABLE 4.2. HEAT RELEASE DATA

	Panel Number				
Peak Values (kW/m^2)	1	2	3	4	5
Horizontal					
25	168,160	~0	104,98	N.I.	N.I.
50	257,222	123,115,152,106	185,162	178,220	191,200
75	251,307	169,191	290,323	256,245	215,186
Vertical					
25	145,163,156,169	N.I.	110,94,121,94	N.I.	N.I.
50	277,319,282,205	145,135	202,174	220,218	188,167
75	322,281	227,175	312,325	339,316	249,211
60 s Average (kW/m^2)					
Horizontal					
25	37,34	~0	28,28	N.I.	N.I.
50	85,84	32,31,45,52	105,105	97,105	64,51
75	109,113	87,84	135,147	161,151	69,70
Vertical					
25	32,28,32,30	N.I.	20,14,24,16	N.I.	N.I.
50	62,93,76,58	44,47	111,107	117,122	49,68
75	110,112	126,112	166,163	181,169	109,86
180 s Averages (kW/m^2)					
Horizontal					
25	12.5,11.3	~0	10.2,10.0	N.I.	N.I.
50	41,39	30,19,22,20	49,48	53,62	35,31
75	52,50	41,41	71,74	66,75	43,48
Vertical					
25	12.2,10.0,14.8,10.3	N.I.	5.6,5.7,9.3,6.8	N.I.	N.I.
50	29,42,30,27	25,24	56,52	55,57	36,44
75	43,49	49,44	82,89	93,74	60,50
Total Heat Release (MJ/m^2)					
Horizontal					
25	2.25,2.04	~0	1.83,1.80	N.I.	N.I.
50	8.84,7.26	5.74,6.11	8.86,8.66	11.01,14.57	6.34,5.82
75	10.14,9.00	8.25,7.99	13.46,14.23	17.04,15.92	14.43,14.52
Vertical					
25	2.19,1.80,2.66,1.85	N.I.	1.00,1.03,1.86,1.22	N.I.	N.I.
50	6.66,8.31,5.39,4.85	6.4,4.48,4.24,4.6	10.43,9.92	10.55,10.43	9.47,11.74
75	7.79,9.06	8.87,7.91	15.22,16.70	18.89,13.53	11.44,9.10

TABLE 4.3. HEAT RELEASE SUMMARY

	Panel Number 1	2	3	4	5
Peak Values (kW/m^2)					
Horizontal					
25	164	~0	101	N.I.	N.I.
50	240	124	174	199	196
75	279	175	307	251	201
Vertical					
25	158	N.I.	105	N.I.	N.I.
50	271	140	188	219	178
75	302	201	319	328	230
60 s Averages (kW/m^2)					
Horizontal					
25	36	~0	28	N.I.	N.I.
50	85	40	104	101	58
75	111	86	141	156	70
Vertical					
25	31	N.I.	19	N.I.	N.I.
50	72	46	109	120	59
75	111	119	165	175	98
180 s Averages (kW/m^2)					
Horizontal					
25	11.9	~0	10.1	N.I.	N.I.
50	40	23	49	58	33
75	51	41	73	71	46
Vertical					
25	11.8	N.I.	6.9	N.I.	N.I.
50	32	25	54	56	40
75	46	47	86	84	55
Total Heat Release (MJ/m^2)					
Horizontal					
25	2.15	~0	1.82	N.I.	N.I.
50	8.06	5.94	8.76	12.79	6.08
75	9.57	8.12	13.85	16.48	14.48
Vertical					
25	2.13	N.I.	1.28	N.I.	N.I.
50	6.30	4.93	10.18	10.55	10.61
75	8.43	8.39	15.96	16.21	10.32

TABLE 4.4. IGNITION TIMES (S)

	Panel Number				
	1	2	3	4	5
Horizontal					
25	31.6	27.9	33.0	N.I.	N.I.
50	7.8	8.0	8.8	8.0	12.2
75	4.8	4.3	3.9	4.5	5.5
Vertical					
25	29.8	N.I.	36.1	N.I.	N.I.
50	7.9	8.0	6.5	8.5	9.5
75	5.8	5.5	5.5	5.5	5.5

TABLE 4.5. FLASHOVER POTENTIAL

Orientation: Vertical

Irradiance: 50 kW/m^2

Function Tabulated: $\frac{\dot{q}''_{peak}}{t_{ign}}$

Panel Number				
1	2	3	4	5
34.3	17.5	28.9	25.8	18.7

TABLE 4.6. RANKINGS

	Best ——> Worst			
Peak, horizontal, 25 kW/m^2	[4 , 5]	2	3	1
60s, horizontal. 25 kW/m^2	[4 , 5]	2	3	1
180s, horizontal, 25 kW/m^2	[4 , 5]	2	3	1
total, horizontal, 25 kW/m^2	[4 , 5]	2	3	1
peak, vertical, 25 kW/m^2	[2 , 4 , 5]	3		1
60s, vertical 25 kW/m^2	[2 , 4 , 5]	3		1
180s, vertical, 25 kW/m^2	[2 , 4 , 5]	3		1
total, vertical, 25 kW/m^2	[2 , 4 , 5]	3		1
Typical at 25 kW/m^2	[4 , 5]	2	3	1
Peak, horizontal, 50 kW/m^2	2	3	[5 , 4]	1
60s, horizontal, 60 kW/m^2	2	5	1	[3 , 4]
180s, horizontal, 50 kW/m^2	2	5	1	3 4
total, horizontal, 50 kW/m^2	[2 , 5]	1	3	4
peak, vertical, 50 kW/m^2	2	[5 , 3]	4	1
60s, vertical, 50 kW/m^2	2	5	1	3 4
180s, vertical, 50 kW/m^2	2	1	5	[3 , 4]
total, vertical, 50 kW/m^2	2	1	[3 , 4 , 5]	
Typical at 50 kW/m^2	2	5	1	3 4
Peak, horizontal, 75 kW/m^2	2	5	4	1 3
60s, horizontal, 75 kW/m^2	5	2	1	3 4
180s, horizontal, 75 kW/m^2	2	5	1	[4 , 3]
total, horizontal, 75 kW/m^2	2	1	3	5 4
peak, vertical, 75 kW/m^2	2	5	[1 , 3 , 4]	
60s, vertical, 75 kW/m^2	5	[1 , 2]	[3 , 4]	
180s, vertical, 75 kW/m^2	[1 , 2]	5	[4 , 3]	
total, vertical, 75 kW/m^2	[1 , 2]	5	[3 , 4]	
Typical at 75 kW/m^2	2	5	1	3 4
Flashover potential	[2 , 5]	[4 , 3]	1	

Note - identical or very close values placed in brackets

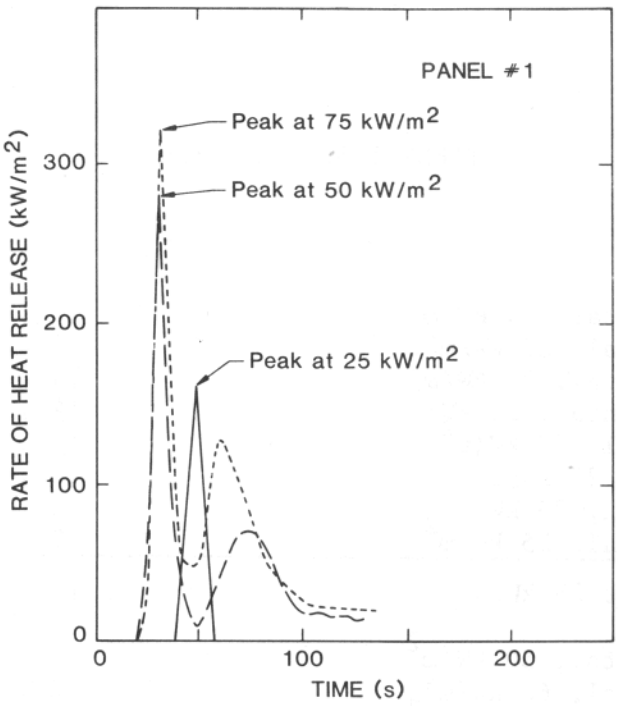

FIGURE 4.1. RESULTS FOR PANEL 1, VERTICAL ORIENTATION

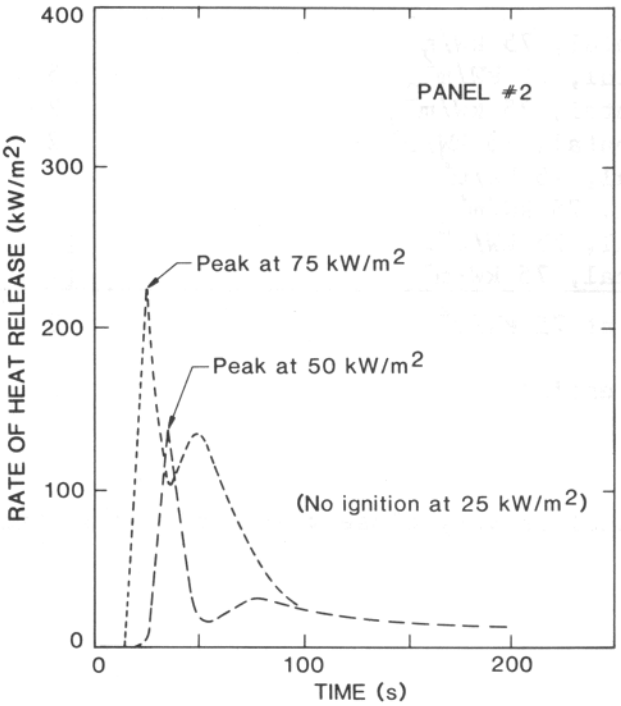

FIGURE 4.2. RESULTS FOR PANEL 2, VERTICAL ORIENTATION

CHAPTER 5. FMRC COMBUSTIBILITY APPARATUS RESULTS ON IGNITION, BURNING AND PYROLYSIS.

A study was undertaken to quantify the fire properties of the five samples of aircraft panel materials. (The list in Table 1, page 3, is repeated here for the convenience of the reader.)

1. Sample 1A (051283), Epoxy Fiberglass

Epoxy glass facing, face and back 1 ply 7781 style woven fiberglass impregnated with epoxy resin, fire retardant, and co-cured to 1/8 cell 1.8 lb Nomex® honeycomb. Weight 0.36 lb/ft^2.

2. Sample 2B (070583), Phenolic Fiberglass

Phenolic glass facing, face and back 1 ply 7781 style woven fiberglass impregnated with a modified phenolic resin, and co-cured to 1/8 cell 1.8 lb Nomex honeycomb. Weight 0.42 lb/ft^2.

3. Sample 3C (051683), Epoxy Kevlar

Epoxy Kevlar® facing, face and back 1 ply 285 style woven Kevlar impregnated with epoxy resin fire retardant, and co-cured to 1/8 cell, 1.8 lb Nomex honeycomb. Weight 0.38 lb/ft^2.

4. Sample 4D (092283), Phenolic Kevlar

Phenolic Kevlar facing, face and back 1 ply 285 style woven Kevlar impregnated with a modified phenolic resin and co-cured to 1/8 cell 1.8 lb Nomex honeycomb. Weight 0.33 lb/ft^2.

5. Sample 5E (090983), Phenolic Graphite

Phenolic graphite facing, 1 ply 8 harness satin, 3 K fiber, T-300 woven graphite, impregnated with a modified phenolic resin, and co-cured to 1/8 cell 1.8 lb Nomex honeycomb. Weight 0.36 lb/ft^2.

The following sections describe the experimental apparatus and procedure employed in the study, detail the experimental results, and present analysis and discussion of these results.

EXPERIMENTAL APPARATUS AND PROCEDURE. In the study, the Factory Mutual Small-Scale Combustibility Apparatus (Figure 5.1) was used. The apparatus and general test procedures are described in detail in References 1-3. In brief, all samples were blackened to maximize their absorption of thermal radiation and placed in an aluminum dish. The samples were cut into 10 cm x 10 cm squares and mounted horizontally on a 10 cm x 10 cm x 1.3 cm thick Cotronics 360 ceramic board (~13 lb/ft^3 density). Each sample was placed inside the apparatus (identified as sample in Figure 5.1) and surrounded by a quartz tube (0.17 m dia and 0.61 m long). In the apparatus, the sample platform was attached to a load-cell assembly (Universal Transducing Cell, Model No. UC3, Gould, Inc., Oxnard, CA)* for monitoring the fuel vapor generation rate.

*Any reference to commercial products does not imply endorsement by the U.S. Federal Government.

Metered dry air was introduced at the bottom of the apparatus at a known rate (measured by electronic flowmeter Model 2015, Thermo System, Inc., St. Paul, MN) and passed through a layer of glass wool for even flow distribution. This air flow rate ensured that the fire ventilation was known. The inlet air oxygen concentration was measured by an oxygen analyzer (Model 755, Beckman Instruments, Inc., Fullerton, CA). In this study, normal air and air diluted with nitrogen was used.

In the apparatus, a small premixed, ethylene-air pilot flame about 0.01 m long was positioned about 0.01 m above the sample surface to ignite fuel vapors for piloted ignition. Four high-density radiant heaters with tungsten quartz lamps (Model 5208, Research Inc., Minneapolis, MN), placed coaxially, were used as a radiant heat source. A single controller (Model 646, Research Inc., Minneapolis, MN) controlled all four radiant heaters. The radiant heat flux at the sample location was precalibrated with a water-cooled heat flux gage (Model 12-10-GTW63, Medtherm Corporation, Huntsville, AL) for different controller settings covering the range from 0 to about 70 kW/m^2.

In the apparatus the fire products were diluted and well mixed with ambient air as they were captured in the sampling duct. The following measurements were made in the duct: total mass and volumetric flow rates of product-air mixtures, using pressure transducers (Model 239, Setra Systems Inc., Natick, MA); bulk gas temperature (K-type chromel-alumel thermocouples); optical transmission through 'smoke' (Photo Sensor, Model UTD-500D, United Detector Technology, California in a 0.10 m path length of a collimated light source across the sampling duct at three wavelengths, 0.46, 0.63 and 1.1 μ) and concentrations of CO_2, CO, total gaseous hydrocarbons, water, and O_2 (CO_2 IR-Analyzer, Model B64; and Hydrocarbon Flame-Ionization Analyzer, Model 400. All instruments were purchased from Beckman Instruments, Inc., Fullerton, CA; for H_2O, System 1200 APS Condensation Dew Point Hygrometer, General Eastern, Watertown, MA; and for O_2, Model OA Oxygen Analyzer, SYBRON/Tayler, Rochester, NY).

The output from all instruments, as well as output from the load cell and inlet air electronic flowmeter, were stored at regular intervals (2 s or longer, depending on the test) by a MINC analog-to-digital data acquisition system (Model LSI 11/03, Digital Equipment Corporation, Northboro, MA).

The general experimental procedure consisted of: 1) initializing the MINC with pertinent sample information, experimental conditions, gas analyzer ranges, etc.; 2) turning on the inlet air flow exhaust blower and pilot flame; 3) weighing the sample and placing it in the apparatus; 4) raising the water-cooled shield around the sample using the computer; 5) turning on the radiant heaters 5 min before the test begins with the controller set at the desired heat flux and taking 1 min of background data; 6) starting the test data acquisition as the shield is lowered by the computer; and 7) measuring the time to ignition. (All other measurements are taken automatically by the computer.) Data acquisition was generally stopped when the sample was consumed.

The test conditions used in the study are summarized in table 5.1. The elemental compositions of the panel materials were not measured in this study; thus, literature data were used to calculate various properties as listed in table 5.2, where k_{O_2} is the oxygen-to-fuel stoichiometric ratio and k_{CO_2}, k_{CO}, k_{H_2O} and k_{HC} are theoretical maximum yields of the compounds.

TABLE 5.1. RADIANT FLUX USED IN THE EXPERIMENTS FOR AIRCRAFT PANEL MATERIALS[a]

Experiments	Samples				
	1A (051283) Epoxy Fiberglass	2B (070583) Phenolic Fiberglass	3C (051683) Epoxy Kevlar	4D (092283) Phenolic Kevlar	5E (090983) Phenolic Graphite
[1] Piloted Ignition[b] (normal air)	7 fluxes (10 to 61 kW/m^2)	9 fluxes (10 to 61 kW/m^2)	8 fluxes (10 to 61 kW/m^2)	10 fluxes (10 to 61 kW/m^2)	8 fluxes (10 to 61 kW/m^2)
[2] Pyrolysis[c] (N_2)	61 kW/m^2	61 kW/m^2	61 kW/m^2	61 kW/m^2	61 kW/m^2
[3] Oxidative Pyrolysis[c] (~10% O_2)	61 kW/m^2 39 kW/m^2	61 kW/m^2 39 kW/m^2	61 kW/m^2 39 kW/m^2	61 kW/m^2 39 kW/m^2	61 kW/m^2 39 kW/m^2
[4] Combustion[d] (normal air)	61 kW/m^2 39 kW/m^2 26 kW/m^2	61 kW/m^2 39 kW/m^2 26 kW/m^2	61 kW/m^2 39 kW/m^2 26 kW/m^2	61 kW/m^2 39 kW/m^2 26 kW/m^2	61 kW/m^2 39 kW/m^2 26 kW/m^2

[a] ~10x10 cm horizontal samples, surface coated with graphite powder; all edges covered with ~1.7 cm wide aluminum foil (~0.5 cm of the surface covered all around); backing ~10x10x1.3 cm thick Cotronics 360 ceramic board (~13 lb/ft^3 density)

[b] premixed ethylene-air pilot flame, ~1 cm long and ~1 cm above the sample surface near the edge

[c] flow rate ~1.7×10^{-3} m^3/s (velocity ~0.07 m/s)

[d] flow rate ~3.4×10^{-3} m^3/s (velocity ~0.14 m/s)

TABLE 5.2. PROPERTIES USED IN THE CALCULATIONS OF HEAT RELEASE RATES AND GENERATION RATES OF CHEMICAL COMPOUNDS

Polymer	Chemical Formula	Net Heat of Complete Combustion (kJ/g)	Air-to-Fuel Stoichiometric Ratio	Theoretical Maximum Yields								
				Combustion					Pyrolysis			
				k_{O_2}	k_{CO_2}	k_{CO}	k_{H_2O}	k_{HC}	k_{CO_2}	k_{CO}	k_{H_2O}	k_{HC}
Epoxy-Novolak	$CH_{1.1}O_{0.20}$[a]	29.8	9.9	2.3	2.70	1.72	0.61	0.27[1] 0.80[2]	0.27	0.34	0.22	0.27
Phenolic foam[b] (32/kg/m^3)	$CH_{1.05}O_{0.24}$	37.6	9.3	2.2	2.61	1.66	0.56	0.25	0.31	0.40	0.26	0.25

[a] From Modern Plastics Encyclopedia, McGraw-Hill, New York, NY, 1972

[b] From Materials Bank Compendium of Fire Property Data, Products Research Committee, National Bureau of Standards, Center for Fire Research, Washington, D.C., 1980

1 assumed Methane

2 assumed $CH_{1.1}$

EXPERIMENTAL RESULTS. The experimental results are presented in tables 5.3 and 5.4, where

$\dot{q}''_e$ = external heat flux from the radiant heaters (kW/m^2);

O_2 = oxygen concentration in the inlet gas supplied to the sample (volume %);

$\dot{G}''_f$ = mass generation rate of fuel vapors per unit surface area of the sample (g/m^2s);

$\dot{G}''_{CO}$, $\dot{G}''_{CO_2}$, $\dot{G}''_{H_2O}$, and $\dot{G}''_{Hvd}$ = mass generation rate of CO, CO_2, H_2O and hydrocarbons respectively per unit surface area of the sample (g/m^2s);

$\dot{D}''_{O_2}$ = mass depletion rate of oxygen per unit sample surface area (g/m^2s);

OD = optical density per unit path length; $(1/\ell)$ ℓn (I_o/I) at three wavelengths of the light source;

$\dot{Q}''_A$ = actual heat release rate per unit sample surface area (kW/m^2);

$\dot{Q}''_C$ = convective heat release rate per unit sample surface area (kW/m^2); and

$\dot{Q}''_R$ = radiative heat release rate per unit sample surface area (kW/m^2).

The data in table 5.4 are for the peak burning or pyrolysis conditions.

ANALYSIS. The data are analyzed in the following manner in order to provide more generally applicable parameters. The attempt here is to provide results that may transcend the scale and specific dependence on the combustibility apparatus. The consistency of these analyses and correlations is one measure of their appropriateness to general predictive calculations, but does not constitute their fundamental validity.

Paint Peeling and Piloted Ignition of the Fuel Vapors for Aircraft Panel Materials. The data for time to paint peeling (t_p) and time to ignition (t_{ig}) at various external heat flux values listed in table 5.3 are found to follow the following relationship:

$$1/t = \frac{\dot{q}''_e - \dot{q}''_{cr}}{E} \qquad (1)$$

where $\dot{q}''_{cr}$ = heat flux at or below which ignition is not expected and E = energy (kJ/m^2) needed for ignition. The data for $\dot{q}''_{cr}$ and E are listed in table 5.5.

Generation Rate of Fuel Vapors ($\dot{G}''_f$). The generation rate of fuel vapors, $\dot{G}''_f$, can be expressed as

Pyrolysis

$$\dot{G}''_f = \frac{\dot{q}''_e - \dot{q}''_{rr}}{L} \qquad (2)$$

where L = heat of gasification of the sample (kJ/g); $\dot{q}''_{rr}$ = surface reradiation loss (kW/m^2).

TABLE 5.3. TIME TO PAINT, PEELING AND (t_p) PILOTED IGNITION (t_{ig}) OF FUEL VAPORS FOR AIRCRAFT PANEL MATERIALS IN SECONDS[a]

Sample	$\dot{q}''_e$ (kW/m^2)										
	10	15	20	26	31	33	35	39	50	56	61
1A (051283) Epoxy fiberglass											
Paint[b]	NP	-	-	23.6	15.5	-	10.8	8.9	6.8	-	4.7
Surface	NI	-	-	45.4	33.1	-	16.9	12.6	9.6	-	7.2
3C (051683) Epoxy kevlar											
Paint[b]	NP	-	-	-	-	-	-	7.6	5.4	-	4.2
Surface	NI	-	266	80.2	18.8	-	-	11.8	8.4	-	6.2
Back surface	-	-	-	49.6	29.7	-	24.5	21.4	-	-	-
2B (070583) Phenolic fiberglas											
Paint[b]	NP	-	32.2	-	13.6[c]	13.8[c]	12.2	9.7	6.8	6.1	5.2
Surface	NI	-	NI	-	NI	NI	142	12.7	10.5	7.6	6.8
4D (092283) Phenolic kevlar											
Paint[b]	90.0	42.1	26.5	18.9	14.0	-	11.6	9.3	7.5	7.0	5.7
Surface	NI	NI	-	28.7	30.9	-	17.4	12.9	9.7	9.2	7.1
5E (090983) Phenolic graphite											
Paint[b]	NP	-	41.2	28.0	18.6	-	15.9	13.6	9.2	-	7.1
Surface	NI	-	NI	NI*	12.1	-	19.0	17.1	11.9	-	8.2

[a] average of 2 to 5 experiments; sample: horizontal, ~10x10 cm, surface coated with fine graphite powder; all edges covered with aluminum foil, including ~0.5 cm of the surface; sample backing: ~10x10x1.3 cm thick Cotronics 360 ceramic board (~13 lb/ft^3 density); pilot flame: premixed ethylene-air, ~1 cm long, ~1 cm above the surface near an edge. [b] peeling time; [c] flame not sustained;

NP-no peeling; NI-no ignition; -: data not taken. *very close to critical heat flux, occasional ignitions at an average time of 366 s.

TABLE 5.4. COMBUSTION/PYROLYSIS DATA FOR AIRCRAFT PANEL MATERIALS[α]

Sample	$\dot{q}''_e$ (kW/m^2)	O_2 (%)	$\dot{G}''_f$ (g/m^{2}s)	$\dot{G}''_{CO}$ (g/m^{2}s)	$\dot{G}''_{CO_2}$ (g/m^{2}s)	$\dot{D}''_{O_2}$ (g/m^{2}s)	$\dot{G}''_{H_2O}$ (g/m^{2}s)	$\dot{G}''_{Hyd}$ (g/m^{2}s)	OD(m^{-1}) 0.46 (μ)	0.63 (μ)	1.1 (μ)	$\dot{Q}''_A$ (kW/m^{2}s)	$\dot{Q}''_C$ (kW/m^{2}s)	$\dot{Q}''_R$ (kW/m^{2}s)	Fuel Vaporized (% wt)
1A (051283)	61	20.9	16.2	1.9	13.7	14.0	3.6	0.25	19.0	6.2	3.4	173	104	69	46
Epoxy fiberglass	39	20.9	12.6	1.4	10.2	13.7	-	0.21	7.8	4.8	2.5	150	74	76	45
	26	20.9	7.0*	0.93*	7.9*	8.3*	2.5*	0.15*	6.9*	4.3*	2.2*	101*	54*	47*	39
	61	9.85	15.1	0.46	1.03	NA	0.86	0.41	8.3	6.5	3.9	NA	NA	NA	44
	39	9.95	9.0	0.13	0.77	NA	-	0.12	4.8	4.3	3.5	NA	NA	NA	41
	61	1.67	12.0	0.32	0.79	NA	-	0.39	8.9	6.6	4.6	NA	NA	NA	43
3C (051683)	61	20.9	17.6	1.45	15.4	16.2	3.7	0.23	9.9	6.4	3.6	194	138	56	74
Epoxy kevlar	39	20.9	14.0	1.38	12.2	14.2	2.8	0.25	6.4	3.8	2.0	164	67	97	65
	26	20.9	7.7*	0.93*	7.9*	9.8*	-	0.14*	4.6*	2.9*	1.4*	110*	53*	57*	51
	61	9.61	11.9	0.68	1.2	NA	-	0.37	7.1	5.5	4.3	NA	NA	NA	66
	39	10.2	6.1	0.20	0.58	NA	-	0.086	2.5	1.7	1.5	NA	NA	NA	48
	61	2.20	-	0.40	0.74	NA	-	0.24	6.2	5.0	3.5	NA	NA	NA	62
	61	2.10	11.0	0.34	0.65	NA	-	0.22	6.8	5.3	3.7	NA	NA	NA	61
2B (070583)	61	20.9	11.9	0.22	15.9	12.9	3.3	0.012	1.7	1.3	0.57	228	69	159	33
Phenolic fiberglass	39	20.9	6.0	0.18	8.7	9.9	1.8	0.013	1.0	0.56	0.37	150	22	128	32
	39	20.9	6.3	0.21	10.6	(10.9)	-	0.021	1.2	0.86	0.44	155	40	115	30
	26	20.9	No Ignition												
	61	9.59	8.1	0.37	0.84	NA	-	0.13	1.4	1.4	0.71	NA	NA	NA	29
	39	9.85	2.7	0.082	0.25	NA	-	0.020	0.28	0.22	0.06	NA	NA	NA	24
	61	2.12	6.0	0.19	0.41	NA	-	0.13	3.5	2.3	1.1	NA	NA	NA	28
4D (092283)	61	20.9	19.5	1.38	21.1	16.4	5.0	0.21	8.2	5.0	2.8	302	102	200	76
Phenolic kevlar	39	20.9	9.4	0.88	14.2	(16.1)	3.4	0.11	3.5	2.4	1.0	216	89	127	56
	26	20.9	5.7	0.57	6.3	(8.8)	1.4	0.055	1.7	1.4	0.63	98	68	30	37
	61	9.53	12.7	0.44	1.23	NA	-	0.29	7.0	5.4	3.7	NA	NA	NA	65
	39	10.4	5.5	0.13	0.50	NA	-	0.080	3.3	2.9	2.0	NA	NA	NA	43
	61	2.01	12.6	0.22	0.65	NA	-	0.20	7.6	5.3	3.6	NA	NA	NA	58
5E (090983)	61	20.9	8.4	0.17	13.7	11.9	2.9	0.020	2.7	1.7	1.1	202	81	121	32
Phenolic graphite	39	20.9	5.6	0.18	9.6	(10.5)	-	0.014	1.7	0.75	0.47	141	35	106	29
	26	20.9	No Ignition												
	61	9.42	-	0.36	0.80	NA	-	0.16	2.8	1.8	0.89	NA	NA	NA	30
	61	9.95	5.6	0.36	0.86	NA	-	0.13	3.2	2.0	0.93	NA	NA	NA	30
	39	10.5	3.5	0.12	0.40	NA	-	0.032	0.62	0.56	0.18	NA	NA	NA	23
	61	2.18	5.3	0.20	0.48	NA	-	0.12	2.4	1.7	0.80	NA	NA	NA	28
	61	2.10	5.7	0.18	0.52	NA	-	0.12	2.4	1.6	0.74	NA	NA	NA	28

[α]For peak burning or pyrolysis conditions; sample surface area ~0.0081 m^2; *unstable combustion; - problems with the measurements
NA = not applicable

Combustion

$$\dot{G}''_f = \frac{\dot{q}''_e + \dot{q}''_{fs} - \dot{q}''_{rr}}{L} \qquad (3)$$

where $\dot{q}''_{fs}$ = flame heat flux (kW/m^2).

If we assume $\dot{q}''_{rr} \approx \dot{q}''_{cr}$ (table 5.5), then values of L and $\dot{q}''_{fs}$ can be calculated from the $\dot{G}''_f$ values using eqs. (2) and (3). The calculated values are listed in table 5.6.

Generation Efficiencies of Heat and Chemical Compounds, Oxygen Depletion Efficiency and "Smoke Mass Attenuation Coefficient". The generation efficiency of heat (χ_i) can be expressed as

$$\chi_i = \dot{Q}''_i / \dot{G}''_f \, H_T \quad , \qquad (4)$$

where i = actual, convective or radiative.

From the data for $\dot{Q}''_i$ and $\dot{G}''_f$ given in table 5.4 and from the data for H_T given in table 5.2, χ_i can be calculated.

The generation efficiencies of chemical compounds (f_j) can be expressed as

$$f_j = \dot{G}''_j / \dot{G}''_f \, k_j \quad , \qquad (5)$$

where j = CO, CO_2, hydrocarbons or H_2O.

From the data for $\dot{G}''_j$ and $\dot{G}''_f$ given in table 5.4 and k_j given in table 5.2, f_j can be calculated. From the carbon atom balance,

$$f_c = 1 - f_{CO} + f_{CO_2} + f_{hyd} \quad , \qquad (6)$$

where f_c = generation efficiency of the mixture of carbon containing compounds other than CO, CO_2, and hydrocarbons.

The oxygen depletion efficiency $\left(d_{O_2}\right)$ can be expressed as

$$d_{O_2} = \dot{D}''_{O_2} / \dot{G}''_f \, k_{O_2} \quad . \qquad (7)$$

where d_{O_2} can be calculated from the data for $\dot{D}''_{O_2}$ and $\dot{G}''_f$ given in table 5.4 and k_{O_2} given in table 5.2.

The smoke mass attenuation coefficient (σ) can be expressed as

$$\sigma = OD / \dot{G}''_f \, a/\dot{V}_T \quad , \qquad (8)$$

where a = surface of the fuel (m^2); and $\dot{V}_T$ = total volumetric flow rate of the fire product-air mixture in the apparatus (0.032 m^3/s in our apparatus). σ can be calculated from the data in table 5.4.

The calculated data for the generation efficiencies of heat and chemical compounds, oxygen depletion efficiency, and "smoke attenuation coefficient" are listed in table 5.7.

TABLE 5.5. CRITICAL HEAT FLUX AND ENERGY FOR THE PILOTED IGNITION OF FUEL VAPORS FOR AIRCRAFT PANEL MATERIALS

Sample	Critical Heat Flux (kW/m^2)		Energy (kJ/m^2)	
	Paint Peeling	Surface	Paint Peeling	Surface
1A (051283) Epoxy fiberglass	17	20	210	280
3C (051683) Epoxy Kevlar	13	19	200	250
2B (070583) Phenolic fiberglass	13	33	250	180
4D (092283) Phenolic Kevlar	8	17	310	310
5E (090983) Phenolic graphite	13	25	350	280

TABLE 5.6. AVERAGE VALUES OF HEAT OF GASIFICATION, CRITICAL AND FLAME HEAT FLUX FOR THE AIRCRAFT PANEL MATERIALS SAMPLE

Sample	$\dot{q}''_{cr_2}$ (kW/m^2)	$\dot{q}''^{a}_{fs_2}$ (kW/m^2)	L (kJ/g)
1A (051283) Epoxy fiberglass	20	15	2.8[b]
3C (051683) Epoxy Kevlar	19	23	3.5
2B (070583) Phenolic fiberglass	33	14	3.5[c]
4D (092283) Phenolic Kevlar	17	17	3.7[c]
5E (090983) Phenolic graphite	25	17	5.9[c]

[a] Normal air, external heat flux 26 to 61 kW/m^2

[b] L = 2.23 kJ/g for epoxy fiberglass from our previous studies

[c] L = 3.74 kJ/g for phenolic foam from our previous study

TABLE 5.7. GENERATION EFFICIENCIES OF HEAT AND CHEMICAL COMPOUNDS, OXYGEN DEPLETION EFFICIENCY AND "SMOKE MASS ATTENUATION COEFFICIENT" FOR AIRCRAFT PANEL MATERIALS

Sample	$\dot{q}''_e$	O_2	f_{CO}	f_{CO_2}	f_{hyd}	f_c	d_{O_2}	f_{H_2O}	$\sigma(m^2/g)$			X_A	X_C	X_R
	(kW/m^2)	(%)							0.46 (μ)	0.63 (μ)	1.1 (μ)			
1A (051283)	61	20.9	0.068	0.31	0.057	0.56	0.37	0.36	4.3	1.4	0.78	0.36	0.22	0.14
Epoxy fiberglass	39	20.9	0.065	0.30	0.062	0.57	0.47	-	2.3	1.4	0.74	0.40	0.20	0.20
	26	20.9	0.077*	0.42*	0.079*	0.42*	0.51*	0.59*	3.7*	2.2*	1.2*	0.48*	0.26*	0.22*
	61	9.85	0.089	0.25	0.101	0.56	NA	0.26	2.0	1.6	0.94	NA	NA	NA
	39	9.95	0.042	0.32	0.049	0.59	NA	-	2.0	1.7	1.5	NA	NA	NA
	61	1.67	0.078	0.24	0.12	0.56	NA	-	2.7	2.1	1.5	NA	NA	NA
3C (051683)	61	20.9	0.048	0.32	0.048	0.58	0.40	0.34	2.1	1.4	0.75	0.37	0.26	0.11
Epoxy kevlar	39	20.9	0.057	0.32	0.066	0.56	0.44	0.33	1.7	1.0	0.53	0.39	0.16	0.23
	26	20.9	0.070*	0.38*	0.067*	0.48*	0.55*	-	2.2*	1.4*	0.68*	0.48*	0.23*	0.25*
	61	9.61	0.17	0.37	0.12	0.34	NA	-	2.2	1.7	1.4	NA	NA	NA
	39	10.2	0.095	0.35	0.052	0.50	NA	-	1.5	1.0	0.91	NA	NA	NA
	61	2.2	0.098	0.23	0.077	0.60	NA	-	2.2	1.7	1.2	NA	NA	NA
2B (070583)	61	20.9	0.011	0.51	0.0040	0.48	0.50	0.50	0.53	0.41	0.17	0.51	0.15	0.36
Phenolic fiberglass	39	20.9	0.019	0.60	0.011	0.37	(0.77)	0.54	0.65	0.42	0.25	0.65	0.13	0.52
	61	9.59	0.11	0.33	0.064	0.50	NA	-	0.64	0.64	0.32	NA	NA	NA
	39	9.85	0.076	0.29	0.030	0.60	NA	-	0.38	0.30	0.12	NA	NA	NA
	61	2.12	0.079	0.22	0.087	0.61	NA	-	2.2	1.5	0.68	NA	NA	NA
4D (092283)	61	20.9	0.043	0.41	0.043	0.50	0.39	0.46	1.6	0.94	0.53	0.41	0.14	0.27
Phenolic kevlar	39	20.9	0.056	0.58	0.047	0.32	(0.79)	0.65	1.4	0.95	0.40	0.61	0.25	0.36
	26	20.9	0.060	0.42	0.039	0.48	(0.71)	0.44	1.1	0.91	0.41	0.46	0.32	0.14
	61	9.53	0.087	0.31	0.091	0.51	NA	-	2.1	1.6	1.1	NA	NA	NA
	39	10.4	0.059	0.29	0.058	0.59	NA	-	2.2	2.0	1.4	NA	NA	NA
	61	2.01	0.044	0.16	0.063	0.73	NA	-	2.2	1.6	1.1	NA	NA	NA
5D (090983)	61	20.9	0.012	0.62	0.0095	0.36	0.65	0.62	1.2	0.75	0.48	0.64	0.26	0.38
Phenolic graphite	39	20.9	0.019	0.66	0.010	0.31	(0.86	-	1.1	0.49	0.31	0.67	0.17	0.50
	61	9.69	0.16	0.47	0.11	0.26	NA	-	2.0	1.2	0.59	NA	NA	NA
	39	10.5	0.086	0.36	0.037	0.52	NA	-	0.65	0.59	0.19	NA	NA	NA
	61	2.14	0.086	0.29	0.087	0.54	NA	-	1.6	1.1	0.52	NA	NA	NA

*unstable combustion

NA = not applicable

Heat and Chemical Compound Generation Parameters. The heat generation parameter (h_i) can be expressed as

$$h_i = H_i/L \quad , \tag{9}$$

where $H_i = \dot{Q}''_i/\dot{G}''_f$.

The chemical compound generation parameter (ξ_j) can be expressed as

$$\xi_j = Y_j/L \quad , \tag{10}$$

where $Y_j = \dot{G}''_j/\dot{G}''_f$.

The calculated data for h_i and ξ_j are listed in table 5.8; data for $\dot{q}''_{rr}$ and $\dot{q}''_{fs}$ are also included.

h_i and ξ_j can be used to estimate the heat release rates and generation rates of chemical compounds in various fire scenarios where heat flux values are known or can be estimated,

$$\dot{Q}''_i = h_i \quad \dot{q}''_e + \dot{q}''_{fs} - \dot{q}''_{rr} \qquad (11)$$

$$\dot{G}''_j = \xi_j \quad \dot{q}''_e + \dot{q}''_{fs} - \dot{q}''_{rr} \quad . \qquad (12)$$

DISCUSSION OF RESULTS. The following discussion tries to interrupt the reading of the results and their relevance to aircraft fire hazards analysis.

Fire Initiation. The critical heat flux data for piloted ignition listed in table 5.5 indicate that phenolic fiberglass (Sample 2B, 070583) requires the highest flux (33 kW/m^2) to initiate ignition, followed by phenolic graphite, 25 kW/m^2, (Sample 5E, 090983). Phenolic Kevlar (Sample 4D, 092283) requires the lowest flux (17 kW/m^2) to initiate ignition. The energy data for piloted ignition listed in table 5.5 indicate that ignition will be quite fast for all samples provided the heat flux is above the critical heat flux.

Although flame heat flux, expected in larger-scale fires, was not quantified, the data for flame heat flux listed in table 5.6, for conditions used in our experiments for small samples, indicate that flame heat flux values do not vary appreciably between various samples. Fire propagation for aircraft panel materials, thus, is expected to depend on the critical heat flux for ignition. The higher the value of critical heat flux, the slower is fire propagation expected for the aircraft panel materials.

Generation of Fuel Vapors. Since the flame heat flux appears to be similar for the aircraft panel materials, the generation rates of fuel vapors would be expected to follow the heat of gasification and surface reradiation (or critical heat flux) (see table 5.6). Phenolic graphite (Sample 5E, 090983) would be expected to have the lowest value for the generation rate of fuel vapors in large-scale fires compared with other materials. For example, at 61 kW/m^2 of external heat flux, in normal air, from table 5.4, $\dot{G}''_f$ = 8.4 and 11.9 g/m^{2}s for phenolic graphite and phenolic fiberglass respectively compared with $\dot{G}''_f$ = 16.2, 17.6 and 19.5 g/m^{2}s for epoxy fiberglass, epoxy Kevlar and phenolic Kevlar respectively.

Thus, in terms of fire initiation (critical heat flux and possibly fire propagation) and generation of fuel vapors, expected in large-scale fires, phenolic fiberglass and phenolic graphite samples appear to be the best samples out of the total five aircraft paneling materials examined in this study.

TABLE 5.8. GENERATION PARAMETERS FOR HEAT AND CHEMICAL COMPOUNDS

Sample	ξ_j (g/kJ)					h_i			$\dot{q}''_{rr}$	$\dot{q}''_{fs}$ [a]
	CO	CO_2	HC	C	H_2O	Actual	Convective	Radiative	(kW/m^2)	(kW/m^2)
1A (051283) Epoxy fiberglass										
Pyrolysis	0.0086	0.026	0.0086	0.20	0.020	NA	NA	NA	20	-
Combustion	0.039	0.29	0.0057	0.20	0.079	4.0	2.2	1.8	20	15
3C (051683) Epoxy kevlar										
Pyrolysis	0.012	0.024	0.0063	0.14	-	NA	NA	NA	19	-
Combustion	0.024	0.25	0.0043	0.16	0.060	3.2	1.8	1.4	19	23
22B (070583) Phenolic fiberglass										
Pyrolysis	0.010	0.025	0.0043	0.16	-	NA	NA	NA	33	-
Combustion	0.0071	0.41	0.00054	0.12	0.083	6.2	1.5	4.7	33	14
4D (092283) Phenolic kevlar										
Pyrolysis	0.0068	0.021	0.019	0.16	-	NA	NA	NA	17	-
Combustion	0.024	0.33	0.0030	0.12	0.078	5.0	2.5	2.6	17	17
5E (090983) Phenolic graphite										
Pyrolysis	0.0075	0.020	0.0034	0.075	-	NA	NA	NA	25	-
Combustion	0.0044	0.28	0.00041	0.058	0.059	4.2	1.4	2.8	25	17

[a] small-sample burning in normal air; data were not measured at higher oxygen concentrations to simulate large-scale flame radiation

Heat Release Rate. The actual and radiative heat release rate parameters for phenolic fiberglass are 6.2 and 4.7 respectively in table 5.8, which are the highest compared with other materials. For phenolic graphite, the actual and radiative heat release rate parameters are 4.2 and 2.8 respectively, which are also higher than the parameters for other materials. However, because of the lower values for the generation rates of fuel vapors, the heat release rates for phenolic fiberglass and phenolic graphite would be expected to become comparable to other materials in large-scale fires. For example, at 60 kW/m^2 in normal air, the actual heat release rates for phenolic graphite and phenolic fiberglass are 202 and 228 kW/m^2 respectively compared with the rates of 173, 194 and 302 kW/m^2 for epoxy fiberglass, epoxy Kevlar, and phenolic Kevlar respectively.

The actual heat release rates of all the aircraft paneling materials are comparable (with the exception of phenolic Kevlar). However, phenolic fiberglass and phenolic graphite show improved characteristics in terms of fire initiation and possibly fire propagation and generation rates of fuel vapors.

Generation of Chemical Compounds. The generation rates of chemical compounds are associated with hazard due to heat smoke, toxic and corrosive

products. The generation of CO_2 and H_2O and depletion of O_2 are generally associated with heat, whereas generation of CO and other organic carbon compounds or inorganic compounds are generally associated with smoke, toxic or corrosive products in fires.

In this study only CO was measured and the mixture of other organic carbon compounds was calculated from carbon atom balance. The generation of smoke was measured indirectly in terms of optical density (smoke attenuation coefficient).

The CO generation parameter in table 5.8 indicates that in pyrolysis the parameter is comparable for all five materials, whereas in combustion the parameter is lowest for phenolic fiberglass and phenolic graphite. Since the generation rate of fuel vapors is lowest for these two materials, it is expected that, in large-scale fires, the generation rates of CO would be lowest compared with other materials. For example, from the data in table 5.4 for an external heat flux of 61 kW/m^2 in normal air, the generation rate of CO is 0.17 and 0.22 g/m^2s for phenolic graphite and phenolic fiberglass compared with the values of 1.38, 1.45 and 1.9 g/m^2s for phenolic Kevlar, epoxy Kevlar and epoxy fiberglass, respectively.

The generation parameter for the mixture of the other organic carbon compounds in table 5.8 indicates that the parameter is lowest for phenolic graphite in pyrolysis and combustion, whereas the parameter for phenolic fiberglass is comparable to parameter for other materials. However, both phenolic graphite and phenolic fiberglass would be expected to show lower values for the generation rates of the mixture of other organic carbon compounds compared with other materials in large-scale fires. For example, at 61 kW/m^2 in normal air, the generation rate of the mixture of other organic carbon compounds in pyrolysis is calculated to be 2.4 and 4.0 g/m^2s for phenolic graphite and phenolic fiberglass respectively, compared with generation rates of 5.5, 7.7 and 7.8 g/m^2s for epoxy Kevlar, phenolic Kevlar and epoxy fiberglass, respectively. At 61 kW/m^2 in normal air, the generation rate of the mixture of other organic carbon compounds in combustion is calculated to be 2.9 and 5.1 g/m^2s for phenolic graphite and phenolic fiberglass respectively, compared with generation rates of 8.4, 9.3 and 10.0 g/m^2s for phenolic Kevlar, epoxy fiberglass and epoxy Kevlar, respectively.

The lower the generation rate of the mixture of other organic carbon compounds, the higher is the optical transmission through smoke. The effect of the lower values of the generation rate of the mixture of other organic carbon compounds on optical transmission through smoke is indicated by the data in table 5.7 for the smoke mass attenuation coefficient; the coefficient has a lower value for all three wavelengths for phenolic graphite and phenolic fiberglass compared with other materials.

CONCLUSION. Based on the study made in the FM Small-Scale Combustibility Apparatus for the five samples of aircraft paneling materials, phenolic graphite and phenolic fiberglass showed the best performance.

It is recommended that larger-scale experiments be performed to validate the conclusions derived from this study.

Although the carbon atom balance appears to indicate lower values for the generation rates of CO and other organic carbon compounds which may be indicative of lower amounts of toxic compounds from phenolic graphite and phenolic fiberglass, it is recommended that direct animal exposure experiments be used for the verification of such indications.

NOMENCLATURE.

a	surface area of sample (m^2)
$\dot{D}''_{O_2}$	mass depletion rate of oxygen per unit surface area of sample (g/m^2s)
d_{O_2}	oxygen depletion efficiency (-)
E	energy for ignition (kJ/m^2)
f_j	generation efficiency of a chemical compound (-)
$\dot{G}''_f$	mass generation rate of fuel vapors per unit surface area of sample (g/m^2s)
$\dot{G}''_j$	mass generation rate of a chemical compound per unit surface area of sample (g/m^2s)
H_T	net heat of complete combustion (kJ/g)
h_i	heat generation parameter (-)
k_j	theoretical maximum yield of a chemical compound (g/g)
k_{O_2}	oxygen-to-fuel stoichiometric ratio (g/g)
L	heat of gasification (kJ/g)
OD	optical density per unit path length (m^{-1})
$\dot{Q}''_i$	heat release rate per unit surface area of sample (kW/m^2)
$\dot{q}''_i$	heat flux per unit surface area of sample (kW/m^2)
$\dot{V}_T$	total volumetric flow rate of fire products air mixture (m^3/s)
Y_j	yield of a chemical compound (g/g)
σ	smoke mass attenuation coefficient (m^2/g)
χ_i	generation efficiency of heat (-)
ξ_j	chemical compound generation parameter (g/kJ)

Superscript

$\dot{}$	per unit of time (s^{-1})
$\ddot{}$	per unit surface area of sample (m^{-2})

Subscript

A	actual
C	convective
cr	critical
e	external
fs	flame to the surface
R	radiative
rr	reradiation

REFERENCES.

5.1 Tewarson, A., Physico-Chemical and Combustion/Pyrolysis Properties of Polymeric Materials, National Bureau of Standards, Washington, D.C., Technical Report No. NBS-GCR-80-295, November 1980.

5.2 Tewarson, A., Experimental Evaluation of Flammability Parameters of Polymeric Materials, Flame Retardant Polymeric Materials, Vol. 3, ed., M. Lewin, S. M. Atlas and E. M. Pearce, Plenum Press, New York, p. 97, 1982.

5.3 Tewarson, A., Quantification of Fire Properties of Fuels and Interaction With Fire Environment, National Bureau of Standards, Washington, D.C., Technical Report FMRC J.I. OEON6.RD, April 1982.

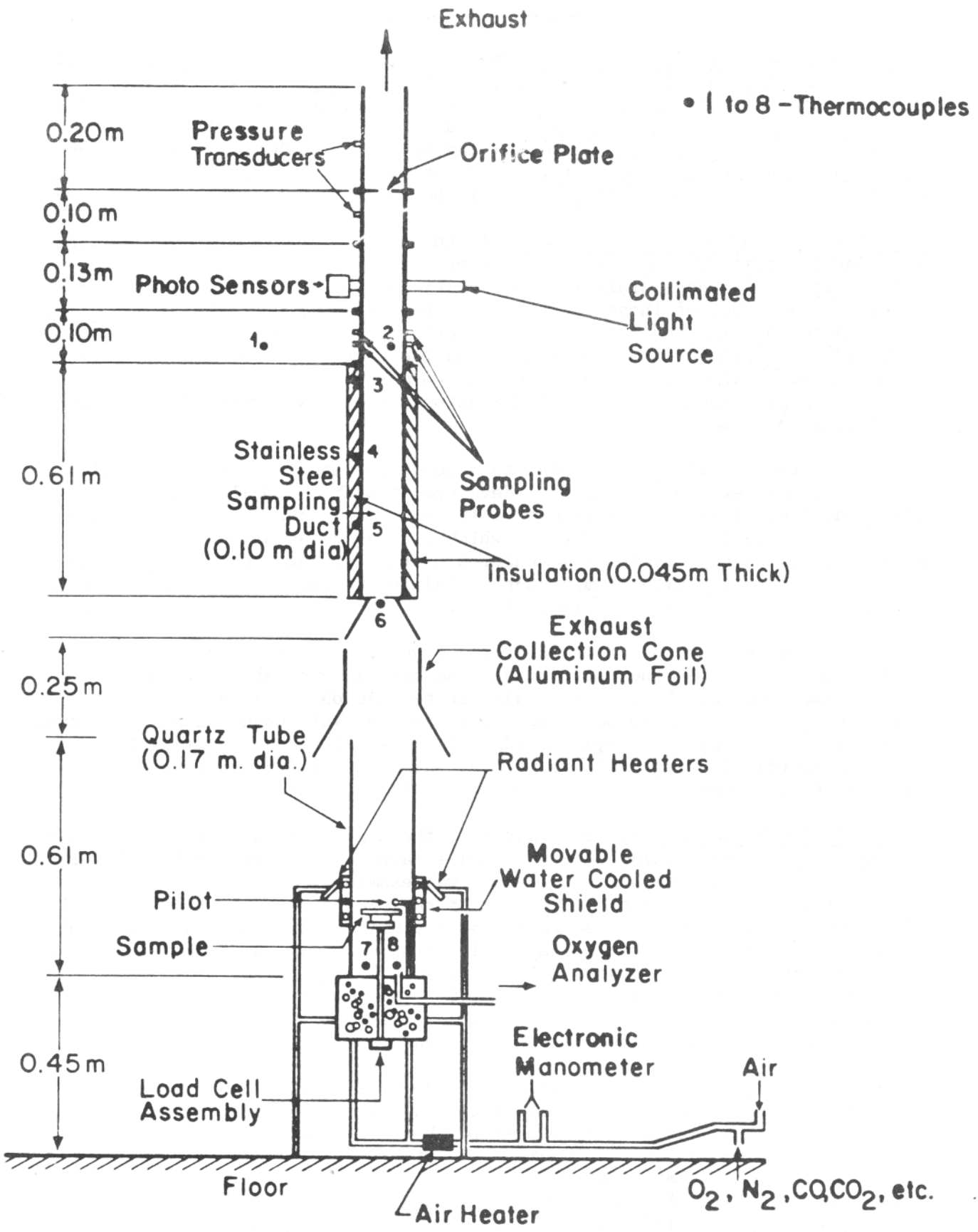

FIGURE 5.1. EXPERIMENTAL APPARATUS

SUMMARY OF RESULTS

The results of this study fall into two categories. First, an assessment of the fire development in several post crash fire simulation experiments conducted by the FAA, and how this fire exposure affects the initial involvement of the cabin lining material. Second, an extensive set of data were derived for specific aircraft cabin lining materials. The details of these data, analyses and their suggested interpretations have been presented in chapters 1-5. Here some main points will be summarized.

ENERGY RELEASE BY CABIN FURNISHINGS. In the analysis of FAA post crash fire experiments (tests 34 and 35) with complete cabin furnishings, the energy release rates of these furnishings were estimated as the fire developed in time. The accuracy of these estimates can be judged by their relative comparisons among the different methods used: calorimetry data of samples coupled with video analysis of fire propagation on the seats and other furnishings; flame height measurements; and an overall conservation analysis of cabin oxygen. These comparisons suggest deviations of approximately 20 to 50% at any instant of time.

In test 35 the regular seats appear to account for about 75% of the total energy release rate during the fire development with the wall panels and carpeting contributing the remainder. The energy release rate grew exponentially with time to about 1000 kW at which flashover was noted at 140 s. Flashover manifested itself as combustion of the ceiling panels followed by their disintegration with flaming debris falling to cause more extensive fire growth on the seats and other furnishings.

In test 34, which had seats with blocking layers, the energy release was similar to test 35 for the first minute, decreased somewhat in the next minute, and then sharply increased similar to that observed in test 35. Flashover was perceived to occur at 210 s, but sporatic unsustained combustion occurred in the upper gas layer at 125 and 155 s. It is interesting to note that the estimated energy release rate at flashover (210 s) in test 34 was essentially the same as in test 35 at 140 s, i.e. 1000 kW.

IGNITION OF CEILING PANELS. In chapter 2, the heat transfer process promoting the ignition of the ceiling panel section adjacent to the external pool fire exposure of the post crash fire scenario was examined. That analysis considers the strong radiative (6 W/cm^2 at the opening) heat of the external fire, its convective effect due to periodic plume capture, and internal cabin energy release as estimated in chapter 1. Prediction of gas temperatures just below ($\sim$ 5 mm) a well insulated ceiling (k = 0.045 W/mK) indicate a maximum of 290 K directly over the first seat and 140 K approximately 2 m away. These results were consistent with experimental measurements only when radiation corrections were made on the thermocouple measurements.

An assessment of an actual aircraft panel was made using these calculations. This was done based on the external pool fire and the internal cabin fire total energy release rate as estimated in chapter 1 for the fully furnished cabins of tests 34 and 35. Although the cabin energy release was considered to be represented as emanating from a point source, it appears the model is acceptable for the early growth period. Indeed, plausible results were computed which gave ceiling ignition (536°C) at 148 s and 204 s respectively

for tests 35 and 34. Since the panel properties assumed are probably very similar to those of the actual panel used in those tests, the computations appear appropriate and are consistent with the flashover times stated previously. Of course, full fire development has not been predicted. It is likely that flashover could develop with a noncombustible ceiling with the same remaining furnishings as in tests 34 and 35, or that a combustible wall-ceiling panel section alone could propagate under the threat of the external pool fire. Only the time to flashover would likely be altered.

MATERIAL FLAMMABILITY DATA FOR PANELS. Five aircraft panel materials were tested in four apparatuses under a range of exposure conditions. These data are numerous and detailed throughout chapters 3 through 5. The panels were honeycomb in core structure with different face layers which accounted for their assigned names: (1) epoxy fiberglass, (2) phenolic fiberglass, (3) epoxy Kevlar, (4) phenolic Kevlar, and (5) phenolic graphite. Since the early stage of fire development would be determined by the panel's ignition and energy release rate characteristics, these results will be compared for the various apparatuses. This underscores the differences in the burning conditions among the various test apparatuses and the burning conditions of the full-scale experiments, and it bears on the use of such laboratory test data in correlating and assessing hazard in full-scale scenarios.

Ignition. In three apparatuses (FMRC combustibility, lateral spread device, and the cone calorimeter) piloted ignition was measured. Ignition will depend on the absorbed heat, surface heat loss, the local attainment of a flammable mixture in the gas phase and the corresponding position of a pilot flame. The data for the five materials are summarized in figures 6.1 through 6.5. Reference to standard heat transfer literature suggests that for the sample sizes used (~ 10 x 10 cm) the flow is nearly turbulent and the convective heat transfer coefficient is essentially identical for vertical and horizontal orientations. Nevertheless, the primary heat loss at the surface is radiative at temperatures preceding ignition. This radiative loss should be identical for each apparatus except where the surface has been blackened in the FMRC apparatus. Still this should have a negligible effect on the emissive loss because non-metallic surfaces have high emissivities at these temperatures. Surface color and polish can have a considerable effect on reflection for source spectra that predominately fall at lower wavelengths than those of infrared or fire sources. The samples were blackened in the FMRC study because that device uses a tungsten-halogen quartz lamp source which would yield predominately low wavelength radiation causing significant surface reflectance for non-black surfaces. Thus, the blackened samples could yield shorter ignition times since more energy would be absorbed. Also the blackened surface might possibly affect the gas phase flammability limit. This effect, however, may have been incidental for these samples because the observed ignition behavior was that the ("Tedlar") surface film would burst or peel away before the honeycomb facing layer sustained ignition. Indeed this peeling affect could be partly responsible for scatter in the ignition data for a given apparatus. The inert backing materials should have a negligible affect on the absorbed heat transfer since all of the samples are good insulators themselves and ignite quickly.

Generally the data are in fair agreement. The most extensive data were taken with the flame spread apparatus described in chapter 3. The best agreement among the data occurred for sample no. 1, epoxy fiberglass. For the other

samples the FMRC data tend to yield shorter ignition times and lower minimum radiative heat fluxes to sustain ignition. The reasons for these differences are not apparent other than those factors mentioned above. Roughly speaking, two classes of behavior appear - one for the epoxy samples and the other for the phenolic samples. Thus it appears that the epoxy and phenolic are the primary decomposing components with the other structural component materials serving as a substrate. The epoxies ignite about twice as quickly and at a flux as low as about 2 W/cm^2 compared to 3 W/cm^2 or higher for the phenolics.

Energy Release. In contrast to the ignition phenomena described above, once combustion commences orientation and sample size will affect the burning rate. The extent to which this is important depends on the flame heat transfer back to the fuel. In the apparatuses used to derive the energy release rate data, the flames are relatively small and probably contribute of the order of 2 to 3 W/cm^2 to the sample. Their small size also implies they are nearly transparent to external radiation so that irradiances of 2 to 7 W/cm^2 are felt by the sample surface. Hence for these cases, one might expect similar but not identical behavior among the devices.

The energy release rates were determined by O_2 consumption in the cone calorimeter, by CO_2 production in the FMRC device, and by flame height in the wall flame heat transfer device. A critical factor to consider is the transient response. For these materials the burning rate is unsteady and the burning time is brief. Although for a complete analysis all of this information may be needed, only peak or average results have been included in this report. For comparative purposes these peak values will be examined among the devices for each material. They are plotted against external irradiance in figures 6.6 through 6.10. Considerable differences exist for samples 1, 2 and 3; but samples 4 and 5 show fairly linear monotonic behavior with external heat flux. The phenolic Kevlar and epoxy fiberglass tend to yield higher energy release rates than the other three samples. The lack of consistency in some of these data does suggest the need to test a larger batch of samples to resolve possible material variations, and to perhaps more fully evaluate the dependence of energy release rate results on the apparatus and its particular measurement technique.

Energy release rate is recognized as an important material variable in fire growth, but there is no generally accepted prescription for how to interpret test data, nor a full appreciation of their application to fire scenarios of larger scale and orientation. Hopefully, the data and analyses contained herein will be a basis for evaluation of aircraft panel flammability performance and its relationship to current FAA full-scale and model experiments.

CONCLUSIONS

The results developed suggest the following:

1. The external pool fire in the FAA post-crash fire experiment dominates the heat transfer to the cabin and is a strong factor in fire growth.

2. The contribution of the seat fire growth is a significant factor in promoting the ignition of typical aircraft wall and ceiling linings. The energy release rates of seats with and without blocking layers were estimated, and in both cases cabin flashover resulted at approximately 1000 kW.

3. It is feasible to predict the ignition of the cabin ceiling panels by using modeling computation, and data on the materials, i.e., thermal ignition properties.

4. For the five panel types tested the minimum heat transfer necessary to provide ignition appears to be influenced strongly by the resin binder (epoxy or phenolic) and not by the face or core materials. For example, the minimum radiant heat flux necessary to ignite the epoxy panels is approximately 2 W/cm^2 and 3 W/cm^2 for the phenolics.

5. The panel peak energy release rates derived from three different apparatuses gives mixed results. This characteristic needs further study.

6. These results should form a basis for analysis of current FAA full-scale and model experiments, and should provide insight into the relevant test data needed to assess the fire hazard of aircraft materials.

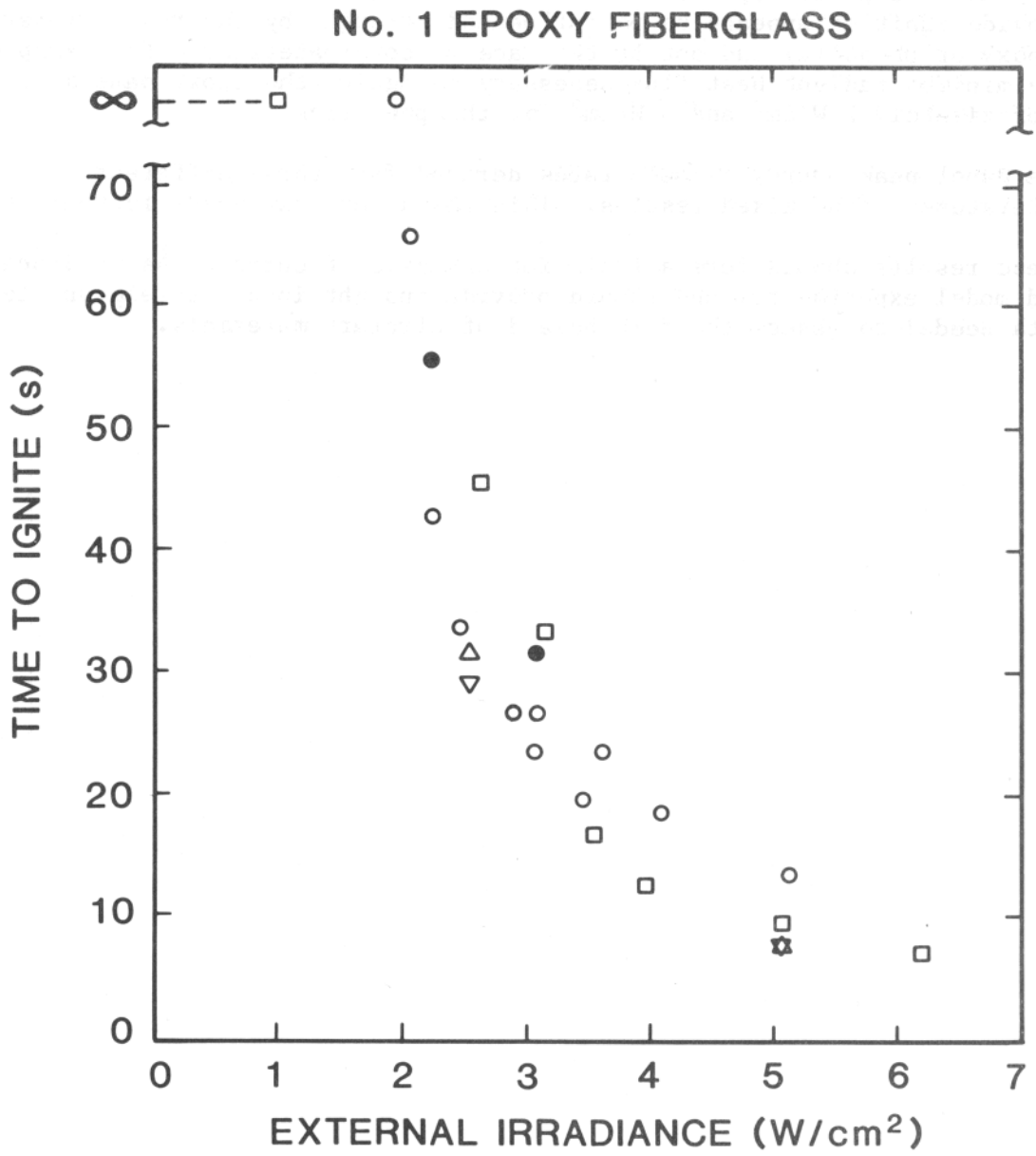

LEGEND	Apparatus	Sample size	Orientation	Backing material Density (kg/m^3)
○	Flame spread	11x11 cm	Vertical	700
●	Flame spread	11x11 cm	Vertical	65
□	FMRC combustibility	10x10 cm	Horizontal	210
△	Cone calorimeter	10x10 cm	Horizontal	~ 100
▽	Cone Calorimeter	10x10 cm	Vertical	600

FIGURE 6.1. IGNITION SUMMARY FOR SAMPLE NO. 1: EPOXY FIBERGLASS

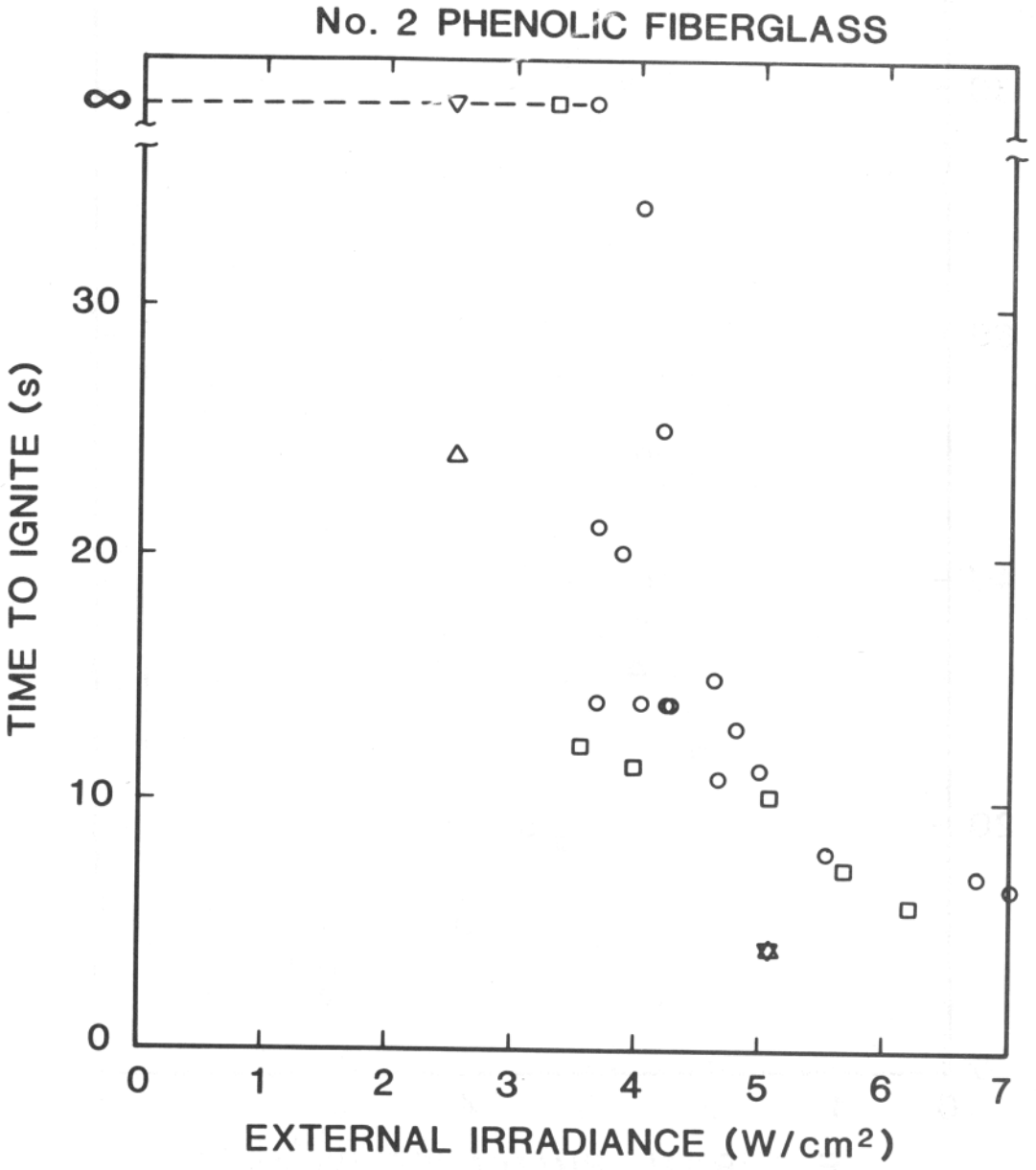

LEGEND	Apparatus	Sample size	Orientation	Backing material Density (kg/m³)
○	Flame spread	11x11 cm	Vertical	700
□	FMRC combustibility	10x10 cm	Horizontal	210
△	Cone calorimeter	10x10 cm	Horizontal	~100
▽	Cone Calorimeter	10x10 cm	Vertical	600

FIGURE 6.2. IGNITION SUMMARY FOR SAMPLE NO. 2: PHENOLIC FIBERGLASS

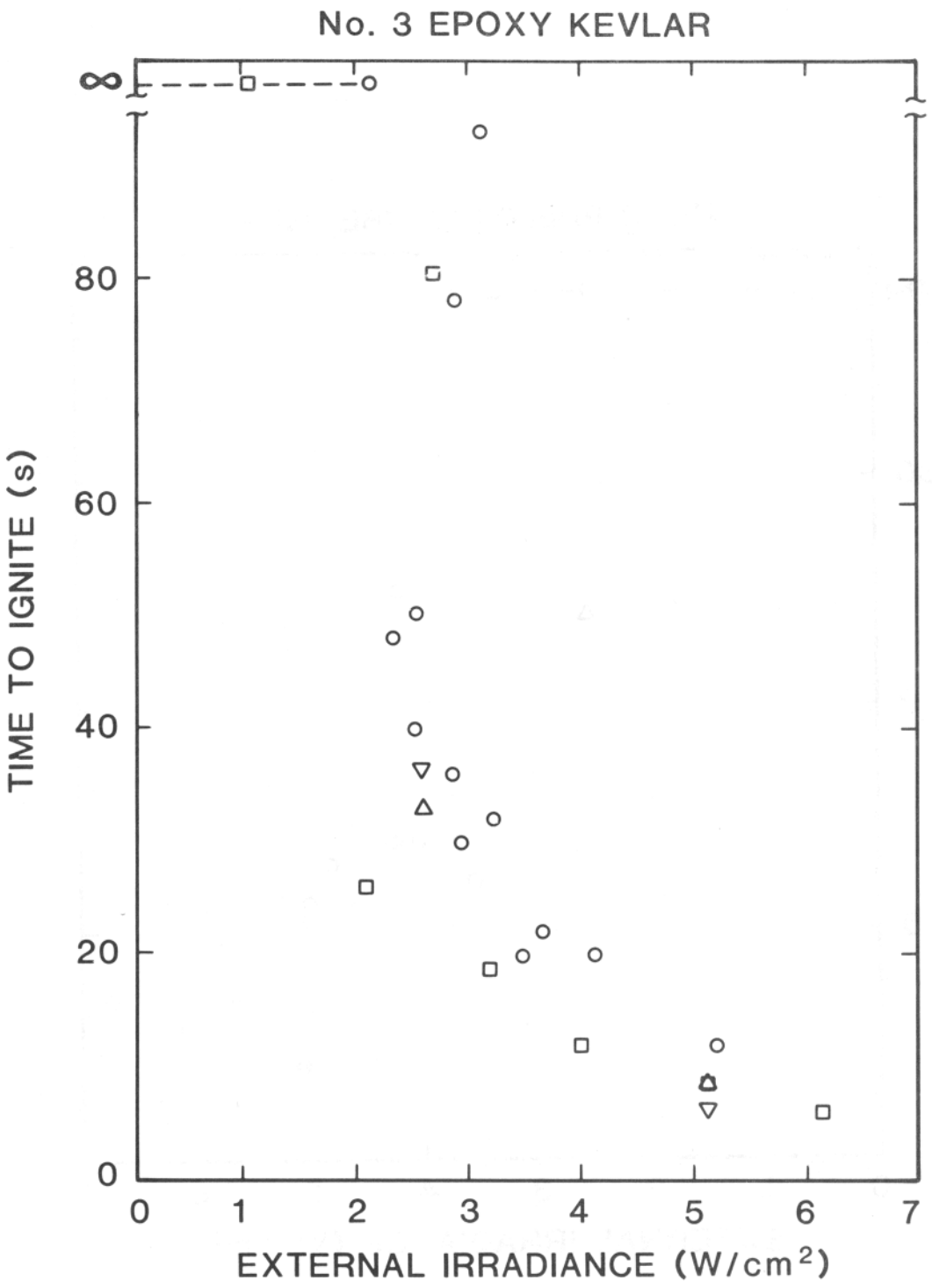

LEGEND	Apparatus	Sample size	Orientation	Backing material Density (kg/m^3)
○	Flame spread	11x11 cm	Vertical	700
□	FMRC combustibility	10x10 cm	Horizontal	210
△	Cone calorimeter	10x10 cm	Horizontal	~100
▽	Cone Calorimeter	10x10 cm	Vertical	600

FIGURE 6.3. IGNITION SUMMARY FOR SAMPLE NO. 3: EPOXY KEVLAR

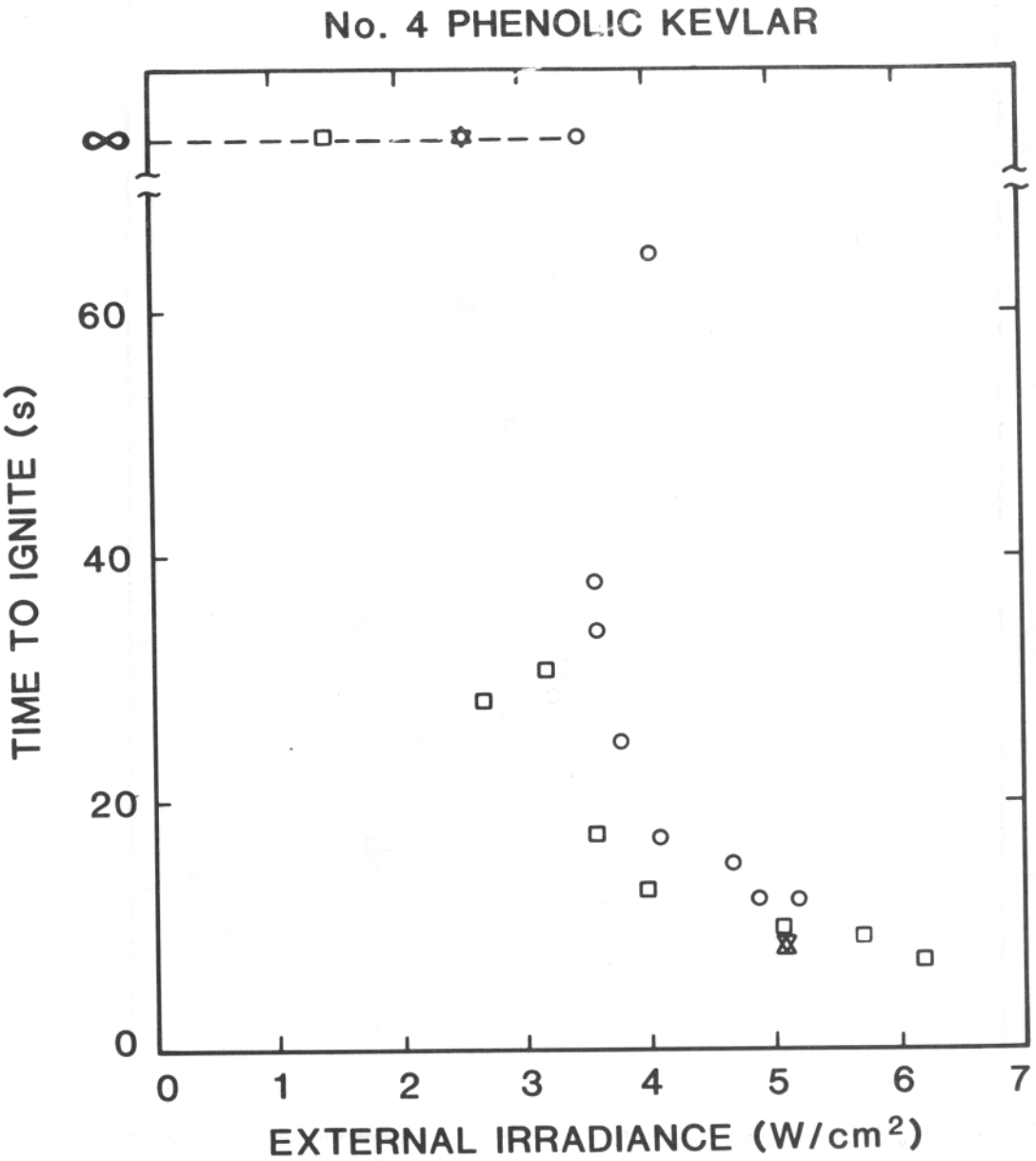

LEGEND	Apparatus	Sample size	Orientation	Backing material Density (kg/m^3)
○	Flame spread	11x11 cm	Vertical	700
□	FMRC combustibility	10x10 cm	Horizontal	210
△	Cone calorimeter	10x10 cm	Horizontal	~100
▽	Cone Calorimeter	10x10 cm	Vertical	600

FIGURE 6.4. IGNITION SUMMARY FOR SAMPLE NO. 4: PHENOLIC KEVLAR

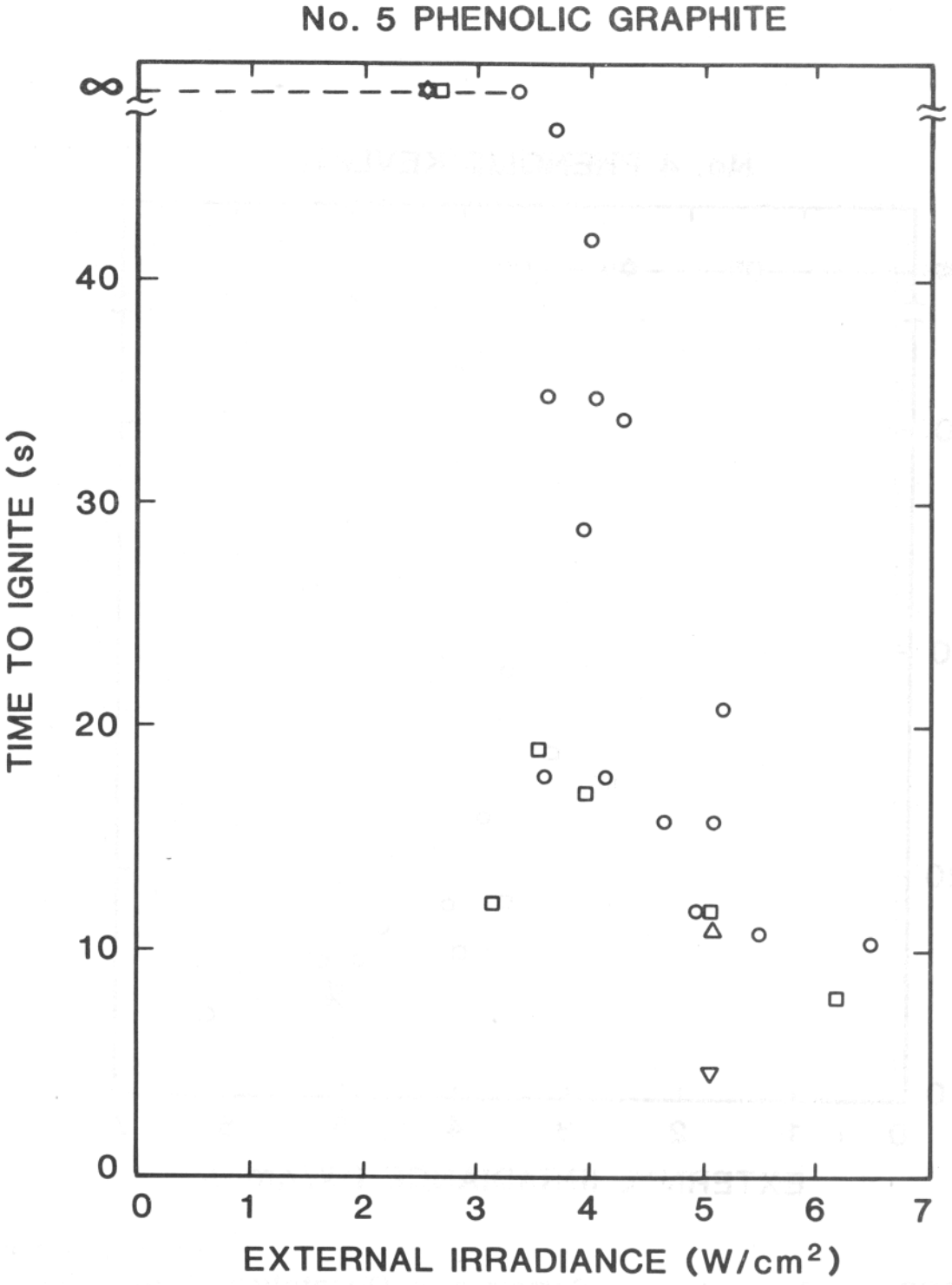

LEGEND	Apparatus	Sample size	Orientation	Backing material Density (kg/m^3)
○	Flame spread	11x11 cm	Vertical	700
□	FMRC combustibility	10x10 cm	Horizontal	210
△	Cone calorimeter	10x10 cm	Horizontal	~100
▽	Cone Calorimeter	10x10 cm	Vertical	600

FIGURE 6.5. IGNITION SUMMARY FOR SAMPLE NO. 5: PHENOLIC GRAPHITE

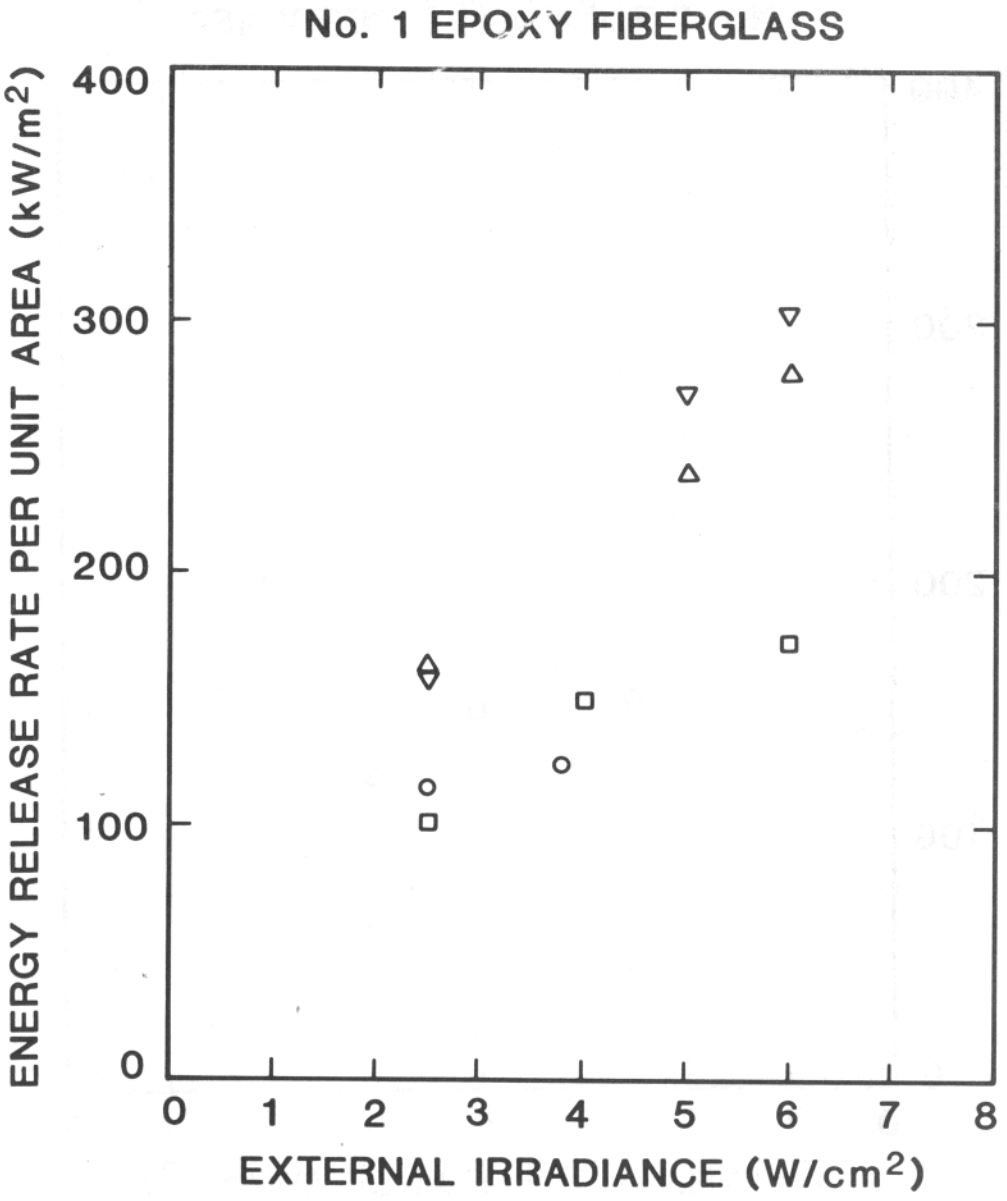

LEGEND	Apparatus	Sample size	Orientation	Backing material density (kg/m3)
o	Flame heat transfer	28x28 cm	Vertical	160
□	FMRC combustibility	10x10 cm	Horizontal	210
△	Cone calorimeter	10x10 cm	Horizontal	~100
▽	Cone calorimeter	10x10 cm	Vertical	600

FIGURE 6.6. PEAK ENERGY RELEASE RATE FOR SAMPLE NO. 1

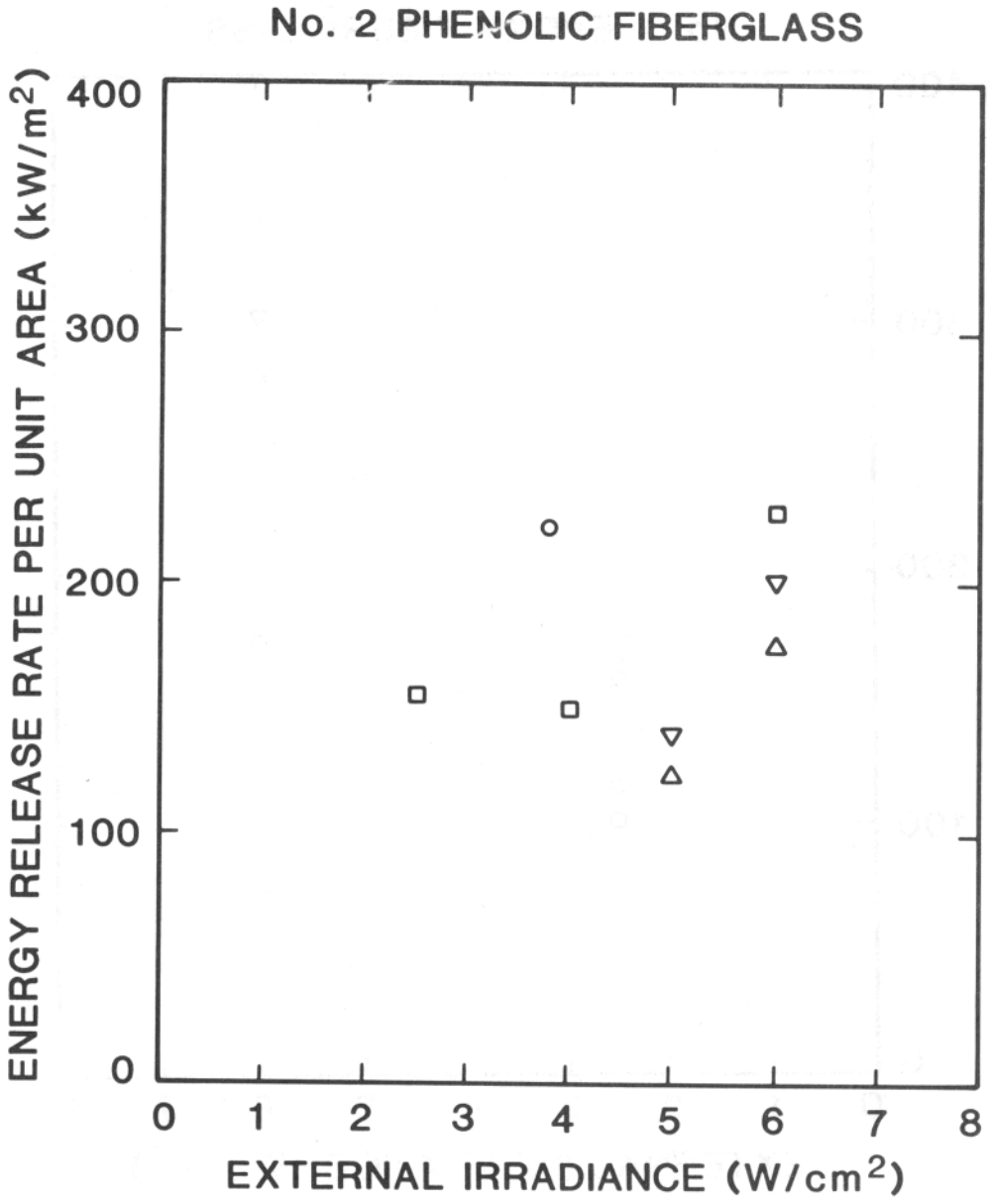

LEGEND	Apparatus	Sample size	Orientation	Backing material density (kg/m^3)
○	Flame heat transfer	28x28 cm	Vertical	160
□	FMRC combustibility	10x10 cm	Horizontal	210
△	Cone calorimeter	10x10 cm	Horizontal	~100
▽	Cone calorimeter	10x10 cm	Vertical	600

FIGURE 6.7. PEAK ENERGY RELEASE RATE FOR SAMPLE NO. 2

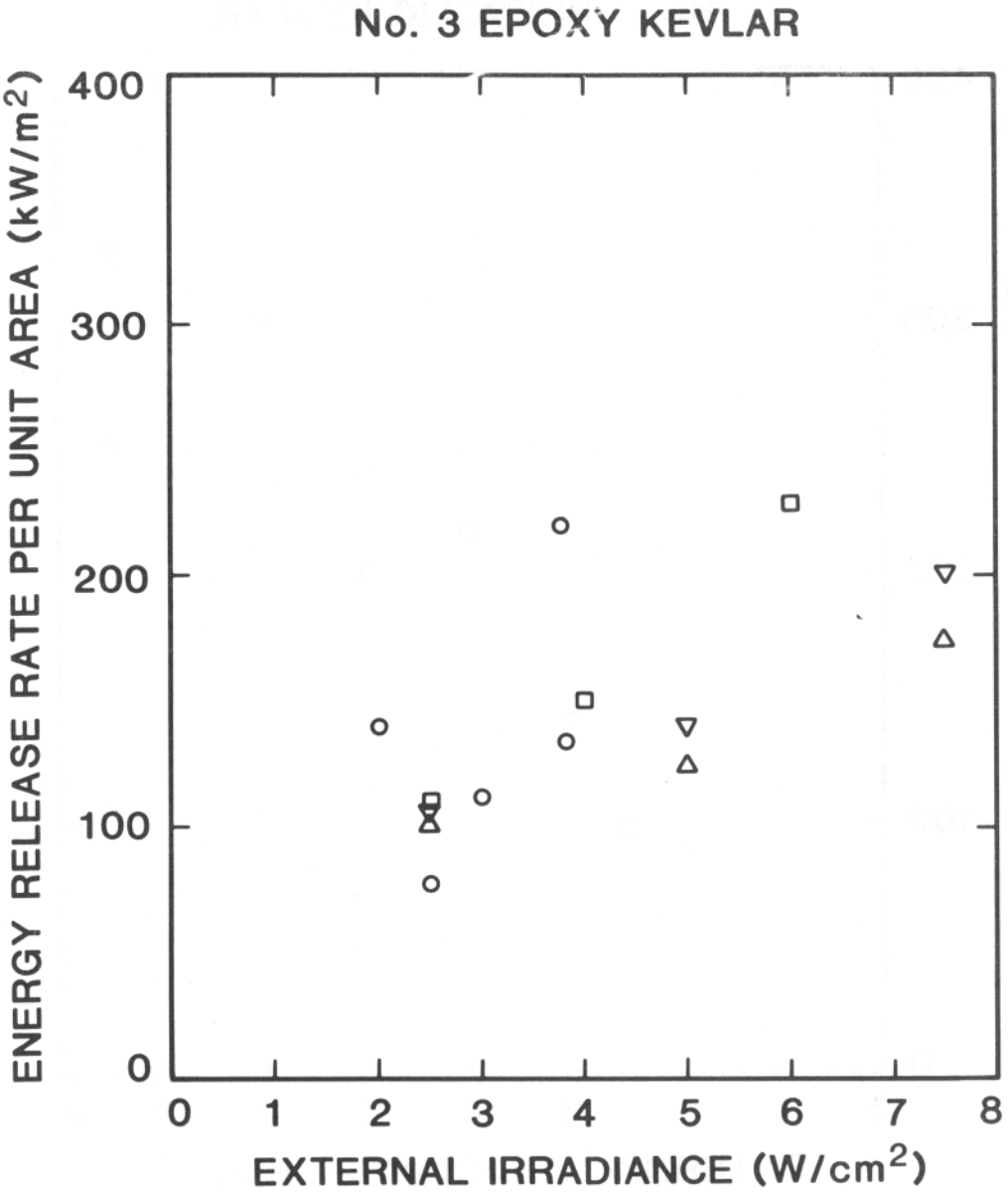

LEGEND	Apparatus	Sample size	Orientation	Backing material density (kg/m³)
○	Flame heat transfer	28x28 cm	Vertical	160
□	FMRC combustibility	10x10 cm	Horizontal	210
△	Cone calorimeter	10x10 cm	Horizontal	~ 100
▽	Cone calorimeter	10x10 cm	Vertical	600

FIGURE 6.8. PEAK ENERGY RELEASE RATE FOR SAMPLE NO. 3

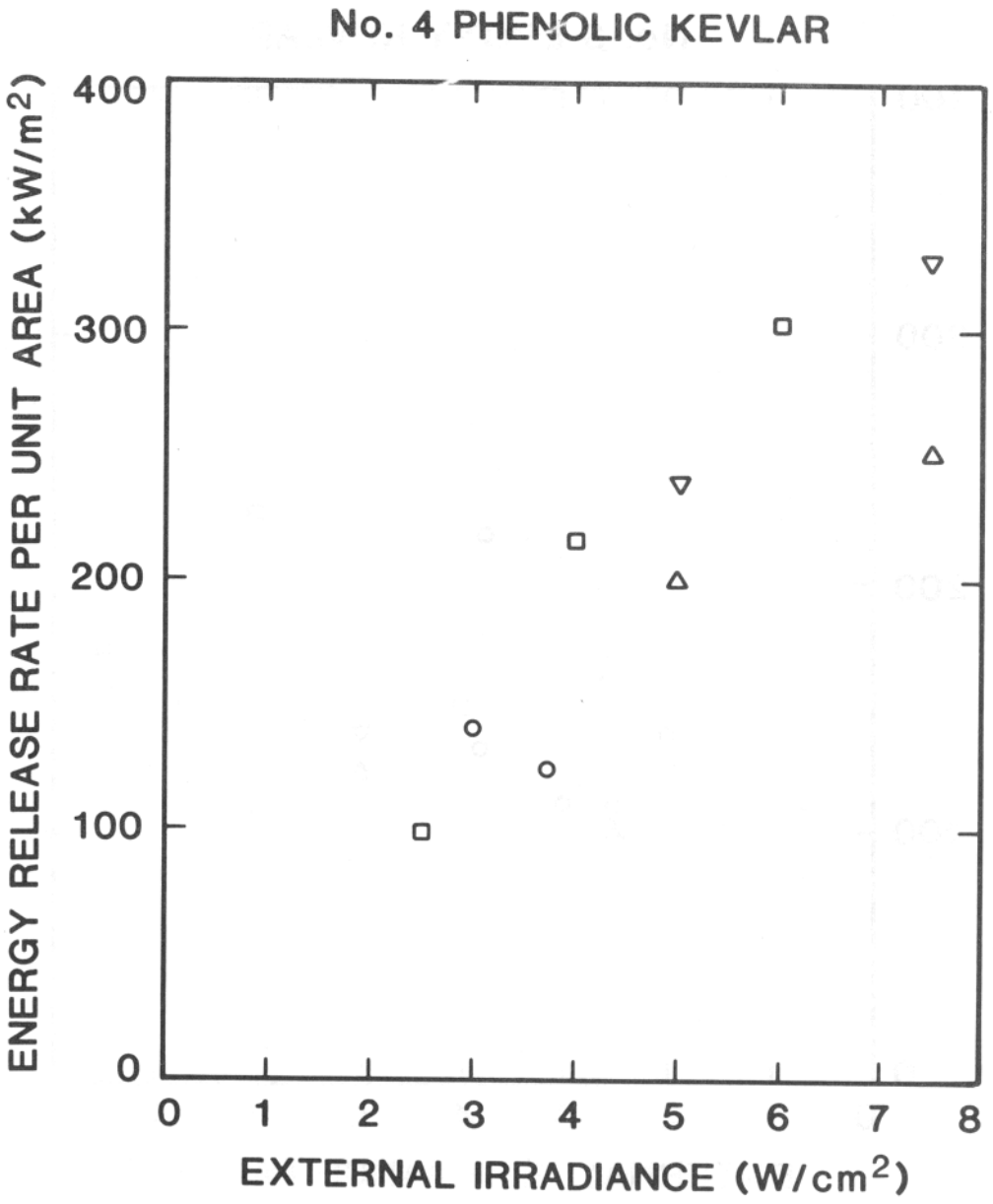

LEGEND	Apparatus	Sample size	Orientation	Backing material density (kg/m3)
o	Flame heat transfer	28x28 cm	Vertical	160
□	FMRC combustibility	10x10 cm	Horizontal	210
△	Cone calorimeter	10x10 cm	Horizontal	~100
▽	Cone calorimeter	10x10 cm	Vertical	600

FIGURE 6.9. PEAK ENERGY RELEASE RATE FOR SAMPLE NO. 4

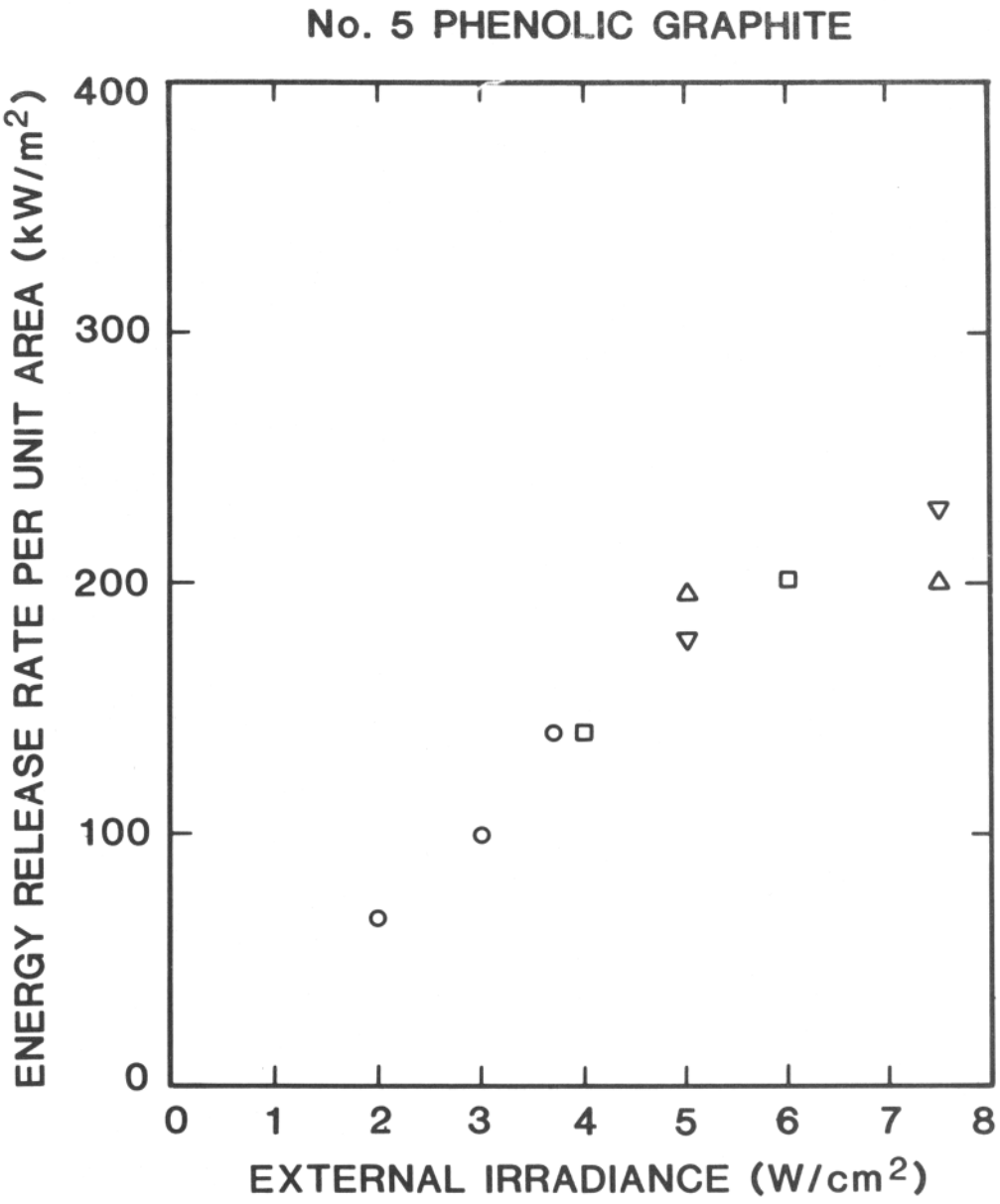

LEGEND	Apparatus	Sample size	Orientation	Backing material density (kg/m^3)
○	Flame heat transfer	28x28 cm	Vertical	160
□	FMRC combustibility	10x10 cm	Horizontal	210
△	Cone calorimeter	10x10 cm	Horizontal	~ 100
▽	Cone calorimeter	10x10 cm	Vertical	600

FIGURE 6.10. PEAK ENERGY RELEASE RATE FOR SAMPLE NO. 5

☆U.S. GOVERNMENT PRINTING OFFICE: 1985—505-080/20096